AN EXAMINATION OF COMPOSITION-PROPERTY RELATIONSHIPS FOR METHOTREXATE-LOADED GLASS IONOMER CEMENTS

by

Lauren Kiri

Submitted in partial fulfillment of the requirements
for the degree of Master of Applied Science

at

Dalhousie University
Halifax, Nova Scotia
November 2014

Table of Contents

List of Tables

List of Figures

Abstract

The addition of chemotherapeutics to bone cements may prevent local cancer progression and failure of stabilization treatments used to manage cancer-related fractures [1]. Significant effort has been made to evaluate the drug loading and delivery potential of conventional bone cements; however all of these materials are burdened to some degree by concerns regarding biocompatibility and strength [2]. Glass ionomer cement (GICs) have been identified as potential alternatives to existing bone cements, though it has been recognized that aluminum (Al) must be removed from the glass phase of existing materials in order to render them biocompatible with bone [3]. Recently, Dickey *et al.* published the first series of Al-free GICs that demonstrate adequate handling and mechanical properties for injectable skeletal applications [4]. In the present study, the best performing GIC was selected from this series to examine its drug loading and delivery potential. Prior to drug loading this material, a Design of Experiments approach was implemented to optimize the cement formulation (powder-liquid ratio and acid concentration) for injectable applications, vertebroplasty and kyphoplasty. The optimized cement was loaded at 0, 1, 5, and 10 wt% with an anticancer agent, methotrexate (MTX), to develop composition-property relationships correlating drug loading with working time, setting time, MTX release, ion release, compressive strength, and cytotoxic effect on NIH-3T3 mouse fibroblast cells. The results of this preliminary examination have shown that MTX addition imparted minimal effects on GIC handling properties and strength. Increased MTX loading significantly increased the concentration of drug released, but release efficiencies remained constant across the different drug loadings. Release was best described by the Korsmeyer-Peppas model, suggesting MTX release was primarily diffusion-mediated. Significant differences in leached ion concentrations were found across the different drug loadings; MTX addition initially increased germanium and silica release, but decreased the release of all ions at 31 days. This may indicate that MTX chemically integrated with the GIC matrix, binding to cations released from the GIC glass component. Finally, all MTX-loaded GICs exhibited a significant cytotoxic effect as compared to the 0 wt% cement, though no differences in cell viability were found between the 1, 5, and 10 wt% loadings. The GIC examined herein is a promising material for drug delivery applications and may present a potentially effective therapy for cancer-related fractures.

List of Abbreviations and Symbols Used

AC	Acid concentration
AP	Adequate precision
R^2_{adj}	Adjusted R-squared
Al	Aluminum
Ca	Calcium
CEX	Cephalexin
CHA	Chlorhexidine-diacetate
CHCl	Chlorhexidine-dihydrochloride
CHG	Chlorhexidine-digluconate
CHX	Chlorhexidine
CPC	Calcium phosphate cement
CS	Compressive strength
CSC	Calcium sulphate cement
CT	Computed tomography
CV	Coefficient of variance
DOE	Design of Experiments
DSC	Differential scanning calorimetry
Ge	Germanium
GIC	Glass ionomer cement
ICP	Inductively coupled plasma
KP	Korsmeyer-Peppas
MBD	Metastatic bone disease
MRI	Magnetic resonance imaging
MTX	Methotrexate
M_w	Molecular weight
Na	Sodium
P/L	Powder-liquid ratio
PAA	Polyacrylic acid
PET	Positron emission spectroscopy
PKP	Percutaneous kyphoplasty
PMMA	Polymethyl Methacrylate
R^2_{pred}	Predicted R-squared
PVP	Percutaneous vertebroplasty
RFA	Radiofrequency ablation
RFI	Radiofrequency ionization
SBF	Simulated body fluid
Si	Silica
SRE	Skeletal-related event
$t_{1/2}$	Release half-life
T_g	Glass transition temperature
TPF	Three point flexure
$t_{plateau}$	Release plateau
t_s	Setting time

t_w	Working time
VCF	Vertebral compression fracture
XRD	X-ray diffraction
Zn	Zinc
Zr	Zirconium

Acknowledgements

I would first like to thank my supervisor, Dr. Daniel Boyd, for both the opportunity to work on this project and for his mentorship and support throughout. Dan, your enthusiasm and encouragement throughout this program were tremendously motivational and inspired me to pursue this project to this point. I undoubtedly benefited from your immense knowledge and expertise.

I would also to thank my committee members, Dr. Robert Abraham and Dr. Mark Filiaggi, for their guidance and insight in completing this project. I am extremely fortunate to have had the chance to collaborate with the both of you; your input to this project was crucial to its completion.

This project would not have been possible without the assistance and support of many people at Dalhousie University: Maxine Langman (Department of Applied Oral Sciences), Gordon Hall (Department of Applied Oral Sciences), Brett Dickey (School of Biomedical Engineering), Nancy Kilcup (School of Biomedical Engineering), Victoria Dickinson (School of Biomedical Engineering), Robbie Sanderson (Department of Physics), and Darren Cole (Department of Biomedical Engineering). I would like to thank you all for your input and help along the way.

I would like to acknowledge the funding resources for this project: NSERC and the Atlantic Canada Opportunities Agency.

Lastly, I would like to thank my parents for their loving support: Brian and Joy Kiri. Thank you for your advice and encouragement in all of my endeavours.

Halifax, October 2014
Lauren Kiri

CHAPTER 1

Introduction

The fundamental objective of this thesis is the examination of composition-property relationships to assess the drug delivery potential of a novel injectable bone cement. The specific clinical context for this work involves the management of metastatic-related vertebral compression fractures. In order to appreciate the findings of the present study, this chapter provides an overview on metastatic bone disease (MBD), MBD-induced vertebral fractures, existing treatment approaches, and limitations with current methods and materials.

1.1 Overview of Metastatic Disease in Bone

Metastasis is the spread of malignant cells from a primary tumour to distant organs or tissues [5]. This process is initiated when malignant cells breakaway from the primary tumour and enter the bloodstream or lymphatic system. Several factors influence this process, including the type, grade, and duration of the primary cancer and the tumour microenvironment [5]. As outlined in Figure 1.1, the disseminated cells must be capable of invading the lumina of the blood vessels and surviving the immune factors in circulation [6]. Once at the target site, the cells extravasate the parenchyma and the tissue undergoes angiogenesis, establishing a secondary malignancy [6]. The location of the secondary tumour is influenced by the biological characteristics of both the malignant cells and the target tissue, as well as the physical properties of the vascular pathways and blood flow [7]. The primary tumour site plays a significant role in establishing the spread pattern, as cancer often metastases to the first collection of blood vessels that the cells encounter after detaching from the primary site. This explains why the lungs, liver, and bone are the most common sites of metastatic deposition [5].

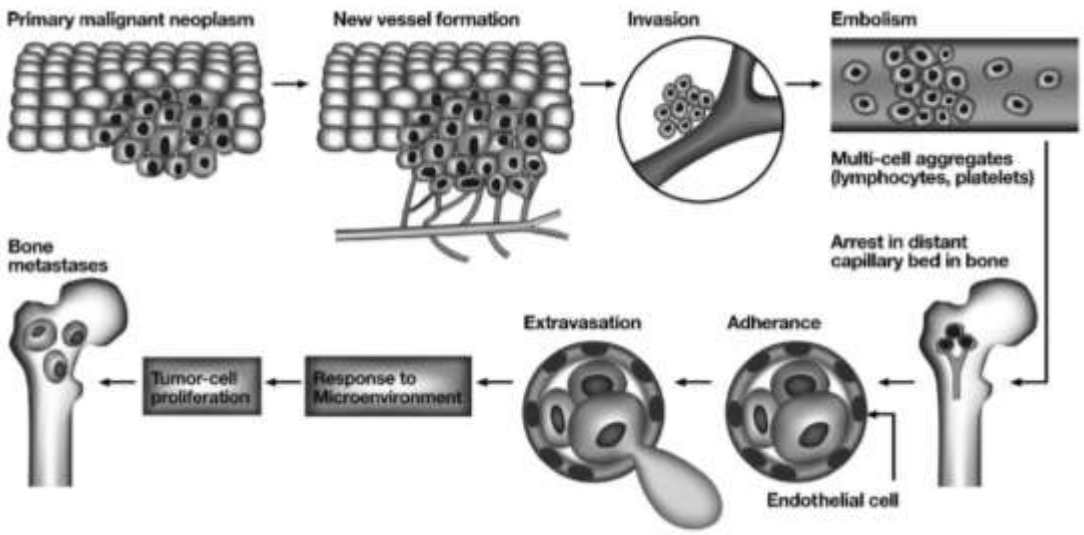

Figure 1.1: Putative mechanisms of metastatic spread to bone [6].

Skeletal metastasis, commonly referred to as metastatic bone disease (MBD), is the third most common type of secondary malignant growth [7]. These growths are primarily localized in vascular regions of the axial skeleton where red marrow is situated, implying the physical properties of the bone marrow cavity, such as the capillary structure and the sluggish blow flow, encourage metastatic development [7, 8]. Additionally, it is understood that growth factors and cytokines released during bone resorption attract malignant cells and facilitate their growth and proliferation [7].

The prevalence of MBD varies depending on the primary cancer type, as outlined in Table 1.1. The American Cancer Society estimates that more than 2 out of every 3 breast and prostate cancers that metastasize spread to bone [9]. Although the mortality rates of these cancers have been steadily decreasing since the 1990s, these diseases, due to their ability to metastasize, remain leading causes of mortality [10]. Overall, advances in cancer treatments have extended lifespan, but have increased the prevalence of metastatic diseases [11].

Table 1.1: Incidence of advanced MBD and median survival time from diagnosis (in months) for leading cancers that result in MBD [6].

Tumour type	Incidence of MBD (%)	Median survival fr. diagnosis (mo.)
Breast	65-75	19-25
Prostate	65-75	12-53
Lung	30-40	6-7
Bladder	40	6-9
Renal cell	20-25	12
Thyroid	60	48
Melanoma	14-45	6

The development of MBD is a devastating event for a cancer patient, as it indicates the cancer is likely incurable [7]. As evidenced from the survival times, outlined in Table 1.1, patients who develop MBD have limited life expectancies [6]. Although the metastasis itself is rarely the direct cause of death, the complications of this disease contribute to a significant degree of morbidity and severely compromise the quality of the remaining life of these patients [7].

1.2 Metastasis of the Vertebral Column

The vertebral column is the skeletal site most often affected by secondary malignant growths [12]. Nearly 30% of all metastases of the axial skeleton are found in the spine and, on average, 5% of all cancer patients suffer from spinal metastases [13, 14]. The thoracic region of the vertebral column is the most prevalent site affected, presenting approximately two-thirds of all spinal lesions. The cervical spine is the second most frequent site, with metastatic infiltration favouring the cervical spine over lumber regions at a 2:1 ratio [14]. Within the vertebrae, malignant cell infiltration typically first occurs in the posterior portion of the vertebral body and over time progresses to the anterior body, lamina, and pedicles [14].

Secondary malignant growth in the spine is unique from other regions affected by MBD, as it may lead to spinal cord compression and compromise neurologic function [14]. Management of these complications, as well as pain and metastatic-induced fractures, has been a major focus of the literature pertaining to MBD [12]. The following subsections discuss the bone weakening mechanism of metastatic

disease and its clinical significance with regards to the vertebral column, followed by the prognosis and clinical course of MBD.

1.2.1 Disturbance of Bone Micro-Environment

MBD results from interactions between malignant cells situated in the bone marrow microenvironment and normal bone cells [7]. Malignant cells may release a number of growth factors and cytokines that indirectly stimulate osteoclast activity, or the cancerous cells may stimulate immune cells and endocrine glands (*eg.* the parathyroid) to release osteoclast-activating factors [7]. When these processes occur, normal bone remodelling may be compromised through accelerated bone resorption and/or increased bone formation [7]. When bone resorption predominates, the metastatic lesion is characterized as lytic. Conversely, heightened bone formation is considered sclerotic [7].

Both tumour-induced osteolysis and osteosclerosis significantly compromise the structural integrity of bone, through either deteriorating bone mineral density (osteolysis) or by causing abnormal growth of unstable bone (osteosclerosis) [7]. Additionally, the large bony masses that result from osteosclerotic processes have been shown to induce ischemic damage through compressing the vasculature within bone [7]. Often, both lytic and sclerotic processes are seen in spinal metastases [15]. Figure 1.2 provides an example of the appearance of lytic and sclerotic lesions in the spine *via* magnetic resonance imaging (MRI) [16]. It is evident from this image that the vertebral bone architecture has been severely compromised; in fact, the vertebral bodies identified by the white arrows are at imminent risk of fracture or spinal cord compression [16].

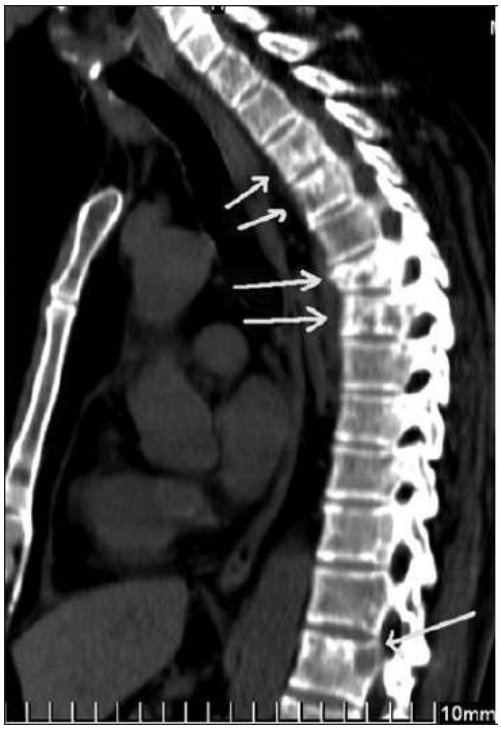

Figure 1.2: Sagittal MRI depicting multiple metastatic lesions that are of both sclerotic- (lighter regions) and lytic-nature (darker regions) [16].

1.2.2 Metastatic-Induced Skeletal-Related Events and Pathologic Vertebral Compression Fractures

Bone is the most common metastatic site that presents clinical complications [9]. These are often referred to as skeletal-related events (SREs) and include pain, impaired mobility, hypercalcaemia, spinal or nerve root compression, and pathologic fracture [7]. The clinical and health-care burdens of MBD are intensified when these SREs present, as additional palliative treatment is required to maintain or improve quality of life [12]. Furthermore, SREs have been correlated with shortened survival times and these complications may directly cause death [15]. For instance, it has been shown that pathologic fracture development increases risk of death by 20-52% in patients with MBD [17]. Consequently, several investigative studies have been conducted to assess incidence, risk factors, and prognosis of SREs in an attempt to advance treatment strategies and improve patient outcomes [12, 17].

Bone pain and pathologic fracture are among the most frequent SREs that result from MBD, as outlined in Table 1.2 [18]. Bone pain is seen in 22% to 75% of patients, while rates of pathologic fracture range between 22% and 39% [12, 17]. Presently, the pathophysiologic mechanisms of pain are not fully understood, but have been hypothesized to be a result of several factors, including tumour-induced osteolysis, tumour-produced growth factors and cytokines, the release of inflammatory mediators, stretch of the periosteum, nerve infiltration, and/or mechanical instability [7, 11, 18]. Numerous groups have reported pain relief in patients who underwent stabilization procedures, which infers mechanical instability is a significant source of debilitation in these patients [19-22]. Furthermore, pain is often indicative of an impending fracture [7].

Table 1.2: Skeletal-related events experienced by patients with bone metastases resulting from breast cancer [18].

Skeletal-Related Event	Incidence
Pain	30%
Any pathologic fracture	34%
Vertebral fractures	20%
Long bone fractures	12%
Fractures in other sites	13%
Hypercalcaemia	19%
Spinal cord compression	8%

Pathologic fractures of the spine are the most prevalent type of metastatic-related fracture [18]. Approximately half of all fractures that result from metastatic involvement occur in vertebral bone [18]. This is in part a result of the spine's dominance in MBD, but also a result of the mechanical loads experienced by these bones [14]. The spine serves as the structural framework of the body, supporting loads over twice the weight of the body during ordinary daily activities [23]. When osteolytic and/or osteoslerotic processes compromise this load-bearing capacity, the vertebral body can collapse under normal physiological loading, causing a vertebral compression fracture (VCF) [14]. The annual incidence of cancer-related VCFs is estimated to be between 75,000-100,000 in the United States [11]. These fractures frequently induce excruciating pain, impair mobility, hinder patient posture, and

result in spinal cord compression [11, 24]. It is unclear whether the pain associated with VCFs is tumour-induced or a result of structural instability; therefore, it is necessary to manage both the disease and instability [11].

1.3 Prognosis and Clinical Course of Skeletal Metastases

The treatment of MBD is based on palliation, not cure [25]. In most cases, the disease cannot be cured by treating the cancerous lesions in bone, since bone is not the primary site from which the cancer originated [25]. However, treatment of MBD is considered valuable, as these patients are at high risk of experiencing SREs and are expected to live for a number of months, sometimes years [25]. As shown above in Table 1.1, median survival times range between 6-53 months, depending on the primary cancer type [6]. The detection time, histological grade, and progression of the bone metastasis have also been identified as prognostic factors [8, 26]. Robson and Dawson found that prostate cancer patients had a median survival time as long as 53 months when the metastatic disease remained confined to the axial skeleton [26]. In this same study, it was found that extraosseous involvement decreased longevity; patients of the same performance status with visceral involvement had a median survival of only 30 months [26]. Limiting metastatic progression in bone can both improve the quality of life and prolong life.

1.3.1 Interventions for the Management of Metastatic-Related VCFs

Despite the high frequency of spinal metastases, management remains controversial [27]. The ideal treatment plan is multidisciplinary and may involve analgesics, bisphosphonates, chemotherapy, radiotherapy, and/or surgery [28]. The decision with regards to what treatment method suits a particular patient is based on the quality of bone and neurologic compromise [28, 29]. The chief aims in the management of this disease are (1) palliating symptoms and managing SREs to improve quality of life, and (2) preventing disease spread to extraosseous sites to prolong life [8, 28].

1.3.1.1 Non-Operative Management for Spinal Metastases

Today, site-directed radiation is the most common treatment method used for painful spinal lesions without neurologic deficit [28]. External beam radiation is effective in approximately 80% of patients with radiosensitive lesions [28]. The dose of radiation is typically limited by the possibility of damaging normal tissue surrounding the tumour. Unfortunately, these conservative measures increase risk of tumour recurrence and treatment failure [24]. Following conventional radiotherapy, pain reduction is typically achieved in 57% to 77% of patients and 50% of patients with neurologic dysfunction see recovery [30]. It is understood that radiotherapy significantly reduces bone density, which puts patients at increased risks of fracture [31]. Consequently, surgical consolidation methods are often required following the administration of radiation to stabilize the weakened bone [14].

Aside from radiotherapy, radiopharmaceuticals, analgesics, bisphosphonates, hormonal therapy, and chemotherapy are used routinely in the nonoperative management of MBD [15, 32-34]. Chemotherapy (chemo) is often used in combination with radiotherapy, as it may prolong life and/or reduce symptoms [28]. On its own, pain relief rates following chemo-administration range from 20% to 80% in patients with MBD [32]. Pain relief in these cases is thought to result from tumour shrinkage; however, the clinical efficacy of chemotherapy is often limited by dose reductions required to avoid systemic toxicity and side effects, and the development of drug resistance [28, 32].

1.3.1.2 Operative Management for Spinal Metastases

Surgical interventions enable removal of the metastatic lesion, as well as fixation [25]. Typically, surgery is considered if the patient life expectancy exceeds six months; however, with advancements in radiotherapy and chemotherapy, this measure has become difficult to determine [25]. Moreover, this increase in average life expectancy has put stress on the orthopaedics community to develop more permanent solutions to fracture fixation/prevention and pain control [25]. The anatomy of the spine serves as a challenge to radical tumour resection; however, options for surgical treatment

have improved drastically in recent years with the development of minimally invasive interventions [28]. Minimally invasive treatment strategies present an attractive means of managing metastatic disease and complications, as these procedures are less aggressive, require reduced recovery time, result in lower complication rates, and have demonstrated clinical success [14]. These methods enable percutaneous access and use image-guidance to target the affected site [35]. Techniques have been developed that either (1) manage the underlying disease through ablating or shrinking the tumour or (2) stabilize the weakened bone [35].

1.3.1.2.1 Minimally invasive approaches to disease control

Tumour ablation involves the direct application of chemical or physical therapies to destroy a specific lesion [35]. Ablation techniques for the spine have been extrapolated from interventional radiology methods used in the treatment of renal, hepatic, and lung malignancies [35]. These techniques include alcohol ablation, radiofrequency ablation (RFA), microwave ablation, cryoablation, laser photocoagulation, and low-temperature radiofrequency ionization (RFI) [35].

Of these methods, RFA is one of the most common [36]. In skeletal malignancy, this method involves introducing an electrode into the vertebral body where a high frequency alternating current (450-600 kHz) is delivered to agitate the ionic molecules of the tissue [36]. This agitation produces frictional heat, elevating the temperature of the local tissue to between 60°C and 100°C. When held for 4 to 6 min, this process causes protein denaturation and induces coagulative necrosis of the tumour [36]. Approximately 80% of patients benefit from this procedure through marked pain reduction [36]. The exact mechanism of pain relief is not clear at this point in time; destruction of sensory nerve fibres, reduction of tumour size, and ablation of tumour cells that produce nerve-stimulatory factors have all been postulated [36]. RFA is contraindicated in patients with excessive osteolysis, as they are at risk of thermal injury to the spinal canal, but has shown significant success in debulking sclerotic lesions [36]. Following RFA, stabilization methods, such as

vertebroplasty, are often used to consolidate the treated area, as the cavities and necrotic tissue produced leave the bone prone to fracture [14, 36].

1.3.1.2.2 Minimally invasive approaches for stabilization: vertebroplasty and kyphoplasty

Both percutaneous vertebroplasty (PVP) and kyphoplasty (PKP) are minimally invasive procedures used to manage pathologic fractures of vertebral bodies [14]. These procedures involve the injection of a bone cement, typically polymethyl methacrylate (PMMA), into the posterior and middle third of the compromised vertebral body, as shown in Figure 1.3 [31, 37]. This is done while the patient is in prone position using a percutaneous, transpedicular approach, typically using an 11- or 13-gauge introducer needle [36]. The needle is guided into place using fluoroscopic or CT guidance. Targeted needle position is attained once the tip of the needle is in the ventral part of the vertebral body [36]. A bitranspedicular approach may be taken to ensure cement injection is as close to the midline of the coronal plane as possible. Once in place, the radiopaque bone cement, in a semiviscous state, is injected [36]. It is crucial the filling pressure remain as low as possible to avoid cement extraversion and to enable quick arrest of the procedure should leakage into the venous plexus or outside the vertebral body occur [36]. Once in place, the cement hardens, stabilizing the fracture and providing immediate pain relief [36]. PKP comprises an additional step, where a balloon is inflated inside the vertebral body prior to cement injection, as shown in Figure 1.3 [31, 38].

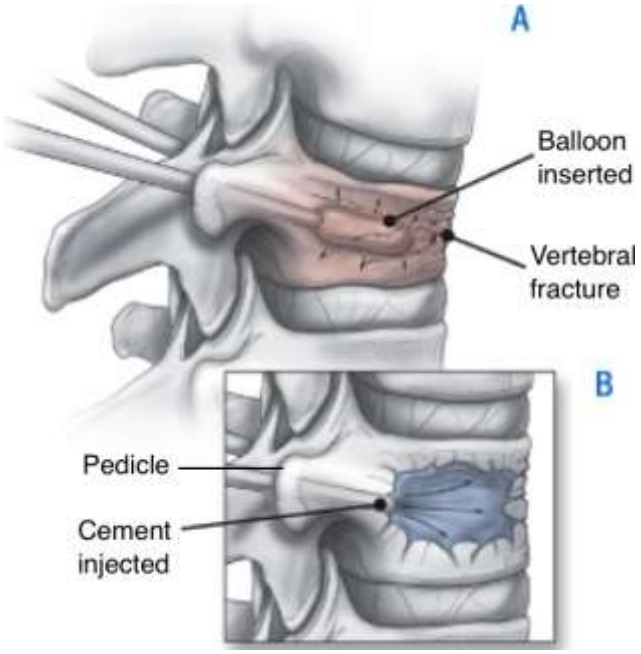

Figure 1.3: Overview of PVP and PKP using a bitranspedicular approach. PKP includes both (A) and (B), while PVP involves only (B), adapted from [37].

In 1981, Harrington was the first to propose the injection of bone cement for the treatment of painful VCFs resulting from cancer [39]. Harrington hypothesized that cement injection into and around the affected vertebral bodies would "fuse" the area, resulting in immediate spinal stability without interfering with cancer therapies, such as radiotherapy [39]. Following this procedure, 13 out of 14 patients reported significant pain reduction and spinal flexion-extension X-rays showed no significant motion. These outcomes persisted through the 45-month follow-up period, ultimately signifying the first success of this procedure in this application [39]. Since this time, a number of groups have reported clinical success when using these techniques in the management of spinal metastases [14]. Throughout the mid 1990s, Cotten *et al.* reported that 97% of 67 patients who underwent PVP for the treatment of osteolytic lesions experienced some degree of pain relief within the first 48 hours [19]. Weill *et al.* reported sustained pain relief in 73% and 65% of 37 patients with malignant spinal lesions at 6 and 12 months post-PVP, respectively [20]. In 2002, Dudeney *et al.* reported significant improvements in pain scores and function, as well as restored vertebral body height in a series of 18 patients who received PKP for the treatment

of osteolytic VCFs resulting from multiple myeloma. These treatment outcomes were maintained at 52 months post-PKP [40]. Similarly, in 2006, Pflugmacher *et al.* reported significant decreases in pain scores in 20 patients who received PKP over a 12-month follow-up period [22].

Pertaining to cancer-related treatment, complications with PVP and PKP range from 2% to 10% in the literature [41, 42]. Symptomatic cement leakage, cement embolism, pulmonary embolism, hematoma, neuro-decline, spinal cord compression, radiculopathy, infection, and adjacent fracture have all been documented as concerns with these procedures [42]. Cement leakage is the most common complication, and it is often seen in regions of highly vascularized tumours and in sites of cortical destruction, where the metastases extend into the paraosseous soft tissues [35]. However, the majority of leakage is non-symptomatic [14]. For instance, Cortet *et al.* reported leakage in 72.5% of patients who underwent PVP for the treatment of osteolytic lesions, but only 4% of these patients presented symptoms [44]. Complications occur more frequently (5-10%) when these procedures are used in the treatment of metastatic disease, as compared to osteoporosis (1-3%) and spinal angiomas (2-5%) [21]. Increased leakage rates seen in cancer patients may be a result of the increased pressures generated *in situ*, as evidenced by the increased injection forces required when tumour cells are present [43]. Severe neurologic complications may arise if cement extravasates into the spinal canal, and pulmonary embolism may develop if the cement leaks into the epidural or paravertebral veins [36, 42]. Concern regarding the extravasation of tumour cells has also been raised [14].

1.3.1.2.3 PVP and PKP in combination therapies

PVP and PKP are limited as they only address half of the issue with metastatic disease in the spine: the instability issue [36]. Consequently, these methods are often used in combination with different cancer therapies, such as radiotherapy or RFA, depending on the characteristics of the cancer [11, 36]. Radiation delivers treatment to the tumour, provides local pain control, delays cancer progression, and is relatively non-invasive. Combining this treatment regime with PVP is an appropriate strategy, as it stabilizes the vertebra, which is further weakened by the radiation [11].

In 2002, Grönemeyer *et al.* reported combining RFA with PVP for the management of osteolytic spinal metastases. In this study, all four treated patients reported significant pain relief and improved neurologic function, and no complications were encountered [45]. Since this time, RFA-PVP combination therapies have been used clinically, as they directly address the metastasis and can debulk osteosclerotic lesions, facilitating cement injection in patients who would not normally be considered good candidates for PVP [11, 14].

An alternative PVP combination therapy discussed in the literature involves the local delivery of chemotherapeutics using the injectable bone cement [46, 47]. Hypothetically, a cement containing antineoplastic agents could exert a direct cytotoxic effect on resident cancer cells, thereby improving the local control of skeletal neoplasms while stabilizing the fracture [1]. This concept of combining structural constructs and drug delivery has succeeded in other areas of medicine, for instance in preventing restenosis of coronary grafts [48]. Local drug delivery systems are appealing, as they improve the therapeutic index of the drug while limiting systemic toxicity, which is a major issue with chemotherapeutics in particular [48]. Accordingly, several groups have conducted investigative studies on the drug delivery potential of currently used bone cements [46, 47]. The following section discusses existing bone cement delivery systems, their limitations, and what an ideal bone cement would comprise.

1.4 Bone Cements as Drug Delivery Systems

Bone cements may be appropriate local drug delivery vehicles for a wide range of orthopaedic applications [49]. There are four broad categories of injectable bone cements discussed across the literature: PMMA, composite resins, calcium phosphate cements (CPCs), and calcium sulphate cements (CSCs). Table 1.3 outlines the basic material components of each of these cement types [49-51]. Although this list comprises CSCs, the rapid degradation of these materials limits their use in the stabilization of VCFs [52]. Cancer patients, in particular, typically require a persistent scaffold for fracture fixation, as bone-regenerating processes are often compromised in this patient population [51]. Consequently, CSCs have been excluded from the subsequent sections discussing drug-loaded bone cements.

Table 1.3: Basic material components and setting characteristics for conventional bone cements discussed in the drug delivery literature, adapted from [49-51].

Cement Type	Basic Material Components	Setting Characteristics
PMMA	• Powder component: pre-polymerized PMMA, inhibitor, radiopacifier • Liquid component: monomer, initiator, stabilizer	Free radical polymerization
Composite resins	• Organic matrix: Bisphenol-A-glycidyl dimethacrylate (Bis-GMA) monomer, viscosity controller • Inorganic filler: glass/ceramic particles • Coupling agent	Free radical polymerization reinforced by filler agents
CPCs	• Powder component: calcium phosphate salts • Liquid component: sodium phosphate solution	Precipitation of hydroxyapatite or carbonated apatite
CSCs	• Sulphate hemihydrate powder	Formation of gypsum when mixed with water

Today, bone cements used in arthroplasty procedures are loaded with antibiotics as a prophylactic measure against orthopaedic inflection [53]. This technique was popularized by Buchholz and Engelbrecht, who showed that the addition of 2 g of gentamicin to 40 g of Palacos PMMA was successful at curing 78% of deep prosthetic infections in 263 patients requiring revision arthroplasty [54]. Since this time,

considerable effort has been made to evaluate the clinical efficacy and safety of this approach [55]. Josefsson and Kolmert compared the infection rates of patients undergoing hip arthroplasty surgeries who were prophylactically treated with either systemic antibiotics or gentamicin-loaded PMMA. At 1 year and 5 years follow up, the group that received systemic antibiotics had a significantly higher infection rate, though no significant difference was found at 10 years [55]. This study also addressed the concern that antibiotic-loaded cements may put patients at risk of long-term toxicity. Over the 10-year period, no cases of nephrotoxicity or ototoxicity and no allergic reactions were reported in the bone cement group; however, interestingly, one patient who received systemic antibiotics had a nephrotoxic reaction [55]. These clinical data suggest antibiotic-loaded bone cement is a safe and effective method for both treating active infections and preventing infection from occurring. Such evidence is the foundation for the continued development and examination of drug-loaded bone cements. To date, composition-property relationships have been described for several drug-loaded bone cement systems. A major focus has been on antibiotics, due to their widespread use as either prophylactics or in the general treatment of bone infections [47]. However, with the increased use of bone cements in oncology, these studies have begun to translate to chemotherapeutics.

In general, the studies on drug-loaded bone cements involve two key aspects: (1) the release kinetics, and (2) the cement-drug interactions. It is important to assess the effectiveness of the cement as a delivery vehicle and understand the underlying mechanisms of release [47]. Equally, it is necessary to verify that drug addition does not compromise the mechanical and rheological behaviour of the material through modifying the physico-chemical properties of the cement [47]. The following subsections review the literature pertaining to drug-loaded bone cements, with focus on cancer-related therapies where possible.

1.4.1 Drug Release from PMMA Cements

PMMA was the original material used in PVP when this procedure was first introduced in 1984, and has remained the widespread accepted norm in recent years [21]. Consequently, the majority of the literature regarding drug-loaded bone cements is with regards to this material. For the most part, the elution kinetics of drugs from PMMA show a biphasic profile, involving an initial burst release within the first 24 hours, followed by a significantly slower, substantiated release thereafter [1, 53, 56, 57]. This biphasic release pattern is not ideal, as sustained, low release levels can induce drug resistance and may cause systemic toxicity [46]. Thomes *et al.* emphasized the ability of bacteria to infect gentamicin-loaded PMMA after prolonged elution of subtherapeutic levels of the drug [58]. Therefore, significant effort has been made to attempt to understand release mechanisms so that elution kinetics may be tailored to maximize therapeutic potential and safety [46].

Despite the widespread use of antibiotic-PMMA systems in orthopaedics over the last 30 years, the elution mechanisms of theses systems are not yet fully understood. Surface release [53, 59], Fickian diffusion [60, 61], and release through cement cracks and pores [53, 62, 63] have all been postulated as release mechanisms. Table 1.4 outlines the key factors that affect drug release from PMMA, as summarized by Anagnostakos *et al.* in 2008 [46].

Table 1.4: Factors affecting drug release from PMMA, adapted from [46].

Cement-Related Factors	Drug-Related Factors	Test-Related Factors
• Composition/brand • Powder/liquid ratio • Surface characteristics (roughness, wettability) • Porosity	• Chemistry • Dose/concentration • Combination (2+ drugs) • State (powder/liquid)	• Fluid refreshment • Load bearing • Temperature

In 2000, Van de Belt *et al.* concluded drug release from PMMA was initially controlled by the cement's surface, while the sustained release was driven by bulk porosity [53]. Wettability has also been identified as an influential factor to drug release, as the hydrophilicity of the cement's surface dictates the ability of fluid to penetrate into the pores of the cement [46]. Generally, surface area is considered the most influential factor, making the cement's surface characteristics and porosity key variables for drug release, and the focus of much of the literature pertaining to this subject [46].

To investigate the role of porosity in drug release, several groups have investigated the effects of cement-mixing technique and cement formulation, two variables that significantly influence air entrapment and monomer boiling, and therefore porosity [64, 65]. Neut *et al.* compared gentamicin release from six different formulations of PMMA that were hand-mixed and vacuum-mixed. Vacuum mixing, which is often done to improve the mechanical properties of PMMA through decreasing porosity, resulted in decreased antibiotic release for five of the six formulations. Surprisingly, vacuum-mixed Palacos R showed higher drug release in comparison to its hand-mixed counterpart. This deviation was attributed to an increase in microporosity (<1 mm diameter), which likely resulted from the heightened rate of monomer evaporation produced during vacuum mixing [64]. These results emphasize the implication of not only mixing technique on drug elution, but also the importance of cement formulation [64].

As cement formulation plays a significant role in dictating porosity, several groups have analyzed the effects of cement additives on release [66-68]. These studies were initially encouraged by the synergistic effects seen when multiple antibiotics were loaded into PMMA [67]. Penner *et al.* showed that combining tobramycin and vancomycin increased drug release by 63% to 103% [67]. Similarly, Anagnostakos *et al.* found that the addition of a glycopeptides to an aminoglycoside increased the elution of the latter [66]. These effects were hypothesized to result from an increase in interconnective porosity with increased concentrations of additives [67]. Consequently, several groups have investigated loading alternative substances, such as glycine, sucrose, and chitosan to enhance antibiotic elution [68-70].

Unfortunately, antagonistic effects were observed by some of these groups; Tunney *et al.* found the addition of chitosan (an antibacterial agent) to gentamicin-loaded PMMA decreased the release of gentamicin without improving the antibacterial properties of the material [68]. Tunney *et al.* speculated that the decrease in gentamicin release might have resulted from the large difference in particle sizes between the two agents. Chitosan retained at the surface of the cement may have physically impeded the release of the drug [68]. These results demonstrate the need to investigate all combinations, as it is not possible to extrapolate results from one combination to another.

Aside from porosity, drug chemistry has also been described as an influential factor to drug release [71]. Klekamp *et al.* found that vancomycin eluted 10-times less effectively than tobramycin under the same test conditions. The authors of this study postulated molecular weight (M_w) might be an influential factor, as the M_w of vancomycin is approximately three-times higher than that of tobramycin [71]. Rosa *et al.* compared release concentrations and durations for different chemotherapeutics, reporting methotrexate release was significantly higher and lasted longer than doxorubicin and cisplatin releases [72]. Again, this study was completed under constant test conditions, concluding the chemical and/or physical altercations of the drug were responsible for the unique release profiles [72].

Aside from the biphasic release nature of drug-loaded PMMA delivery systems, these materials are burdened by relatively low release efficiencies (percentage of drug released as compared to the initial loading). Low release efficiencies are unpractical from both a cost and therapeutic standpoint, but also potentially dangerous, as a local reservoir of high drug concentration remains entrapped within the patient [46]. Picknell *et al.* reported that only 2.2% (methicillin) to 11% (cloxacillin) of the initial antibiotic loading was released from a Palacos PMMA system over a 4-day *in vitro* experiment [59]. Bayston *et al.* reported that only 6% of an initial gentamicin load was released from Palacos PMMA over a 5-day *in vitro* experiment [73]. Wasserlauf *et al.* found that only 6%, 3.3%, and 3.4% of the initial chemo-load was released from methotrexate-loaded, cisplatin-loaded, and 5-

fluorouracil-loaded PMMA cements, respectively [74]. These studies do not encompass the entire duration of elution due to their length and the difficulty of detecting very low drug levels at longer time points [59]. In the study completed by Wasserlauf *et al.*, the release duration was limited by drug detection limits: methotrexate release was only quantifiable for 224 days; cisplatin release for 98 days; and 5-fluorouracil 110 days [74].

To elucidate the release mechanism, numerous studies interpret drug release based on kinetic models. Table 1.5 outlines some of the most common models applied to drug eluting bone cements [75, 76]. An example of this approach can be found in the study published by Diez-Pena *et al.,* which characterized the release of gentamicin from CMW-1 PMMA through application of the Korsmeyer-Peppas (KP) model and the Noyes-Whitney model [77]. This group added a constant term, *b*, to the KP equation to represent the burst release, and found relatively good correlation at low drug loadings (approximately 3 and 10 wt% gentamicin). At higher concentrations (approximately 17 and 24 wt% gentamicin), the release deviated, but correlated well with the Noyes-Whitney equation [77].

Understanding the effects of the cement on drug activity, as well as the effects of drug loading on the cement are also critical to the success of these systems. The high curing exotherm temperature of PMMA has been raised as a concern in the literature, as many drugs are sensitive to heat [48]. However, numerous groups have published results that negate this concern [48, 57, 78]. Healey *et al.* showed that native chromatograms of pamidronate and doxorubicin matched those of the drugs released from PMMA, concluding the exothermic process did not chemically change these drugs [48]. Similarly, Hernigou *et al.* confirmed that MTX remained biologically active after the curing reaction using both chromatography and an *in vivo* dog model [78].

Table 1.5: Common kinetic models used to compare release profiles of drug loaded bone cement systems [75, 76].

Kinetic Model	Equation	Summary
Noyes-Whitney	$\mathbf{dM/dt=DS(C_s-C_t)}$ *M: mass transfer, t: time, D: diffusion coefficient, S: surface, C_t: concentration at t, C_s: equilibrium solubility*	The rate of mass transfer or dissolution following first-order kinetics.
Higuchi	$\mathbf{Q=A(D(2C-C_s)C_st)^{1/2}}$ *Q: drug released; t: time; A:area; C: initial drug concentration; C_a; drug solubility; D: diffusion constant* Simplified: $\mathbf{Q=K_Ht^{1/2}}$ *K_H: Higuchi constant*	Cumulative percentage of drug released *vs.* square-root-time – describes Fickian diffusion assuming the following: 1) the initial drug concentration is higher than the drug solubility, (2) the size of the drug particle is smaller than the release device, (3) the material does not swell or dissolve, and (4) the diffusion coefficient of the drug is independent of time or position.
Korsmeyer-Peppas	$\mathbf{M_t/M_{infinity}=Kt^n}$ *$M_t/M_{infinity}$: fraction of drug released at time, t; K: release rate constant; n: release exponent*	When applied to the first 60% of the drug release, *n* may be derived: $n < 0.45$ Fickian diffusion, $0.45 < n < 0.89$ non-Fickian transport, n=0.89 relaxational transport, $n > 0.89$ anomalous transport.
Weibull	$\mathbf{M=M_0[1-exp(-(t-T)^a/a]}$ *M: drug released; M_0: total drug released; t: time; T: lag time; a: scale parameter; b: shape of the dissolution curve*	An empirical formula used to compare the shape and scale of dissolution/release curves.
Hopfenberg	$\mathbf{M_t/M_{infinity}=1-[1-k_0t/C_0a_0]^n}$ *$M_t/M_{infinity}$: fraction of drug released at time, t; k_0=erosion rate constant; C_0: initial concentration of drug, a_0: radius/thickness; n: 1, 2, or 3 for slab, cylinder, or sphere, respectively*	The release from surface-eroding devices, such that erosion is the rate-limiting step and that time dependent diffusional resistance has no effect.

From an elution standpoint, liquid antibiotics have shown superior results in comparison to powdered agents [62]. However, liquid antibiotics severely compromise the mechanical properties of PMMA and therefore only powdered antibiotics are incorporated in PMMA today [62]. It is generally accepted that PMMA can be loaded with antibiotics up to a 10 wt% threshold without significant compromise to mechanical properties [46]. This statement is supported by the results of Lautenschlager *et al.,* who reported loading up to 4.5 g of gentamicin into 40 g of Simplex-P PMMA did not compromise compressive strength (CS) from a clinical standpoint, but that loadings exceeding this threshold significantly decreased CS [79]. Klekamp *et al.* also found that adding 1-3 g of vancomycin or 1.2-2.4 g of tobramycin to 40 g of Palacos or Simplex PMMA did not significantly affect CS [71]. However, this group observed a proportional decrease in fatigue with increased drug loading, recommending that dynamic mechanical testing should be completed to validate the generally accepted 10 wt% claim [71]. Decreased mechanical properties with increased drug loading is quite uniform across the PMMA literature regardless of the drug or cement type; however, the mechanism behind this observation has not been determined [48]. Some authors postulate this results from increases in porosity, while others hypothesize decreased strength results from alterations of the cement matrix [62].

★★★

Overall, there are several gaps in the literature pertaining to drug-loaded PMMA, and much of what is reported is contradictory. This makes drawing conclusions regarding the efficiency and practicality of these systems difficult. Although antibiotic-loaded PMMA is currently used clinically, several aspects of these systems remain unclear: the mechanism of drug release, the duration of drug release, the effect of the cement on the drug, the effect of the drug on the cement, and the long-term side effects are just a few [46]. Nonetheless, the combination of structural constructs and drug delivery is a growing force in the medical literature. Drug-loaded bone cements may expand the scope of these materials through developing a dual system that addresses two major concerns with metastatic-related VCFs: disease control and structural

support [48]. Accordingly there has been a continued effort to understand and characterize drug release from newer PVP/PKP bone cement systems: composite resins and CPCs.

1.4.2 Drug Release from Composite Resin Cements

Composite resins present a newer class of bone cements that aims to play on the advantages of both acrylic materials and bioactive ceramics [80]. Due to their acrylic resin matrix, drug-loaded composite resins exhibit similar release behaviour to what was described for PMMA: relatively low release efficiencies and biphasic release profiles [81, 82]. DiCicco *et al.* hypothesized composite resins would yield lower release efficiencies than PMMA, as these materials exhibit a higher degree of crosslinking and thus lower porosity [81]. Interestingly, Cortoss™, a commercially available composite resin, eluted antibiotics at a significantly higher concentration than Simplex P PMMA. This led the authors to conclude that the hydrophilicity of Cortoss™ had a greater effect on release than the higher porosity of Simplex P [81]. It appears that even though release may be primarily a surface phenomenon in these systems, the hydrophilic nature of composite resins plays a more prominent role in dictating drug release in comparison to porosity [81].

As with PMMA, drug release from composite materials is biphasic and dependent on the initial drug loading [82]. Otsuka *et al.* reported early (first 4 days) cephalexin (CEX) release from a composite material showed good linearity with square-root-time, indicating the rate-limiting step of this drug release system was diffusion-controlled, as outlined by the Higuchi equation (Table 1.5) [82]. However, at later time points, CEX release did not correlate with the Higuchi equation. This deviation was attributed to hydroxyapatite precipitation, as evidenced *via* Fourier-transform infrared analysis [82]. This grou*p* found that the rate of CEX release increased across 1, 2, and 5 wt% drug loadings, but that the release efficiency decreased with increased drug loading (approximately 10% to 5% after 2 weeks) [82]. For the 5 wt% CEX-loaded cement, approximately 5.4% of the initial drug load was release with 72.8% remaining entrapped within the cement [82]. The authors

attributed this difference in %-released and %-entrapped to CEX degradation within the cement matrix [82].

In terms of mechanical properties, Otsuka *et al.* found that CEX addition (0- to 5 wt%) significantly decreased CS (180 to 127 MPa) [82]. The authors speculated this observation resulted from either drug adsorption onto the interface between the glass-ceramic particles or increased porosity, while DiCicco *et al.* attributed changes in strength to polymerization effects [81, 82]. Nonetheless, even at the highest CEX loading, Otsuka *et al.* found that the composite cement demonstrated significantly higher CS (127 MPa), as compared to PMMA [82]. Since this study, Otsuka *et al.* published a number of reports aiming to optimize the release and strength of this material through adjusting either the ceramic component or the water-soluble component of the material [83, 84]. These reports indicate that the properties of antibiotic-loaded composite resins may be tailored through adjusting the proportions of different material components to optimize material properties and drug release [83, 84].

1.4.3 Drug Release from Calcium Phosphate Systems

A large proportion of conventional CPCs, comprising mono-, di-, tri-, and/or tetra-calcium phosphates and/or calcium carbonates, are biodegradable [85]. However, the matrix degradation rates of these materials tend to be significantly lower than their drug release rate, as evidenced by the constant porosity of these matrices during drug delivery [47]. Consequently, CPCs are often considered diffusion-controlled systems, and are therefore often analyzed by application of Higuchi's law (summarized in Table 1.5) [47]. Across the literature, good correlation has been found between the initial release phase of CPC systems and the Higuchi equation; however, the precipitation of hydroxyapatite crystals complicates this behaviour over time [86, 87]. Otsuka *et al.* found that the release of 6-mercaptopurine, cephalexin, and norfloxacin from self-setting apatite systems only correlated with the Higuchi equation for the first 100-250 hours of release [86, 87]. Like composite resins,

hydroxyapatite formation is a crucial parameter that dictates the release kinetics of drug-loaded CPC systems [86, 87].

The duration of drug release from CPCs varies across the literature, depending on the drug, cement formulation, and *in vitro* test setup [47, 88, 89]. Hamanishi *et al.* reported that the initial drug loading was a significant factor in determining release duration for CPCs; the addition of 1 and 5 wt% vancomycin modulated release duration between 2 and 9 weeks *in vitro* [90]. Drug-loaded CPCs have shown significantly higher release efficiencies in comparison to PMMA and composite resin drug delivery systems: Hamanishi *et al.* found that up to 95% of the initial drug load was released from a vancomycin-CPC system within 2-9 weeks, while Bohner *et al.* reported release efficiencies between 58-100% for a gentamicin-brushite-polyacrylic acid cement [90, 91]. However, drug release from some CPCs has been found to be significantly faster than that of PMMA, which has raised concerns, as the therapeutic doses administered from CPCs do not typically meet the 7-10-day requirement for the treatment of active infections [47, 91].

In terms of physico-chemical alterations, the addition of antibiotics to CPC systems typically increases setting time and decreases CS [47]. Takechi *et al.* reported significant decreases in CS when increased concentrations of flomoxef sodium were added to a CPC system. This group attributed this observation to an increase in porosity with drug addition [92]. Ratier *et al.* also observed decreases in CS with antibiotic (tetracycline) addition; however, the chemical properties of the drug were discussed as the cause of CS reduction in this study. When tetracycline complexed with calcium was added, no effects to CS were observed, which lead the authors to suggest that the uncomplexed drug chelated Ca-atoms in the cement matrix [93].

In terms of anticancer agents, Yang *et al.* examined the physico-chemical effects of methotrexate addition (0 to 1 wt%) on a CPC. This group observed significant decreases in CS (40-38 MPa), though not below the minimum requirements for vertebral bone, and no effects to setting time [88, 89]. Conversely, Tani *et al.* reported doxorubicin could be loaded into a CPC (5 to 10 mg per 10 g mixed

calcium phosphate powder) without compromising CS [94]. However, a limitation pointed out by these authors was the effects of chemo-loading on the bioactivity of the material. Although the control CPC demonstrated bone resorption and remodelling in a rabbit model, this group observed slowed bone formation around the doxorubicin-loaded implant, suggesting the addition of the chemotherapeutic limited the bioactivity of the material [94].

★★★

In considering the bone cement delivery systems described above, it is evident there are a number of deficiencies with the release behaviour and drug loading potential of current materials. PMMA and composite resin cements, the most widely used materials in PVP and PKP, demonstrate low release efficiencies, while CPCs may not provide adequate dose duration [51, 52]. At present, there is a significant lack of understanding of the mechanisms of release, as well as the drug-cement interactions [46]. However, aside from the delivery role of these materials, conventional bone cements themselves present numerous limitations.

1.4.4 Limitations with Existing PVP/PKP Bone Cements

Although PMMA is generally considered safe, its biocompatibility has been subject to major criticism. PMMA sets at a relatively high exotherm, contains a cytotoxic monomer component, produces noxious fumes, shrinks upon curing, and does not integrate with host bone tissue [49, 80, 95-102]. Interestingly, the former two points have been identified as possible tumour therapies [48]. These phenomena have been shown to cause bone resorption and impair bone regeneration, which is often presented as negative side effects of the material when used in the treatment of osteoporotic fractures [48]. However, the potential necrotic nature of PMMA may actually be beneficial when used to treat metastatic lesions [48].

As a result of these controversies, there has been a continued effort to develop improved bone cements. This work has resulted in the creation of composite resins, which combine the advantages of acrylic cements with those of ceramics. As briefly

mentioned, Cortoss™ is a commercially available composite resin that was specifically developed for use in PVP and PKP. In comparison to PMMA, Cortoss™ sets at a lower exotherm temperature (63°C), provides increased strength (163 MPa), and is maintained at constant injection viscosity due to its specialized extrusion cannula [80]. Furthermore, the dispersion of ceramic particles throughout the resin has the potential to chemically integrate with host bone tissue [50, 103, 104]. Although composite resins may address some of the concerns identified with PMMA, these materials remain burdened, to some degree, by their acrylic component. The setting temperature of these materials is significantly lower than that of PMMA; however, it remains higher than the threshold for impaired bone regeneration: 44-47°C for 1 min [95, 96]. Additionally, composite resins contain allergenic components and the *in vitro* cytotoxicity of different monomer components has been raised as a concern [105].

CPCs negate these issues identified with acrylics, but are burdened by a unique set of factors. Conventional CPCs are highly osteoconductive and, in some cases, biodegradable, which are not valued properties in the treatment of metastatic-related fractures [51]. It is generally accepted that metastatic-related fractures require a permanent fixation, as host bone regenerating capabilities are often compromised [51]. However, the leading disadvantage with the use of CPCs in PVP and PKP is their lack of injectability [52]. CPCs exhibit thixotropic properties when extruded through a cannula and undergo a phase separation [52]. This ultimately limits the application of these materials in PVP and PKP and reduces their load-bearing capacity [52, 106].

1.4.5 The Ideal Bone Cement Delivery System

Today, the central theme in the bone cement literature involves the need to develop a material that addresses the shortcomings and concerns identified with current materials. In 2001, Heini and Berlemann published a review of the PVP literature, summarizing the properties that would comprise an ideal bone cement for PVP and PKP [80]. The conclusions of these authors are outlined in Table 1.6 [80].

Table 1.6: Clinically relevant properties that would comprise an ideal PVP bone cement, adapted from [80].

Properties of an Ideal Bone Cement
• Constant viscosity/injectability for 5-10 min
• High radiopacity
• Setting time of approximately 10 min
• Low setting temperature
• Mechanical properties similar to those of natural bone*
• Adhesion/integration with host bone tissue
• Non-toxic
• Low cost

*Controversial; 30 MPa is typically used across the bone cement literature [4].

Although current materials meet a combination of these points, there remains the need to develop a material that addresses this Table in full. Equally as important, and in the context of this research, the drug delivery aspects of clinical cements require substantial improvements. The primary goals of bone cement delivery systems are to deliver therapeutic drug concentrations to the affected tissue without compromising the structural integrity of the bone cement [48]. In order to achieve these objectives, the following limitations with current systems must be addressed: (1) low release efficiencies must be improved to provide effective and safe therapeutic doses, (2) release mechanisms must be characterized in order to design controlled, predictable delivery systems, and (3) the cement-drug interactions must be fully analyzed to predict changes in cement properties and drug activity [48, 53]. It is evident from the literature, no material satisfies the criteria in Table 1.6 or these required release characteristics.

1.5 Glass Ionomer Cements for the Restoration of MBD-Related VCFs

Glass ionomer cements (GICs) have been identified as potential alternatives to existing bone cements and may satisfy many of the requirements identified by Heini and Berlemann [80]. GICs are used clinically in dental practice as restorative and luting cements. These materials set *via* a neutralization reaction between a basic glass powder and an aqueous solution of polyalkenoic acid, usually polyacrylic acid (PAA), as outlined in Figure 1.4 [107]. When mixed, the acid attacks the glass network, liberating metal cations that crosslink the polyanion chains of the acid. This reaction is a continuous process, which is evidenced by increases in CS, translucency, and the ratio of bound-to-unbound water over time [108]. Ultimately, the set cement consists of a polysalt matrix that is reinforced by reacted and unreacted glass particles [108].

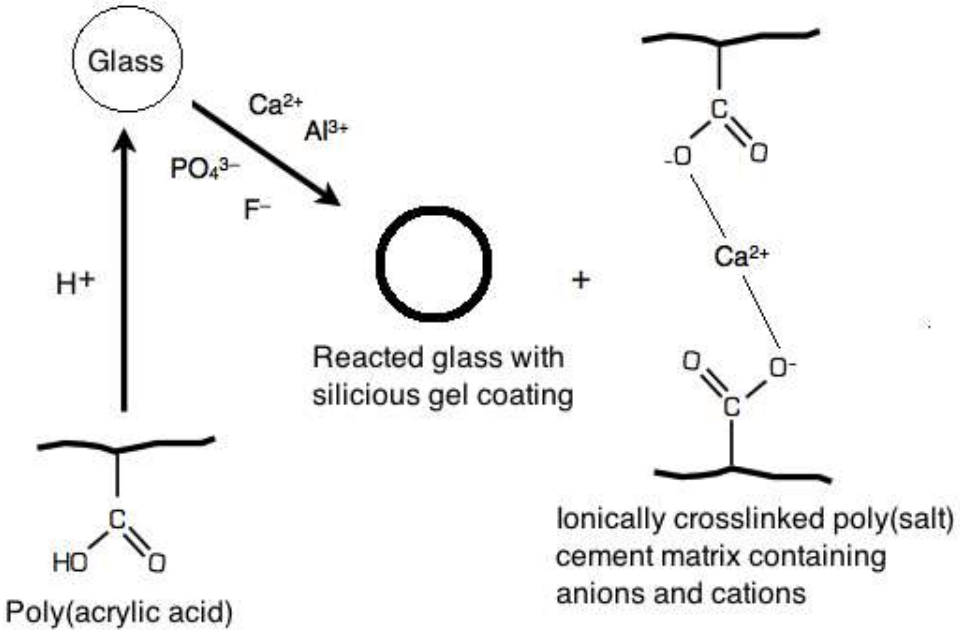

Figure 1.4: Summary of the GIC setting reaction, adapted from [107].

Conventional GICs are inherently radiopaque, chemically adhere to the mineral phase of bone, set at a negligible exotherm temperature, and present clinically practical handling and mechanical properties for PVP and PKP [4, 97, 108]. It was these positive inherent attributes that initially encouraged the adaptation of these dental materials to bone; however, their use was soon after arrested due to toxicity concerns with aluminum (Al) in the glass phase [3].

Throughout the 1990s several groups reported using conventional Al-GICs in neuro-otological applications and skull-based procedures [157-160]. A number of these reports supported the continued use of these materials in such applications, documenting no toxic reactions, adherence of the GIC to bone, ease of handling, adequate strength, and no adverse side effects [157-160]. However, as the use of Al-GICs in bone continued, reports of serious complications arose. In 1994, both Renard *et al.* and Hantson *et al.* reported fatal subacute encephalopathy in four patients who underwent neuro-otological bone augmentation using such materials. These authors attributed these complications to elevated Al levels (63-185 mg/L) in the cerebrospinal fluid (safe: <5 μg/L) of these patients [109]. Al-related toxicity was also reported as the cause of impaired osteoblastic function and bone mineralization when an Al-GIC was used in revision hip arthroplasties in 2000 [3]. It is worth mentioning that this study involved patients in whom all other interventions were contradicted, which complicates these findings [3]. The concluding remarks of these groups who reported Al-related complications cast doubt on the biocompatibility of Al-GICs and recommend against their use in orthopaedic surgery [3, 109, 110]. Unfortunately, these conclusions have ultimately removed conventional GICs from the list of potential orthopaedic materials without further investigation into their biocompatibility and with disregard to their previous successes.

1.5.1 The Development of Al-Free GICs

Although Al-related concerns have contraindicated GIC-use in orthopaedics, the remarkable combination of handling properties, strength, radiopacity, and bioactivity provided by these materials have encouraged a continued effort to develop Al-free GICs. Since the early 2000s, several groups have attempted to develop an Al-free GIC [97, 103, 111-114]. The majority of these investigations involved zinc-based glasses, as zinc oxide acts as both a network modifier and a network former, similar to Al [4, 115]. In 1994, Darling and Hill were the first to report development of a zinc-based glass, though the resulting Zn-based GICs (Zn-GICs) were hydrolytically unstable [115]. Since this time, a substantial amount of research has focused on developing and improving Zn-GICs [115]. As it stands, Zn-GICs demonstrate acceptable biocompatibility and strength (60 MPa) [97, 111], but set within 1-2 min, preventing them from use in injectable applications [112, 113]. Unfortunately, achieving a balance in these two properties has proven challenging, as outlined in Figure 1.5 [97, 103, 111-114].

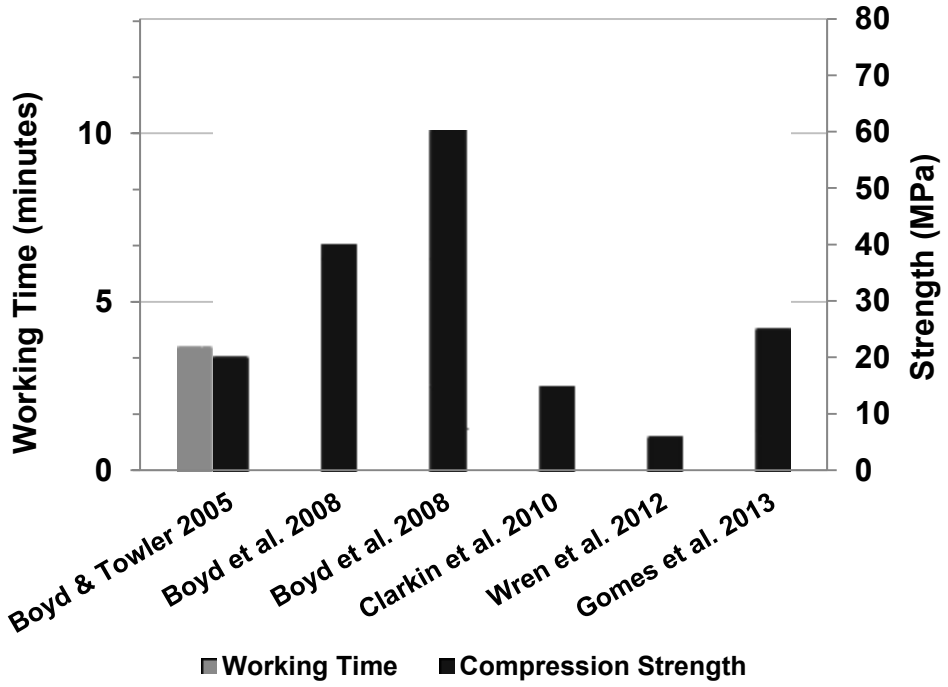

Figure 1.5: Evolution of Zn-GICs over time, adapted from [97, 103, 111-114].

In 2008, Boyd *et al.* reported that adding trisodium citrate to a series of Zn-GICs increased working time (t_w) from 20-120 sec while maintaining CS at approximately 60 MPa [97]. In 2010, Wren *et al.* reported that adding titanium to the glass network increased t_w to approximately 180 sec while maintaining CS at 45 MPa [116]. In 2010, Clarkin *et al.* reported decreasing M_w and acid concentration produced increases in t_w from 17-132 sec, but reduced CS three-fold [112]. In 2012, Wren *et al.* reported the addition of gallium to the glass network increased t_w to approximately 4 min, but significantly reduced CS from 80 MPa to only 6 MPa [113]. Overall, although these efforts proved it was possible to adjust material properties through adjusting various GIC components, none of these studies produced cements of adequate t_w [80].

In fact, until recently, there existed no Al-free GIC with both appropriate handling characteristics and strength. In 2013, Dickey *et al.* published the first series of germanium-inclusive glasses that, when mixed with PAA (50% wt%) at a 2.0/1.5 glass-powder-to-liquid-acid ratio (P/L), produced cements with t_w in the range of 5-10 min, setting times (t_s) between 14-36 min, and CS in excess of 30 MPa for the first 30 days [4]. This series, titled the Dal Glass (DG) series, is the first set of Al-free GICs that meets the criteria in Table 1.6. These glasses were developed through manipulating a previously developed Zn-based glass (composition: 0.48SiO_2, 0.36 ZnO, 0.12CaO, 0.04SrO_2) through a sequence of glass component substitutions and additions. The authors took a novel approach to glass design and investigated the effects of altering the network modifying components, as well as the network forming components of the glass on GIC handling and mechanical properties [4]. Historically, the main focus has been on adjusting only the network modifying agents, leaving silica (Si) as the network former. Zirconium (Zr) and sodium (Na) were substituted (1:1 molar ratio) in place of calcium (Ca), and germanium (Ge) in place of Si. No clear trend in the effects of Zr and Na on GIC setting was observed; however, surprisingly, Ge addition significantly increased the setting reaction of the cement, without compromising strength. The extended setting reaction was hypothesized to be a result of either (1) the lower bond angles within GeO_4 tetrahedra in comparison to SiO_4, which may have created smaller network cavities, thereby trapping cations and

delaying their release, or (2) the ability of GeO_4 tetrahedra to take on higher coordination, $[GeO_5]^-$ or $[GeO_6]^{2-}$, which would require more charge compensation, thereby reducing the number of network modifying cations and reducing the reactivity of the glass [4].

Of the 11 different glass compositions developed by Dickey *et al.*, DG209 (composition: 0.36ZnO, 0.04SrO, 0.215SiO_2, 0.215GeO_2, 0.025ZrO_2, 0.025NaO, 0.12CaO) demonstrated an optimal combination of workability and strength: t_w=5 min, t_s=14 min, and 1-day CS>30 MPa which increased over time [117]. It should be noted that these properties were measured using a P/L of 2.0/1.5 and an acid concentration (AC) of 50 wt%. This formulation (P/L and AC) is widely used in the Al-free GIC literature [117].

At this point in time, the exact role of Ge in the glass network is not fully understood; however, it is apparent that, when added in controlled proportions, Ge extends the setting reaction of these materials without sacrifice to mechanical strength [4]. To date, a preliminary biocompatibility investigation has been completed by Victoria Dickinson, a MASc student in the School of Biomedical Engineering at Dalhousie University [118]. The results of this study found the DG glasses and cements to be biocompatible with NIH-3T3 mouse fibroblast cells by means of an MTT assay. Additionally, ion release analysis showed that Ge^{4+}, Si^{4+}, Na^+, and Sr^{2+} were released from the cements in concentrations (maximum) of 200, 45, 32, and 5 ppm, respectively [118]. Therefore, the DG-cements may address the biocompatibility concerns with Al-GICs, offering an appealing alternative to existing bone cements.

It was the aim of this thesis to investigate the drug loading and delivery potential of the DG-GIC with the best-suited properties for PVP/PKP to expand the therapeutic potential of the material. Conventional GICs have been investigated for antibiotic delivery, as dental infections often result in treatment failure [119]. The subsequent section discusses the current understanding and role of GICs in drug delivery applications.

1.5.2 Drug Release from GICs

The approach of combining structural restoration with drug delivery has been applied to GICs used in dentistry as well. The majority of the literature on this subject pertains to chlorhexidine (CHX), a cationic bactericidal that is effective against bacteria associated with dental carries [119-122]. In general, CHX-release profiles from GICs typically resemble the biphasic release profiles discussed for PMMA, and similar release factors have been investigated in an attempt to determine the driving mechanisms for release: surface release, diffusion, and porosity [119-122]. However, the setting reaction of GICs is entirely different than that of PMMA (Table 1.3), and therefore unique theories pertaining to drug-cement interactions have been proposed [120].

Farret *et al.* reported less than 10% of the initial drug load was released from a CHX-loaded GIC and that CHX-addition significantly compromised the CS of the material [120]. To explain these observations, the authors postulated that CHX interacted with the cationic binding sites of the GIC. It was proposed that the drug partook in the neutralization setting reaction, and through chemically binding to the cement matrix, compromised the structural integrity of the material [120]. These findings are consistent with what was seen by Palmer *et al.*; increased drug loading (0 to 13 wt%) increased the amount of drug released from the cement, but decreased CS [122]. However, it is difficult to conclude that these findings are solely a result of CHX loading since the P/L of the cement was decreased to accommodate the powdered drug [122]. Takahashi *et al.* also reported decreases in CS when CHX was added in quantities greater than 1 wt%, though this group found that the initial drug loading had no effect on the release efficiency [121].

It has become evident that drug chemistry greatly influences the release behaviour of drug-loaded GICs. Ribero and Ericson found that CHX-digluconate (CHG) was released more quickly than CHX-diacetate (CHA) from a conventional GIC. Since CHA is a less soluble compound than CHG, the authors speculated the release of CHA was more dependent on matrix deterioration and erosion in comparison to CHG

[123]. Comparably, Jedrychowski *et al.* studied the mechanical alterations of a GIC loaded with either CHG or chlorhexidine dihydrochloride (CHCl), which is similar to CHA in the way it has poor solubility. This group found the CHCl-cement had mechanical properties closer to controls than the CHG-cement [124].

★★★

At present, there are no reports of chemo-loaded GICs, as these materials have remained limited to use in dentistry. The recent advancements made with regards to Al-free GICs may address the material-related concerns identified with conventional bone cements, allowing GICs to retranslate back to orthopaedics. The following research outlined in this document presents the first investigative analysis of drug loading this novel class of bone cements (the DG-series), as well as the first attempt to load a GIC with an anticancer agent.

1.6 The Problem Statement

The addition of antineoplastic agents to injectable bone cements may be an appropriate treatment for managing spinal metastases [1]. Hypothetically, the local release of chemotherapeutics could exert a direct cytotoxic effect on resident cancer cells, while providing structural support to the affected vertebra [1]. At this point in time, the effects of chemo-addition on GIC matrices are not known. GICs have recently re-translated from dentistry to orthopaedics due to the advancements made in the development of Al-free materials; Dickey *et al.* reported the first set of Al-free GICs that balance appropriate handling properties with strength, and Victoria Dickinson has since demonstrated their biocompatibility *in vitro* [4, 118]. To expand the therapeutic potential of this novel class of bone cements, this thesis presents the first investigative analysis on the chemo loading and delivery potential of GICs. In this study, the cement formulation of the DG-GIC comprising the best-suited properties for PVP/PKP was optimized and loaded at various concentrations with the anticancer agent, methotrexate (MTX). Subsequently, composition-property relationships were established, relating MTX loading to handling characteristics, mechanical properties, drug and ion release, and cytotoxicity.

CHAPTER 2

Research Objectives, Hypotheses, and Rationales

The overarching objective of this thesis work was to examine the drug loading and delivery potential of the best-suited DG-GIC for PVP/PKP (developed by Dickey *et al.*) using the anticancer agent, MTX. The work of this thesis was divided into six sections, as outlined in Figure 2.1. To start, a preliminary experiment was conducted in which DG209 glass powder was synthesized and characterized to confirm repeatability of structural characteristics to those published [4]. In this preliminary experiment, an upper threshold of MTX addition was derived, from which four discrete MTX loadings were established. The first formal experiment of this thesis used a Design of Experiments (DOE) approach to optimize the DG209-GIC formulation (P/L and AC) in terms of clinically desired t_w, t_s, and CS. MTX was added to this optimal formulation at the four discrete loadings and cement composition was correlated with the observed effects on handling properties, MTX release, ion release, CS, and cytotoxicity. For comparison purposes, drug and ion release, CS, and cytotoxicity were quantified at three distinct time points: 1, 7, and 31 days. Composition-property relationships were derived in an attempt to understand the effect of the drug on the material, the effect of the cement on the drug, and the mechanisms of drug release from the GIC. The following chapter outlines the objectives, hypotheses, and rationales for each experiment, as well as the foundation for the selection of the DG-GIC (DG209) and the drug (MTX).

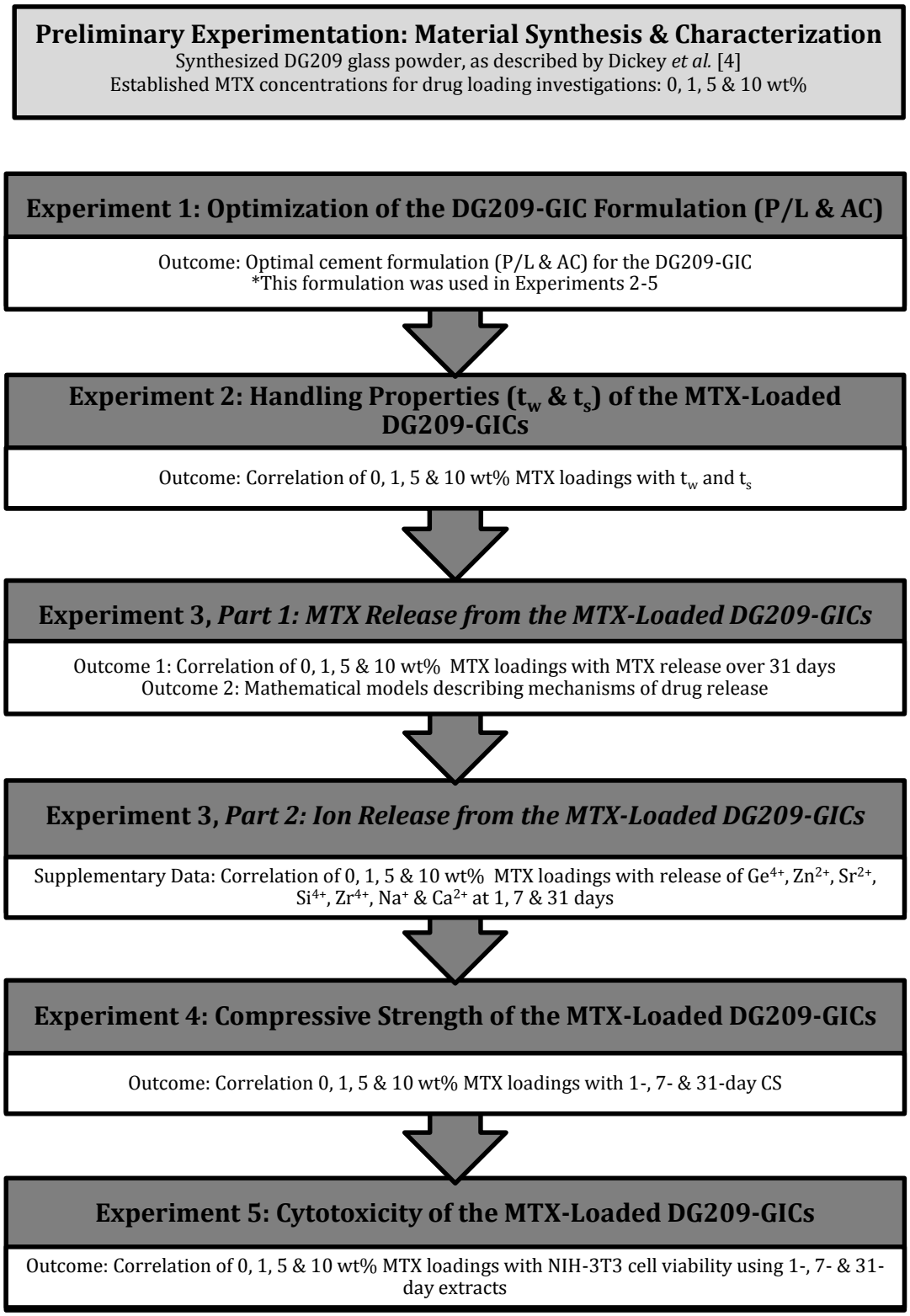

Figure 2.1: Summary of the experimental plan for this thesis work.

2.1 Selecting the GIC Matrix

The DG-GICs comprise the first Al-free GICs that demonstrate practical t_w and t_s for injectable skeletal applications, paired with appropriate strength [4]. The composition of each of these materials, and their measured t_w and t_s are summarized in Table 2.1 [4]. Since these data were originally published, the CS of each GIC was measured at 1, 7, 30, and 180 days. These data have identified DG209 as the best-suited material for PVP/PKP. The DG209-GIC stands as the only cement that demonstrates CS that exceeds 30 MPa (maintained over 180 days), paired with clinically practical t_w and t_s.

Table 2.1: DG Compositions (molar fraction) and handling properties; the GIC used in the present work is highlighted in red, adapted from [4].

	Zn	Sr	Si	Ge	Zr	Na	Ca	t_w (min:s)*	t_s (min:s)*
Zn-GIC	0.36	0.04	0.48	0	0	0	0.12	1:17	2:05
DG201	0.36	0.04	0	0.447	0.0335	0.0335	0.087	5:18	13:58
DG202	0.36	0.04	0	0.48	0	0	0.12	5:58	16:06
DG203	0.36	0.04	0.215	0.215	0.05	0.05	0.07	7:05	104:19
DG204	0.36	0.04	0.48	0	0.05	0.05	0.02	7:08	NO SET
DG205	0.36	0.04	0	0.38	0.05	0.05	0.12	4:58	14:07
DG206	0.36	0.04	0.447	0	0.0335	0.0335	0.087	1:09	3:16
DG207	0.36	0.04	0.38	0	0.05	0.05	0.12	0:22	1:03
DG208	0.36	0.04	0	0.48	0.05	0.05	0.02	10:02	35:55
DG209	**0.36**	**0.04**	**0.215**	**0.215**	**0.025**	**0.025**	**0.12**	**5:02**	**14:13**
DG210	0.36	0.04	0.223	0.223	0.0335	0.0335	0.087	6:56	36:05
DG211	0.36	0.04	0.24	0.24	0.025	0.025	0.07	7:54	75:23

*t_w and t_s measured using P/L=2.0/1.5 and AC=50 wt%.

The DG209-GIC is the only material of this series that appears to satisfy the requirements of a PVP/PKP bone cement, as outlined in the literature and summarized in Table 1.6. Based on its potential clinical utility, the DG209-GIC was selected for the bases of this thesis.

2.2 Selecting the Chemotherapeutic Agent

With regards to bone cement delivery systems, MTX is one of the most commonly investigated chemotherapeutic agents in the literature due to its relevance to breast and prostate cancer, the two leading contributors to MBD. Furthermore, the efficacy of MTX increases with extended exposure, as cell sensitivity increases with time; the drug's time-effect is greater than its dose-effect. This makes MTX an ideal chemotherapeutic for slow, extended, local delivery [125].

MTX is a folic acid derivative and folate antagonist that has been used as a cytotoxic antineoplastic since the 1940s. Its anticancer effects depend on its structural similarities to folic acid, depicted in Figure 2.2 [126]. MTX is a structural analog to folic acid, but differs by an amine group in place of a hydroxyl group on C4, and a methyl group in place of a hydrogen atom on N10. The drug inhibits the reduction of dihydrofolates, which prevents the transport of one-carbon groups in the synthesis of purine nucleotides. Consequently, MTX interrupts DNA synthesis, repair, and cellular replication. Actively proliferating cells, such as malignant cells, are more prone to the effects of MTX than normal tissues and therefore the drug can be used to inhibit growth of malignant tissues without irreversible damage to normal tissues [127, 128].

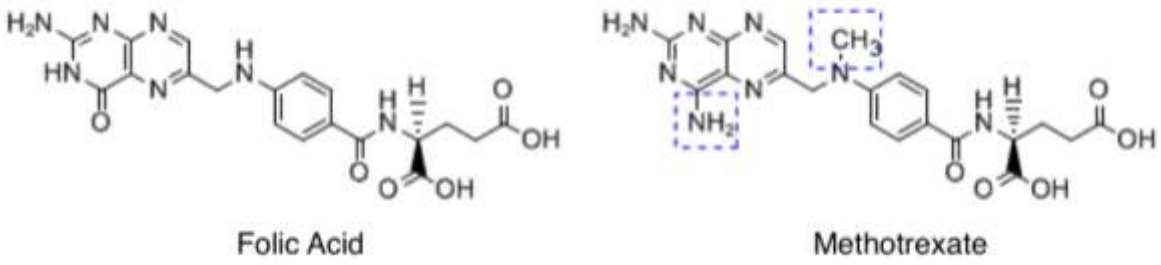

Figure 2.2: Structural comparison of folic acid and methotrexate; the blue boxes highlight the differences between the two compounds, adapted from [125].

For this research, MTX was selected to test the drug loading and delivery potential of the DG209-GIC. This selection was founded upon three key aspects: (1) the relevance of MTX to the MBD, (2) the potential advantage of using MTX in local, sustained delivery systems, and (3) the ability to compare the results of the present work to the literature.

2.3 Preliminary Experimentation: Material Synthesis & Characterization

2.3.1 Objectives

- To synthesize DG209 glass powder and validate that (1) the material contained no identifiable crystalline species, and (2) the material had the same glass transition temperature (T_g) as that reported be Dickey *et al.* [4].
- To establish an upper threshold at which MTX could be loaded into the DG209-GIC based on t_w and t_s analyses.
- To define four discrete MTX loadings for use in Experiments 2-5 using the established upper threshold as a basis.

2.3.2 Rationale

Validation that the DG209 glass synthesized in this experiment was characteristic of that developed by Dickey *et al.* was critical to the work of this thesis. Four batches of DG209 glass powder were synthesized to provide a bulk of material sufficient for the completion of this work. Each glass batch was characterized *via* X-ray diffraction (XRD) to ensure amorphous structure devoid of identifiable crystalline species, and analyzed using differential scanning calorimetry (DSC) to determine T_g. The T_g of each glass batch was statistically compared to that reported by Dickey *et al.* [4]. Verification of amorphous glass structure and statistically similar T_g were used to confirm repeatability of structural characteristics [4].

To establish four discrete MTX loadings for the development of composition-property relationships throughout this research, a screening experiment was conducted prior to commencing Experiments 2-5. An upper threshold of MTX addition was approximated using t_w and t_s analyses to provide a basis for defining the different loadings. This upper threshold was defined by the highest MTX concentration that persisted to produce a *cohesive*, *settable* cement. As MTX is a dicarboxylic acid, it was proposed the drug may chemically interact with the neutralization setting reaction of the DG209-GIC. Previous studies have demonstrated the effects of increased AC on GIC properties; higher ACs increase the reactivity of the cement, as evidenced by decreases in t_w and t_s [112, 129]. In the literature, t_w is frequently used to relate the basic rheology of dental and bone cements, while t_s is used to approximate the time it takes the material to harden (validating whether the material sets) [4]. In the present work, MTX was added to the DG209-GIC at increasingly higher concentrations until the material failed to provide a cohesive cement paste or did not set.

2.4 Experiment 1: Optimization of the DG209-GIC Formulation (P/L and AC)

2.4.1 Objectives

- To use a DOE approach to investigate the effects of P/L and AC on the handling and mechanical properties of the DG209-GIC.
- To derive an optimal formulation (*ie.* P/L and AC) for the DG209-GIC using the resulting regression equations derived from the DOE.

2.4.2 Hypotheses

i. It was hypothesized that increases in P/L and AC would increase setting rate, evidenced through decreases in t_w and t_s, and increase the CS of the DG209-GIC.

ii. It was hypothesized that a DOE approach could be used to optimize *both* P/L and AC such that t_w=5-10 min, t_s<20 min, and CS>30 MPa.

2.4.3 Rationale

The DG209-GIC is the first Al-free GIC that demonstrates adequate handling characteristics while maintaining appropriate strength for injectable skeletal applications. Ideally, a PVP/PKP bone cement should comprise the properties outlined in Table 2.2 [2, 4, 80]. From a clinical standpoint, sufficient time for injection is required, the cement should set as quickly as possible once in place, and the material should match the mechanical properties of native bone [80]. In the literature, these three key properties are approximated using the ISO9917 tests for t_w, t_s, and CS (respectively). It should be mentioned that t_w is not an exact measure of injectability; however, it is reported extensively in the dental and bone cement literature for comparison purposes of basic rheology [4].

Table 2.2: Delivery specific criteria for a PVP/PKP bone cement [2, 4, 80].

Property	Target
t_w	5-10 min
t_s	< 20 min*
CS	> 30 MPa

*Minimal t_s desired, therefore t_s ~10 min when considering time for injection.

The effects of P/L and AC on the DG209-GIC were unknown prior to this thesis, and an optimal formulation was not previously derived for this material. The t_w of the DG209-GIC published by Dickey *et al.* (t_w=5:02 min:sec; GIC mixed at P/L=2.0/1.5 and AC=50 wt%) borders the minimum threshold for what is considered acceptable for use in PVP and PKP [4]. Consequently, this experiment aimed to investigate whether it was possible to extend t_w without compromising t_s or CS through adjusting the P/L and AC of the DG209-GIC. The *individual* effects of P/L and AC on GIC performance have been well documented in the GIC literature [97, 130, 131]. Adjustments to these components significantly influence the setting chemistry of GICs and, consequently,

the properties of the material [132]. In general, it is understood that increasing either P/L or AC increases the reactivity of the setting material, as evidenced by decreases in t_w and t_s [97, 130, 131]. Both increases in P/L and AC have been shown to increase CS; increased P/L increases the proportion of reinforcing glass particles, while increased AC increases the extent of matrix entanglement [97, 130]. Based on these reports, the present work investigated whether the properties of the DG209-GIC could be optimized through adjusting the P/L and/or AC.

A novel approach was implemented in order to establish an optimal formulation, whereby P/L and AC were adjusted *concomitantly*. Design Expert 8.0.4 was used to develop a DOE in which both P/L and AC were varied to establish composition-property relationships that described their combined effects. A central composite, response surface design was selected to augment a simple first-order design to a second-order design without requiring a full three-level factorial experiment. This reduced the necessary experimental work substantially (t_w, t_s, and CS were measured at only 13 different P/L-AC combinations) through using multiple linear regression to generalize the responses. Using the acquired models and the target parameters for t_w, t_s, and CS (Table 2.2), the desirability function approach was implemented to determine a single, optimal set of P/L and AC.

2.5 Experiment 2: Handling Properties (t_w and t_s) of the MTX-Loaded DG209-GIC

2.5.1 Objective

To examine the effects of MTX addition (0, 1, 5, and 10 wt%) on the t_w and t_s of the optimized DG209-GIC.

2.5.2 Hypothesis

Since MTX is a dicarboxylic acid, it was hypothesized that increased MTX loading would increase the reactivity of the setting process, evidenced by decreases in t_w and t_s.

2.5.3 Rationale

In this experiment, composition-property relationships were established correlating MTX loading to t_w and t_s in order to investigate the effects of drug addition from both a clinical and chemical standpoint. As the effect of MTX addition on GIC matrices was unknown prior to this study, the effects of MTX addition on t_w and t_s were studied separate from the material optimization in Experiment 1. The aim of this thesis was not to derive an optimally drug-loaded GIC, rather to investigate the effects of drug loading on the GICs properties and the suitability of the GIC to act as a delivery vehicle.

Across the literature, t_w and t_s are commonly reported to compare the ease of handling of different bone cements [4]. These measures offer a simplistic approach for relating the approximate rheology of different cements. Furthermore, t_w and t_s provide a foundation for developing hypotheses regarding setting reactivity; decreases in t_w and t_s may be indicative of increased reactivity [112].

2.6 Experiment 3: MTX and Ion Release from the MTX-Loaded DG209-GICs

Experiment 3 investigated the release behaviour of the MTX-loaded DG209-GICs. This experiment was divided into two sections: Part 1 involved characterization of MTX release from the optimized GIC (Experiment 1) as a function of time, while Part 2 examined the effects of MTX loading on ion release from the DG209-GIC.

2.6.1 Part 1: MTX Release

2.6.1.1 Objectives

- To quantify MTX release from each MTX loaded DG209-GIC (0, 1, 5, and 10 wt%) over a 31-day incubation period in simulated physiological conditions.
- To apply mathematical models to each release profile to (1) describe drug release, and (2) elucidate the mechanisms of release.

2.6.1.2 Hypotheses

i. Consistent with what has been reported for antibiotic-releasing GIC systems, it was hypothesized that increased MTX loading would increase the quantity of drug released from the cement [122].

ii. It was hypothesized that the release efficiency*, the release half-life ($t_{1/2}$), and the time at which the release plateaus ($t_{plateau}$) would be independent of drug loading, as drug release from conventional GIC delivery systems is believed to result from surface characteristics and diffusion [121].

iii. Also consistent with conventional GIC delivery systems, it was hypothesized that mathematical models describing diffusion would fit the acquired release

*Release efficiency: Percentage of the initial drug load released.

profiles significantly better than those based on erosion-mediated release [123].

2.6.1.3 Rationale

In vitro release has been recognized as an important element in the development of local delivery systems. However, establishing *in vitro* conditions is a complex process that significantly impacts release kinetics and the applicability of acquired data. Numerous experimental factors were considered in designing this experiment, including the incubation environment, sink conditions, the stability of the drug, and the detection limits of the drug. The following Rationale aims to summarize the justifications for the selected experimental components.

In the present study, MTX-loaded DG209-GIC cylinders were incubated in phosphate buffered saline (PBS) at 37°C under dynamic conditions (2 Hz rotating mixer). This only very roughly approximated physiological conditions, but provided a constant environment to enable accurate comparisons across the acquired data. Since MTX is only stable in solution for 1 to 7 days when stored at 4-8°C [133], a specialized elution schedule was developed: PBS was changed at 1 hour, daily for 10 days, and on days 30* and 31. This ensured MTX was only in solution in the incubation environment for a maximum of 24 hours to minimize risks of chemical change, which could influence UV spectroscopy readings and the drug's activity (required for the MTT assay, Experiment 5). To further reduce such risks, collected extracts were stored at 4°C until analyzed using UV spectroscopy to quantify MTX concentrations (maximum storage period: 7 days), and frozen at -20°C thereafter (maximum storage period: 30 days) [133].

To accommodate sink conditions throughout the release period while maintaining detectable drug concentrations, the following PBS volumes were used:

*Note: Extracts taken on day 30 were not included in the analysis. In these samples, MTX was in solution at 37°C for 10 days prior to its collection, which may have adversely affected its chemical structure and/or activity.

10 ml for the first hour and first day, 5 ml for the second day, and 2.5 ml for the remaining sampling time points [134]. Sink conditions are defined as the volume of medium at least three times the volume required to form a saturated solution [134]. These conditions provide consistent measures of dissolution through ensuring release is not inhibited by the saturation point of the solution. PBS was selected as the extract medium, as MTX is insoluble in water [134]. The solubility of MTX in PBS is approximately 1 mg/ml, and therefore PBS volumes were maintained such that MTX concentrations in release extracts did not exceed 0.333 mg/ml [135]. The volume required to dissolve three-times the maximum amount of MTX loaded into a cement sample was calculated as approximately 100 ml (27.7 mg MTX per 10 wt% MTX cement sample in 100 ml PBS meets this requirement). However, it was estimated that no more than 10% of this initial drug loading would be released at any one time point, and therefore initial PBS volumes were reduced to 10 ml. This assumption was validated experimentally once drug release data was acquired.

The detection limit of MTX in PBS was pre-determined through taking UV spectroscopy readings of a serial dilution; 0.25 μg/ml was the derived detection limit. To establish the volumes of PBS listed above, a preliminary release experiment was conducted using the 1 wt% MTX DG209-GIC (minimum) in order to predict when the extracts may approach the detection limit. It became apparent that the burst release terminated before 1 day and therefore PBS volumes were halved for the subsequent time point (day 2). MTX concentrations of the 2-day extracts were significantly lower than necessary to meet sink conditions. This indicated that the PBS volumes required to compensate the slow, sustained release phase could be further reduced. PBS volumes of 2.5 ml were used for the remaining time points to provide sufficient material for UV spectroscopy, ICP analysis (Experiment 3, Part 2), and cytotoxicity testing (Experiment 5). Full methodological details are provided below in Chapter 3.

Resulting release profiles were compared in Prism 6 to develop composition-property relationships correlating drug loading with concentration of MTX released, release efficiency, $t_{1/2}$, $t_{plateau}$, and kinetic models. Release efficiency, $t_{1/2}$, and $t_{plateau}$ are reported extensively across the drug release literature [74, 75]. Release efficiency

quantifies the percentage of drug released relative to the initial loading, providing the therapeutic dose eluted from the material, as well as the amount of drug held within the cement. The $t_{1/2}$ represents the time point at which half of the total drug release occurs, while the $t_{plateau}$ signifies the point at which the drug release levels off. The $t_{plateau}$ is of particular interest, as it may represent the point at which the burst release terminates and the sustained release begins. Kinetic models were applied to support predictions regarding release mechanism and to draw comparisons with the peer-reviewed literature. Table 1.5 outlines the models that are commonly applied to bone cement delivery systems [73, 76].

2.6.2 Part 2: Ion Release

2.6.2.1 Objective

To quantify the concentration of constituent ions released at 1, 7, and 31 days from the 0, 1, 5, and 10 wt% MTX DG209-GICs using inductively coupled plasma (ICP).

2.6.2.2 Rationale

This experiment was considered supplementary to the other experiments and did not have a formal hypothesis. It was proposed that correlation of MTX loading with ion release might provide support for theories involving the chemical interactions of MTX in the GIC matrix (developed from Experiments 2-5). Therefore, this experiment was conducted in an attempt to augment the understanding of these composition-property relationships. Additionally, it is well known that ionic dissolution products can affect several different biological responses [136]. Therefore, this study was conducted to rule out any effects of ion species on cell viability (Experiment 5); knowledge of ionic content is valuable information for interpreting cytotoxicity results.

2.7 Experiment 4: Compressive Strength of the MTX-Loaded DG209-GICs

2.7.1 Objective

To investigate whether MTX loading compromised the mechanical integrity of the GIC matrix through measuring the CS of the 0, 1, 5, and 10 wt% MTX DG209-GICs at 1, 7, and 31 days.

2.7.2 Hypothesis

It was hypothesized that increased MTX loading would decrease the CS of the DG209-GIC, but that all DG209-GICs (MTX-loaded or not) would show increases in CS over time.

2.7.3 Rationale

Compressive testing serves as a preliminary tool for examining the effects of drug loading on the mechanical integrity of the cement. Cement cylinders synthesized in this experiment were prepared (synthesized and incubated) using identical methods to those used in Experiments 3 and 5. This enabled accurate correlation between the data acquired from these experiments. Testing was conducted at 1, 7, and 31 days in order to cross-reference CS with MTX release, ion release, and cell viability data, as well as CS data published in the peer-reviewed literature pertaining to drug-loaded GICs.

The compressive testing methods used in the present work were adapted from ISO 9917 [137]. In the past, the validity and reproducibility of this test for strength has been challenged in the literature [138, 139]. Fleming *et al.* stated that the test offers no context for strength, as the stress at failure calculation does not take failure mechanism into consideration; uniaxially compressed cylinders may collapse under a combination of tensile and shear stresses [138]. In 2012, Fleming *et al.* investigated the appropriateness of CS testing in comparison to two other alternative strength test

methods commonly reported in the literature: the three point flexural (TPF) test and the biaxial test. This study found that TPF and biaxial test results showed significantly higher statistical power in comparison to CS. The authors reported CS is limited to a measure of "quality", rather than a predictive value that may be used to interpret strength [138].

Nonetheless, the ISO 9917 test for CS is the only strength test specified for GICs, and it has remained the most commonly cited method for assessing the mechanical properties of GICs over the last 20 years [138, 139]. In 2011, Dowling *et al.* addressed the debate on the reliability of this test method, reporting no significant inter- or intra-operator variability between two operators and three GICs [139]. Although the 2012 paper by Fleming *et al.* questions the predictive clinical utility of this test, ISO 9917 remains a common method for drawing mechanical-related comparisons across the GIC literature.

In the present study, a single operator completed all CS testing under constant laboratory conditions. Although the reproducibility of ISO 9917 remains under scrutiny, these consistencies reduced risk of variability across the data set, enabling the development of relevant composition-property relationships to correlate MTX addition with strength. The results of this study are intended to provide a *preliminary* examination of the effects of MTX addition on strength. The "quality aspect" of this test was considered sufficient for drawing the necessary conclusions for this thesis.

2.8 Experiment 5: Cytotoxicity of the MTX-Loaded DG209-GICs and Validation of Drug Activity

2.8.1 Objectives

- To test the cytotoxicity of the 1, 5, and 10 wt% MTX DG209-GICs in comparison to a 0 wt% MTX cement control using percent-cell viability measured *via* an MTT assay.
- To investigate whether the activity of the released MTX was affected through comparing cell viabilities of the MTX DG209-GIC extracts to cell viabilities of fresh MTX solution of similar concentrations.

2.8.2 Hypotheses

i. As MTX competitively inhibits the metabolism of folic acid, it was hypothesized MTX-loaded cement extracts would yield significantly lower NIH-3T3 mouse fibroblast cell viability than the 0 wt% MTX cement extract control at each time point (1, 7, and 31 days).

ii. As per Section 2.6.1.2, increased MTX loading would increase the amount of drug released from the cement. Consequently, it was hypothesized the extracts taken from cement specimens of higher drug loading would yield lower NIH-3T3 mouse fibroblast cell viability.

2.8.3 Rationale

In vitro elution testing was conducted to test the cytotoxicity of the released MTX in order to (1) develop composition-property relationships for the drug loaded GICs in terms of cytotoxicity and (2) determine whether the cement affected the cytotoxicity of the drug. Elution testing, as opposed to the direct contact or agar diffusion test methods, was selected in order to accommodate prolonged test periods from which extracts could be collected and analyzed using UV spectroscopy and ICP. Cement

samples were incubated in simulated physiological conditions for 31 days, as discussed previously in Section 2.6.1.3.

One of the major challenges in conducting elution testing was selecting the release medium. Tissue culture water, PBS, and simulated body fluid (SBF) have all been identified as appropriate media for *in vitro* cell testing; however, each release medium is burdened by a unique set of limiting factors – tissue culture water is not buffered and risks damaging cells due to its relatively low pH, PBS lacks the organic compounds found in the *in vivo*, and SBF compositions are inconsistent across the literature [136, 140]. PBS was used for release testing, due to its ability to solubilize MTX [141]. Solubility data is crucial for determining sink conditions, which dictate the minimum volume of media that may be used. Additionally, PBS is used extensively across the literature for testing the release of chemotherapeutics from different types of bone cements. This allowed for relevant comparisons between the present study and the literature.

The NIH-3T3 mouse fibroblast cell line was chosen to test the activity of the released MTX. Surely, a number of cell lines would suit as MTX is an antifolate and thus inhibits the normal cellular processes of all actively proliferating cells. Since the primary objective of this experiment was to evaluate whether the released MTX was active or not, the simple, robust NIH-3T3 cell line was used. To assess cell viability, a MTT (3-(4,5-dimethylthiazol-2-yl)-2,5-diphenyltetrazolium bromide) assay was performed. This method is used extensively in the peer-reviewed literature as a colorimetric means of quantifying mitochondrial activity, which is indicative of cell viability.

CHAPTER 3

Materials & Methods

3.1 Preliminary Experimentation: Material Synthesis, Characterization, and Preparation

3.1.1 DG209 Glass Synthesis & Preparation

Four batches of DG209 glass were synthesized using the rapid quench method. Analytical grade reagents were weighed out as per Table 3.1 (Sigma-Aldrich Co., Oakville, Canada). The powder mixture of reagents was mixed for one hour in a mechanical mixer (Twin shell dry blender, Patterson-Kelly, USA) and then packed into a 50 ml platinum crucible (Alfa Aesar, Ward Hill, USA), which was fired (1500°C ± 10°C, 1 hour) in a high temperature furnace (Carbolite RHF 1600, Hope, UK), and then quenched into deionized water at room temperature. The resulting glass frit was dried overnight in a vacuum oven (100°C), and then ground using a planetary ball mill (Pulversette 7, Fritsch, Germany) and sieved to yield a powder of <45 μm particle size (Cole-Parmer, Montreal, Canada). Glass powders were then annealed in the high temperature furnace at 30°C less than their average T_g for three hours, and left to furnace cool. All glasses were subsequently stored in a desiccator prior to subsequent analysis [4].

Table 3.1: DG209 composition.

Reagent	Mole Fraction
ZnO	0.360
SrO	0.040
SiO_2	0.215
GeO_2	0.215
ZrO_2	0.025
Na_2O	0.025
CaO	0.120

3.1.2 DG209 Glass Characterization

3.1.2.1 X-ray Diffraction Method

Powder samples for each glass were analyzed via X-ray diffraction using a Bruker AXS D8 diffractometer (Department of Physics, Dalhousie University, Canada). The system comprised Cu-Kα radiation, a Göbel mirror, a Vantec-2000 area detector, and a Cu target X-ray tube. Glass powders were pressed into hollow square wafers. A monochromator in the incident beam path limited the wavelengths striking the specimen to Cu Kα1,α2. The X-ray beam was incident on the specimen at approximately 6° and the curved position detector collected all scattered X-rays in the following scan angle range: $10° < 2\theta < 120°$ (step size: 0.033°). The collection time for the XRD spectra was approximately 1800 sec [142].

3.1.2.2 Differential Scanning Calorimetry Method

Each of the four batches of synthesized DG209 glass powder (n=3) were analyzed with a differential scanning calorimeter (Q200 DSC, TA Instruments, Brossard, Canada). For each run, approximately 30 mg of glass powder was placed into a stainless steel closed pan, while the reference pan was left empty. The sample was heated at 10°C/min to a maximum temperature of 1000°C [4]. Q Series software (TA Instruments, Grimsby, Canada) was used to determine the T_g (point of inflection).

3.1.3 DG209 Cement Preparation

DG209 cements were formed by mixing prepared glass powder and aqueous PAA, M_w=12,700 g/mol, AC=50 wt% (Advanced Healthcare, Tonbridge, UK) on dental mixing pads using a dental spatula at P/L=2.0/1.5 (as reported by Dickey *et al.*) [4].

3.1.4 Preliminary MTX Loading Method for Establishing Upper Threshold of Drug Addition

MTX powder (M9929, Sigma-Aldrich Co., Oakville, Canada) was added to the DG209-GIC in concentrations as follows: 0, 5, 10, 20, and 30 wt%*. For each MTX loading, cements were prepared as per Section 3.1.3, and t_w and t_s were measured (n=3). The t_w was measured in ambient air using a stopwatch, and was defined as the period of time from the start of mixing during which it was possible to manipulate the material without having an adverse effect on its properties [137]. The t_s was measured in a 37°C room by filling an aluminum mould (10 mm x 8 mm x 5 mm) to excess, which was placed on an aluminum plate (75 mm x 100 mm x 8 mm) wrapped in aluminum foil. Sixty seconds prior to the cement's t_w, a Gilmore needle (mass=453 g, flat tip diameter=1.1 mm) was placed on to the surface of the material. This was repeated in approximate 10 sec intervals until the cement could no longer take the full weight of the indenter for 5 sec; the indenter tip failed to make a full circular impression in the cement when viewed at 2x magnification [137]. The maximum MTX loading that produced a *cohesive*†, *settable*‡ cement was defined as the upper threshold for MTX loading. Using this maximum loading, a total of four discrete MTX loadings were defined.

*The cement was incohesive at MTX loadings greater than or equal to 30 wt%.

†For the purpose of this thesis, a "cohesive" cement pertains to a homogenous, unified cement paste, while an "incohesive" cement refers to a material demonstrating lack of integration, characterized by crumbling or visible discontinuities.

‡For the purpose of this thesis, a "settable" cement refers to a material that sets as per the ISO9917 definition of setting time.

3.2 Experiment 1: Optimization the DG209-GIC Formulation (P/L and AC)

3.2.1 Experimental Design

A central composite design of experiments (Design Expert 8.0.4, Stat-Ease Inc.) was developed relating the effects of (a) P/L and (b) AC on t_w, t_s, and CS. A quadratic user-defined design consisting of 13 experiments representing different P/L-AC combinations was constructed, as summarized in Table 3.2. These discrete GIC formulations, herein referred to as *design points*, were determined based on previously determined constrained ranges [*] (*design space*) for each factor: P/L between 1.0/1.0 and 2.0/1.0 w/w, and AC between 40 and 60 wt%. Four design points were set at the vertices, four were set at the axial check-blends, and one was set at the centroid of the design space. This centroid point was repeated five times to increase experimental precision. For each design point, cements were prepared and t_w, t_s, and CS were measured as follows.

3.2.2 DG209 Cement Preparation

DG209 cements were formed by mixing prepared glass powder and aqueous PAA, M_w=12,700 g/mol (Advanced Healthcare, Tonbridge, UK) on dental mixing pads with a dental spatula using the P/L-AC combinations listed in Table 3.2.

3.2.3 Determination of t_w and t_s

The t_w was measured in ambient air using a stopwatch, and was defined as the period of time from the start of mixing during which it was possible to manipulate the material without having an adverse effect on its properties [137]. The t_s was measured in a 37°C room by filling an aluminum mould (10 mm x 8 mm x 5 mm) to

[*]A preliminary screening step was completed prior to the commencement of this experiment to determine the ranges of P/L and AC that produced cements with practical working characteristics (a *cohesive*, *settable* cement) using the methods detailed in Section 3.2.3 for measuring t_w and t_s.

excess, which was placed on an aluminum plate (75 mm x 100 mm x 8 mm) wrapped in aluminum foil. Sixty seconds prior to the cement's t_w, a Gilmore needle (mass=453 g, flat tip diameter=1.1 mm) was placed on to the surface of the material. This was repeated in approximate 10 sec intervals until the cement could no longer take the full weight of the indenter for 5 sec; the indenter tip failed to make a full circular impression in the cement when viewed at 2x magnification [137]. Both measurements were performed in triplicate for each design point.

Table 3.2: Summary of design points: P/L and AC.

Design Point	P/L	AC (wt%)
1	2.0/1.0	60
2	1.0/1.0	40
3	1.5/1.0	50
4	1.5/1.0	50
5	1.5/1.0	60
6	2.0/1.0	40
7	1.0/1.0	60
8	1.0/1.0	50
9	1.5/1.0	40
10	2.0/1.0	50
11	1.5/1.0	50
12	1.5/1.0	50
13	1.5/1.0	50

3.2.4 Determination of CS

To determine CS, stainless steel split ring molds (diameter=4 mm, height=6 mm) were filled to excess with cement, covered with acetate, clamped between two stainless steel plates, and incubated (37°C). After 1 hour, the assembly was broken down, cement flash was removed, and the ends of the samples were ground flat using wet 800 grit silicon carbide paper. Cement specimens were removed from the molds and incubated in distilled water (37°C) for 24 hours under static conditions. The cylinders were removed from the incubation environment and immediately loaded on an Instron 3344 mechanical testing device (Instron, Norwood, USA; 2 kN load cell, 1 mm/min crosshead speed). Five samples for each design point were tested [137].

3.2.5 Generation of Models

The resulting t_w, t_s, and CS data were modeled using Scheffé multiple comparison equations and backward regression analysis to determine significant model coefficients. A second-order polynomial equation was fitted for the t_w response; a power transformation (lambda=0.75) was applied to the t_s response, which was then modeled using a second-order polynomial fit; and a third-order polynomial equation was used to model the CS response. The resulting reduced polynomials were analyzed by ANOVA to show significant model terms.

3.2.6 Optimization and Validation

Target ranges of t_w, t_s, and CS (Table 3.3) were inputted to the desirability function to interpolate an optimal P/L and AC. Using the derived P/L and AC, the DG209-GIC was prepared as per Section 3.2.2, and t_w, t_s, and CS were measured as per Sections 3.2.3 and 3.2.4. These measurements were compared (ANOVA) to the model predictions for t_w, t_s, and CS to assess the predictive power of the model and validate the properties of the optimized formulation.

Table 3.3: Design criteria inputted to Design Expert to obtain an optimal P/L and AC.

Factors	Goal	Lower Limit	Upper Limit	Importance
t_w	maximize	-	-	+++
t_s	in range	minimum	2000 sec	+++
CS	in range	32 MPa	maximum	+++

3.3 Experiment 2: Handling Properties (t_w and t_s) of the MTX-Loaded DG209-GIC

MTX powder (M9929, Sigma-Aldrich Co., Oakville, Canada) was added to the cement at 0, 1, 5, and 10 wt%* of the cement. The MTX powder was added to the liquid acid to obtain a homogenous dispersion prior to being combined with the basic glass powder, and cements were prepared as per Section 3.2.2 using the optimized P/L and AC (Experiment 1) in a fume hood. For each MTX loading, t_w (n=3) and t_s (n=3) were measured as described in Section 3.2.3 with the following modifications: (1) t_w measurements were performed in a fume hood, and (2) t_s measurements were performed using a 37°C oven placed in a fume hood.

3.4 Experiment 3: MTX and Ion Release from the MTX-Loaded DG209-GICs

3.4.1 Part 1: MTX Release

3.4.1.1 Quantification of MTX Release

Cylindrical specimens (n=5) were synthesized for the 0, 1, 5, and 10 wt% MTX cements as per the methods detained in Section 3.2.4. Each cylinder was immersed in 10 ml phosphate buffered saline (PBS; P5493, Sigma-Aldrich Co., Oakville, Canada) and incubated at 37°C in a 2 Hz rotating mixer (Max Q4000, 4320, Thermo Scientific, OH, USA). At sampling intervals (1 hour; daily for 10 days; and at 30 and 31 days), the cylinders were removed and placed into fresh PBS (volume=10 ml for the first hour and first day, 5 ml for the second day, and 2.5 ml for the remaining sampling times) while maintaining sink conditions. All incubating solutions were stored at 4°C for a maximum of 7 days, and at -20°C thereafter in the absence of light (maximum 30 days). The concentration of MTX was quantified by UV emission spectroscopy

*Drug loadings established from the methods described in Section 3.1.4.

(BioTek Instruments Inc., Version 3.2) using an absorbance wavelength of 303 nm [57].

3.4.1.2 Generation and Application of Mathematical Models to MTX Release Data

Cumulative MTX release profiles were analyzed using non-linear regression (Prism 6, GraphPad Software Inc., La Jolla, USA). Exponential models were statistically compared and data was fitted to zero-order, first-order, Higuchi, Korsmeyer-Peppas, and Hopfenberg models, and statistically analyzed to show model adequacies.

3.4.2 Part 2: Ion Release

Using the 1-, 7-, and 30-day extracts collected from Section 3.4.1.1, 1 ml of each extract was diluted to 7 ml using 2% (v/v) HNO_3. Calibration standards were prepared using 2% (v/v) HNO_3 from standard solutions of 1000 mg/L Zn, Sr, Si, Ge, Zr, Na, and Ca solutions (Perkin Elmer Atomic Spectroscopy Standards), as shown in Table 3.4.

Table 3.4: Standard ion concentrations (ppm).

Standard	Zn^{2+}	Sr^{2+}	Si^{4+}	Ge^{4+}	Zr^{4+}	Na^{+}	Ca^{2+}
1	10	10	10	25	10	10	10
2	1	1	1	10	1	1	1
3	0.1	0.1	0.1	1	0.1	0.1	0.1
4	0.01	0.01	0.01	0.1	0.01	0.01	0.01
5	0	0	0	0	0	1000	0
6	0	0	0	0	0	500	0
7	0	0	0	0	0	100	0
8	0	0	0	0	0	50	0

The concentration of each ionic species listed in Table 3.4 was measured for each experimental extract using ICP optical emission spectroscopy (Perkin Elmer Optima 8000). Dilute extract concentration were compared to derived calibration curves, using WinLab32 ICP software.

3.5 Experiment 4: Compressive Strength of the MTX-Loaded DG209-GICs

MTX powder (M9929, Sigma-Aldrich Co., Oakville, Canada) was added to the cement at 0, 1, 5, and 10 wt%. The MTX powder was added to the liquid acid to obtain a homogenous dispersion prior to being combined the basic glass powder, and cements were prepared as per Section 3.2.2. Compressive strength (n=5) was measured for each DG209-GIC after being incubated for 1, 7, and 30 days as per the methods detailed in Section 3.2.4, but with using the storage conditions outlined in Section 3.4 (PBS, 37°C, 2 Hz rotating mixer) [137].

3.6 Experiment 5: Cytotoxicity of the MTX-Loaded DG209-GICs and Validation of Drug Activity

NIH-3T3 cells at passage 17 (200 µl) were seeded at a density of 3 x 10^4 cells/ml in 96-well plates. PBS (n=5) was used as a negative control and DMSO (n=5) was used as a positive control. The 96-well plates were incubated for 24 hours in a cell culture incubator (37°C, 10% CO_2), after which 20 µl of each relevant experimental extract (0.20 µm sterile-filtered; n=3) was added to the appropriate well as shown in Figure 3.1. Another plate was used to test the cell viability of fresh MTX solutions prepared at concentrations similar to what was derived from the MTX release tests (Section 3.4.1.1). The setup for this assay is shown in Figure 3.2. The plates containing MTX were incubated (37°C, 10% CO_2) for 72 hours. A 5-mg/ml solution of MTT reagent (M2128, Sigma-Aldrich, Oakville, Canada) was prepared in PBS (0.20 µm sterile-filtered), and each well was exposed to the prepared MTT at a volume of 10% of the culture media volume. The plates were stored in the incubator (37°C, 10% CO_2) for 3 hours, after which the well contents were dumped and 100 µl of DMSO was added to solubilize the formazan crystals. The absorbance of each well was measured using a plate reader set at an absorbance wavelength of 492 nm. Cell negative control wells (PBS) were assumed to have 100% metabolic activity corresponding to cell viability

of 100% [142]. The percentage of cell viability of the cells exposed to experimental extracts was calculated relative to this, as follows:

$$Cell\ Viability\ \% = 100\% \times \frac{OD_{extract}}{OD_{control}}$$

where $OD_{extract}$ is the mean optical density measurement of the experimental extract and $OD_{control}$ is the mean optical density measurement of the negative control.

<table>
<tr><th></th><th>1</th><th>2</th><th>3</th><th>4</th><th>5</th><th>6</th><th>7</th><th>8</th><th>9</th><th>10</th><th>11</th><th>12</th></tr>
<tr><td>A</td><td colspan="5" rowspan="3">0 wt% MTX</td><td colspan="5" rowspan="3">5 wt% MTX</td><td rowspan="8">PBS (no cells)</td><td rowspan="8">DMSO (no cells)</td></tr>
<tr><td>B</td></tr>
<tr><td>C</td></tr>
<tr><td>D</td><td colspan="5" rowspan="3">1 wt% MTX</td><td colspan="5" rowspan="3">10 wt% MTX</td></tr>
<tr><td>E</td></tr>
<tr><td>F</td></tr>
<tr><td>G</td><td colspan="5">PBS</td><td colspan="5">Medium</td></tr>
<tr><td>H</td><td colspan="5">DMSO</td><td colspan="5"></td></tr>
</table>

Figure 3.1: Diagram of a 96-well plate with MTX extracts from different loadings. A different plate was used for 1-, 7-, and 31-day extracts.

<table>
<tr><th></th><th>1</th><th>2</th><th>3</th><th>4</th><th>5</th><th>6</th><th>7</th><th>8</th><th>9</th><th>10</th><th>11</th><th>12</th></tr>
<tr><td>A</td><td rowspan="8">1 mg/ml</td><td rowspan="8">0.5 mg/ml</td><td rowspan="8">0.1 mg/ml</td><td rowspan="8">50 µg/ml</td><td rowspan="8">5 µg/ml</td><td rowspan="8">PBS</td><td rowspan="8">DMSO</td><td colspan="3" rowspan="8">Medium</td><td rowspan="8">PBS (no cells)</td><td rowspan="8">DMSO (no cells)</td></tr>
<tr><td>B</td></tr>
<tr><td>C</td></tr>
<tr><td>D</td></tr>
<tr><td>E</td></tr>
<tr><td>F</td></tr>
<tr><td>G</td></tr>
<tr><td>H</td></tr>
</table>

Figure 3.2: Diagram of a 96-well plate with fresh MTX solutions in the range of collected extracts.

3.7 Statistical Analysis

One-way analysis of variance (ANOVA) was used to compare the different drug loadings in Experiments 2-5 (Prism 6, GraphPad Software Inc., La Jolla, USA). The mean values of each measurement (t_w, t_s, T_g, CS, MTX release, ion release, and cell viability) were compared using the Tukey post-hoc test and the Brown-Forsythe test was applied to each ANOVA. Bar graphs demonstrate the measurement means, standard deviations, and statistical results using the following convention: $p \leq 0.05$ (*), $p \leq 0.01$ (**), $p \leq 0.001$ (***), and $p \leq 0.0001$ (****).

CHAPTER 4

Results & Discussion

This chapter aims to establish composition-property relationships for the MTX-loaded DG209-GIC to attempt to understand the effects of the drug on the material, the effects of the cement on the drug, and the mechanisms of MTX release from the GIC. The following subsections present the results obtained from the experiments outlined in Figure 2.1.

4.1 Preliminary Experimentation: Material Synthesis and Characterization

The primary objectives of this section were to (1) synthesize the DG209 glass, verify the material contained no identifiable crystalline species, and determine T_g to confirm repeatability of structural characteristics, and (2) determine the maximum threshold at which MTX could be loaded into the DG209-GIC in order to establish discrete drug loadings for subsequent testing.

4.1.1 DG209 Glass Characterization

X-ray diffraction results for the four batches of DG209 glass are provided in the Appendix. Resulting XRD patterns are characteristic of materials that are primary amorphous. Results for batches 1, 2, and 3 demonstrate narrowed peaks, which may be indicative of residual crystallinity. However, all glass batches demonstrated significantly similar t_w and thus residual crystallinity was considered negligible. Overall, XRD results satisfy the first part of the first objective of this experiment, suggesting all four batches were primarily amorphous, as published [4].

Differential scanning calorimetry results are also provided in the Appendix. No significant difference was found between the T_g of the four glass batches. The standard deviations (SD) for Batches 1, 2, and 4 fall within the accuracy of the system (± 2%); however, the SD of Batch 2 exceeded this accuracy, indicating there was likely some degree of variability throughout this batch. The average T_g across the four batches was calculated as 615°C, which is statistically similar to that reported by Dickey *et al.* [Dickey]. Using the averaged T_g, the annealing temperature was derived for subsequent material processing as follows: $T_{g\ (average)}$ - 30°C. Overall, T_g analysis satisfied the objective of this experiment through confirming repeatability across the four batches of synthesized glass, and suggesting the produced material matched that reported in the literature [4].

4.1.2 Preliminary MTX Loading Investigation: Results and Derivation of Drug Loadings

Results for the preliminary drug loading are summarized in Table 4.1. At 30 wt% MTX, it was not possible to obtain a cohesive cement paste. At 20 wt% MTX, the material did not set as per Section 3.2.3. At 15 wt% MTX, the material set in 556 sec; however, the material crumbled when removed from the mould. This may be indicative of chemical interference within the structural matrix of the cement. At 10 wt% MTX, the material satisfied the selection criteria – a cohesive, settable cement paste was obtained. Consequently, 10 wt% was established as the upper threshold for MTX loading.

Although it is apparent from these results the exact threshold of MTX addition fell between 10 and 15 wt%, 10 wt% was taken as the maximum loading on the basis that it is significantly higher than what is typically seen in the literature: <1 to 5 wt% for MTX-loaded PMMA investigations [1, 74, 78, 143]. For comparison purposes, the 1 to 5 wt% range was investigated; however, to further investigate the chemical effects of drug addition on the cement, it was desired that a significantly higher loading be analyzed as well. Therefore, 0, 1, 5, and 10 wt% loadings were selected to develop the composition-property relationships in Experiment 2-5.

Table 4.1: Preliminary drug loading investigation: (a) t_w for various MTX loadings; (b) t_s for various MTX loadings.

(a)

MTX Loading (wt%)	Average t_w (min:sec)
0	5:10
5	4:10
10	2:50
20	2:40
30	N/A

(b)

MTX Loading (wt%)	Average t_s (min:sec)
0	10:50
5	12:20
10	11:00
15	9:20
20	N/A

4.2 Experiment 1: Optimization of the DG209-GIC Formulation (P/L and AC)

A DOE approach was used to predict composition-property relationships for the DG209-GIC, and the resulting regression models were used to derive an optimal formulation (P/L and AC) according to a predetermined set of properties, specific to PVP (Table 2.2). It was hypothesized that the t_w of the DG209-GIC could be extended through careful material adjustments to improve its clinical utility. Heini and Berlemann stated that around 10 min of constant viscosity is required for controlled application in PVP [80]. Generally, 5-10 min of t_w is considered acceptable; however, in considering the recommendation of Heini and Berlemann, prolonging the t_w of the DG209-GIC is desirable.

4.2.1 General Responses

Table 4.2 outlines the general trends observed for t_w, t_s, and CS in response to varied P/L and AC. Figure 4.1 provides a graphical representation of the resulting models for these material responses, further depicting such trends.

Table 4.2: General trends in t_w, t_s, and CS in response to increase P/L and increase AC.

Factor Adjustment	Material Response	
↑ **P/L**	↓ t_w	540-120 sec when AC=40 wt% 450-120 sec when AC=50 wt% 640-100 sec when AC=60 wt%
	↓ t_s	700-140 sec when AC=40 wt% 1940-310 sec when AC=50 wt% 5220-720 sec when AC=60 wt%
	↑ CS*	24-54 MPa when AC=50 wt% 28-53 MPa when AC=60 wt%
↑ **AC**	↓ t_w	540-370 sec when P/L=1.0/1.0 250-180 sec when P/L=1.5/1.0 120-100 sec when P/L=2.0/1.0
	↑ t_s	700-5220 sec when P/L=1.0/1.0 280-1440 sec when P/L=1.5/1.0 140-720 sec when P/L=2.0/1.0
	↑ CS	21-28 MPa when P/L=1.0/1.0 26-45 MPa when P/L=1.5/1.0 21-53 MPa when P/L=2.0/1.0

*Note: No change in CS with ↑ P/L for AC=40 wt% (21 MPa)

Although discouraged by manufacturers, P/L and AC are often adjusted by practitioners to adjust the properties of conventional GICs for a specific dental application (*ie.* restoration, luting, or sealing) [131]. Consequently, the *individual* effects of P/L and AC on GIC performance have been well documented. Decreasing P/L ratio has been reported to increase both t_w and t_s, while decreasing CS [130, 131, 144]. It is accepted that these changes result from both a decrease in the reactivity of the material and the decreased proportion of reinforcing glass particles [130]. Conversely, increases in AC have been correlated with decreases in t_w and t_s, and increases in CS. Boyd *et al.* hypothesized that these observations resulted from increased reactivity of the neutralization reaction, as well as increases in the extent of matrix entanglement [97].

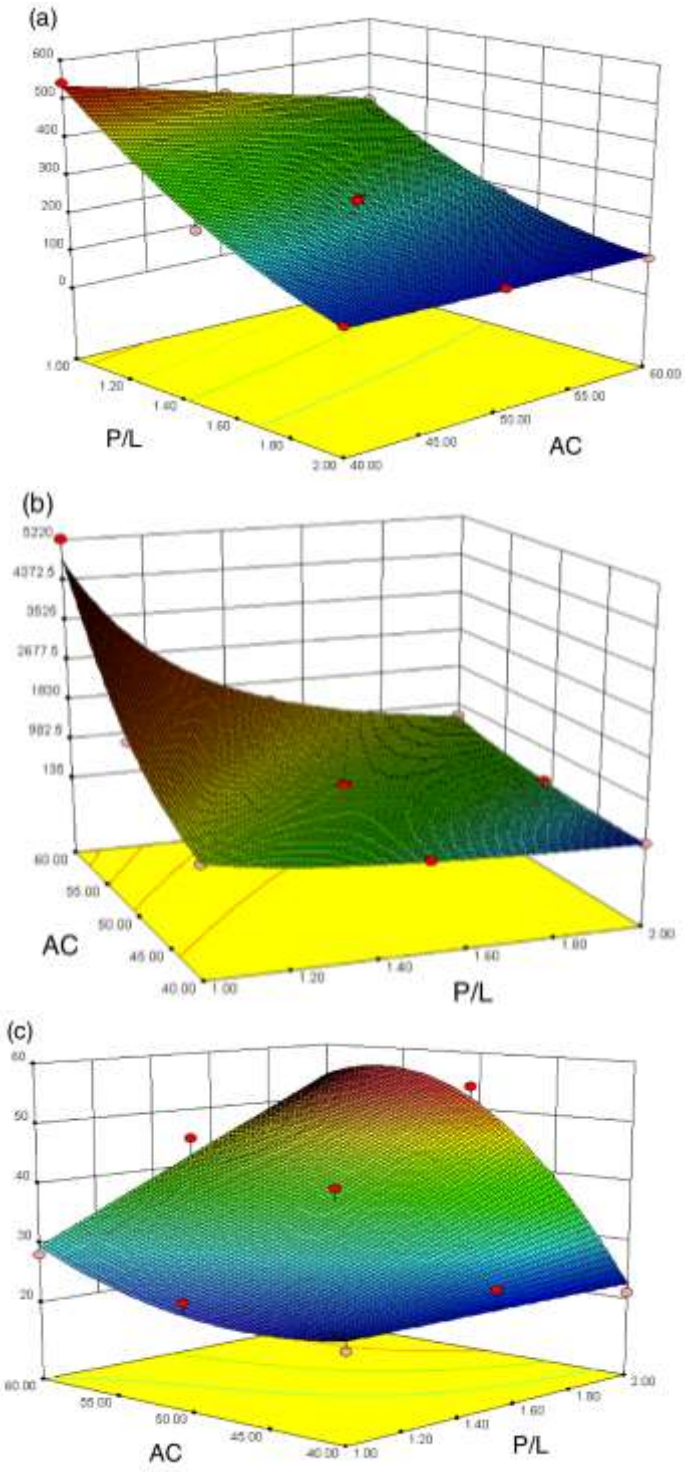

Figure 4.1: 3D contour plots showing the effect of varying P/L and AC on (a) t_w (sec), (b) t_s (sec), and (c) CS (MPa). Red circles indicate data points above the model; pink circles indicate data points below the model.

As outlined in Table 4.2, the responses modeled for t_w and CS are consistent with that reported for conventional GICs; increases in both P/L and AC decreased t_w and increased CS [129, 130]. However, unexpectedly, the response modeled for t_s was contrary to the literature; increases in AC with constant P/L increased t_s. At this point in time, the cause for this observation is unknown. Boyd et al. reported similar deviations in the t_s-AC trend when Sr was added to a Zn-glass at a molar fraction of 0.08 [97]. This group observed standard t_s-AC trends when Sr=0.0-0.04 molar fraction, which lead the authors to suggest Sr interfered with the effects of AC [97]. Although conclusions regarding these deviations cannot be drawn at this point in time, it is evident adjustments to glass composition significantly influence the effects of AC on setting behaviour.

4.2.2 Interpretation of Models and Optimization

The primary objective of this experiment was to determine the DG209-GIC formulation that produced the optimum balance in t_w, t_s, and CS (Table 2.2). Using the responses observed in the first part of this experiment, regression models were generated to mathematically describe the composition-property relationships, such that the optimal P/L-AC combination could be interpolated (Table 3.3) [145]. The backward regression method was used to automatically derive significant model coefficients, and the reduced polynomial models were further analyzed by ANOVA to show significant model terms. Table 4.3 summarizes the actual model terms and adequacies. Both the t_w and t_s responses show high model adequacies since (i) the adjusted R-squared (R^2_{adj}) and predicted R-squared (R^2_{pred}) values are within 0.20 of the R-squared, (ii) Prob>F values are less than 0.05, (iii) coefficients of variation (CV) are less than 10%, and (iv) adequate precision (AP) are greater than 4. The CS model also meets these requirements with the exception of (i) [142, 146].

In general, a high R-squared value indicates the data are close to the regression model; however, it cannot indicate whether the model is adequate. R-squared cannot distinguish between apparent increases in the goodness of fit due to additional model terms and over-modelling/modelling noise of the system. These

concerns were therefore addressed by computing R^2_{adj} and R^2_{pred} values; R^2_{adj} adjusts the R-squared value based on the number of model terms, while R^2_{pred} investigates concerns of over-fitting. Relatively high values were obtained for both values; therefore, the goodness of fit of each model was considered satisfied [146]. The Prob>F values represent the *p*-values for the test. Small *p*-values, as seen in Table 4.3, indicate that there is at least one significant effect in each model. The CV, which is the ratio of the standard error of estimates to the mean of the observed responses, is a measure of reproducibility, and the AP represents the range in the predicted response relative to the associated error. Both of these parameters were satisfied for the three models [146].

Table 4.3: Final regression equations and summarized ANOVA (CV: coefficient of variance; AP: adequate precision).

Response	Regression models	R^2	R^2_{adj}	R^2_{pred}	Prob>F	CV(%)	AP
t_w	$t_w = 1964.36 - 1297.29P/L - 15.55AC + 7.40P/L*AC + 194.76P/L^2$	0.9931	0.9897	0.9797	<0.0001	5.14	52.794
t_s	$1/\sqrt{t_s} = 0.066 + 0.098P/L - 0.0033AC - 0.00125P/L*AC + 0.0000336AC^2$	0.9978	0.9968	0.9893	<0.0001	2.47	110.634
CS	$CS = 577 - 470P/L - 22.49AC + 18.75P/L*AC + 0.216AC^2 - 0.175P/L*AC^2$	0.9639	0.9381	0.6617	<0.0001	7.83	17.524

Given the adequacy of the models and the acquired data, the criteria listed in Table 2.2 were used to interpolate a single formulation using the desirability objective function. Using this approach, the geometric mean of all individual desirability functions was computed, and a relative importance was assigned to each response (Table 4.4). The limits of the desirability ranges were adjusted several times to yield the best possible balance in predicted t_w, t_s, and CS that maximized the desirability function; Table 4.4 outlines the best possible set. Figure 4.2 depicts, using a 2D surface plot, the desirable region for this optimal formulation. Based on this data, P/L=1.2/1.0 and AC=56% were predicted as the best in class formulation.

Table 4.4: Optimization design criteria.

Factors	Goal	Lower Limit	Upper Limit	Importance
t_w	maximize	-	-	+++
t_s	in range	minimum	2000 sec	+++
CS	in range	32 MPa	maximum	+++

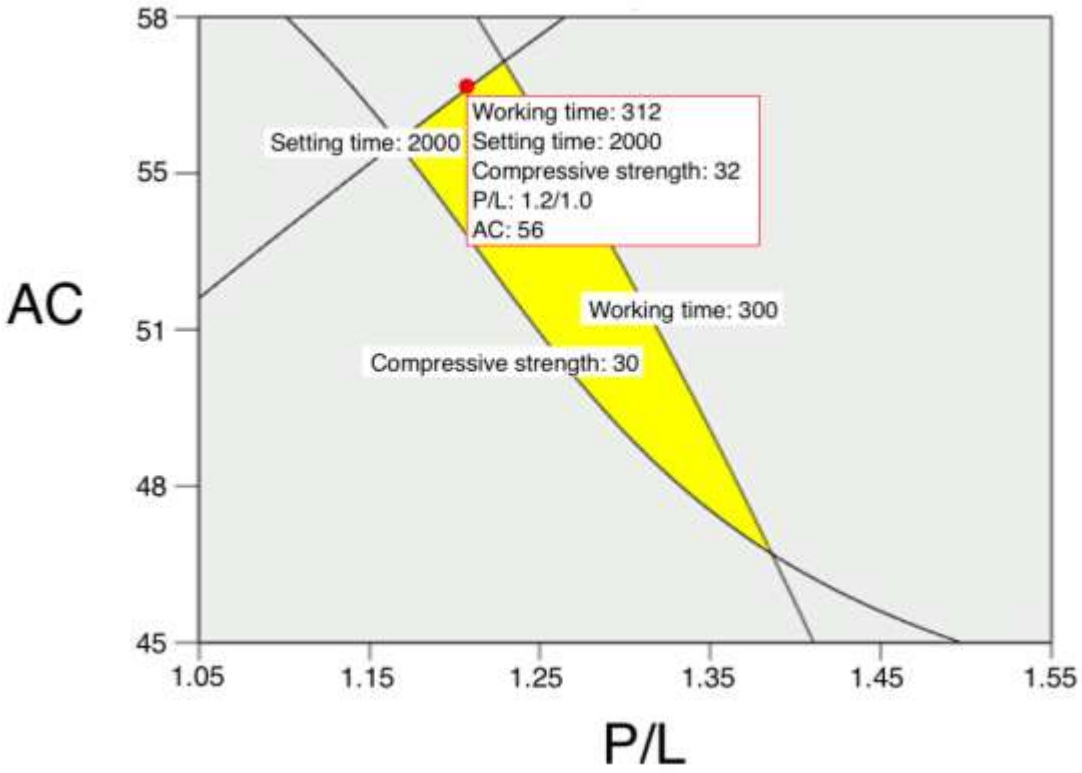

Figure 4.2: Overlay plot showing the region of the optimal formulation; the yellow region satisfies the design parameters.

Using this formulation, t_w, t_s, and CS were measured to validate the model predictions. Table 4.5 summarizes the predicted and experimental values obtained.

Table 4.5: Comparison of model generated predictions and experimental measurements using P/L=1.2/1.0 and AC=56%, and experimental measurements when using P/L=1.5/1.0 and AC=50% (centroid design point).

Factor	Predicted (P/L=1.2/1.0, AC=56%)	Experimental (P/L=1.2/1.0, AC=56%)	Experimental (P/L=1.5/1.0, AC=50%)
t_w (min:s)	5:10	3:40	4:10
t_s (min:s)	33:20	34:00	10:40
CS (MPa)	32	28.5	39

The measured t_w deviated from the predicted t_w significantly, while the measured t_s and CS were not significantly different from what was predicted (1-way ANOVA). It is questionable, however, whether this deviation in t_w is real, or whether it is due to experimental error. The reliability of the ISO standards for dental materials has been subject to major criticism, as mixing technique, environment conditions, operator experience, and fatigue have all been identified as possible causes for variability across results [138]. Nonetheless, the centroid design point (P/L=1.5/1.0 and AC=50%) yielded a combination of t_w, t_s, and CS that more closely matched the desired criteria (also shown in Table 4.5). This cement formulation was selected as optimal and was used for subsequent experimentation instead of the formulation derived by the model.

★★★

While the individual effects of P/L and AC on GICs are well established, there are currently no studies that report the effects of adjusting *both* P/L and AC, and significant question remains about their combined effect on GIC properties. Therefore, Design Expert 8.0.4 was used to develop a DOE in which *both* P/L and AC were varied to establish composition-property relationships that described their combined effects. A central composite, response surface design type was selected because it enables augmentation of a first-order design to a second-order design without requiring a full three-level factorial experiment. A first-order design consisting of four factorial points was augmented through simply adding orthogonal axial points and replicating the center point. These points are in accordance with Scheffe's proposal that the interesting points of a design space are at the top, the middle of the sides, the middle of the faces, and the center of gravity. The responses were modeled using multiple linear regression, and the F-test was used to validate their adequacies. The quadratic and cubic responses modeled for t_w and CS, respectively, captured the mean structure; however, no polynomial response adequately described the raw t_s response. To address the non-normality of the variance in this response, and improve the quality of fit, a transformation was applied to the t_s data. The Design Expert Box-Cox plot recommended applying a power

transformation of lambda=0.75. When applied, the transformed data demonstrated a definite improvement in the ANOVA.

Although the regression models have been adequate in predicting the P/L and AC for a particular set of factors, the models proved to be a poor predictor of an optimal P/L and AC. This likely indicates a problem with the desirability approach, since the models showed relatively high adequacies. The desirability function uses response functions and target value specifications to derive a single function, which is maximized to determine near optimal conditions. The quality of the output is determined by the size of the prediction variance, which depends on the design matrix itself [161]. Any issues in the robustness of the procedures used to acquire the data may result in small changes in the inputted variables, resulting in big changes in the responses, and thus the model's predictive power [162]. As mentioned above, the procedure for t_w has been subject to major criticism; this is also the case for t_s and CS as well [132].

4.2.3 Summary of the Optimization of the DG209 Cement Formulation

The wide range in t_w, t_s, and CS observed in this experiment suggest that the DG209-GIC may be tailored, like conventional GICs, through adjusting the P/L and/or AC. The response of these properties to varied P/L and AC encompass the desired criteria for PVP/PKP (Table 2.2): t_w ranged from 100 to 640 sec, t_s varied between 140 and 5220 sec, and CS was modulated from 21 to 53 MPa. Unfortunately, the generated composition-property relationships were insufficient in predicting an optimum formulation; experimental t_w differed statistically from that predicted by the model. The poor optimization power of the regression models may be attributed to the variance within the acquired data and/or the suboptimal methods used to acquire the data [138]. A single design point within the DOE, the centroid: P/L=1.5/1.0 and AC=50%, provided superior properties as compared to the formulation derived by the models. Therefore, this formulation was used for the drug loading and release experiments discussed in the subsequent sections.

4.3 Experiment 2: Handling Properties (t_w and t_s) of the MTX-Loaded DG209-GIC

This experiment examined the effects of MTX addition on the handling properties of the optimized DG209-GIC. Figure 4.3 summarizes the measured t_w and t_s for the 0, 1, 5, and 10 wt% MTX DG209-GICs. The addition of MTX significantly decreased t_w from 230 to 190 sec; however, there was no significant difference in t_w found between different MTX loadings (1-way ANOVA) (Figure 4.3). The 5 wt% MTX DG209-GIC had a significantly higher t_s than the 0, 1, and 10 wt% MTX DG209-GICs; however, no general trend in t_s was observed in this loading range.

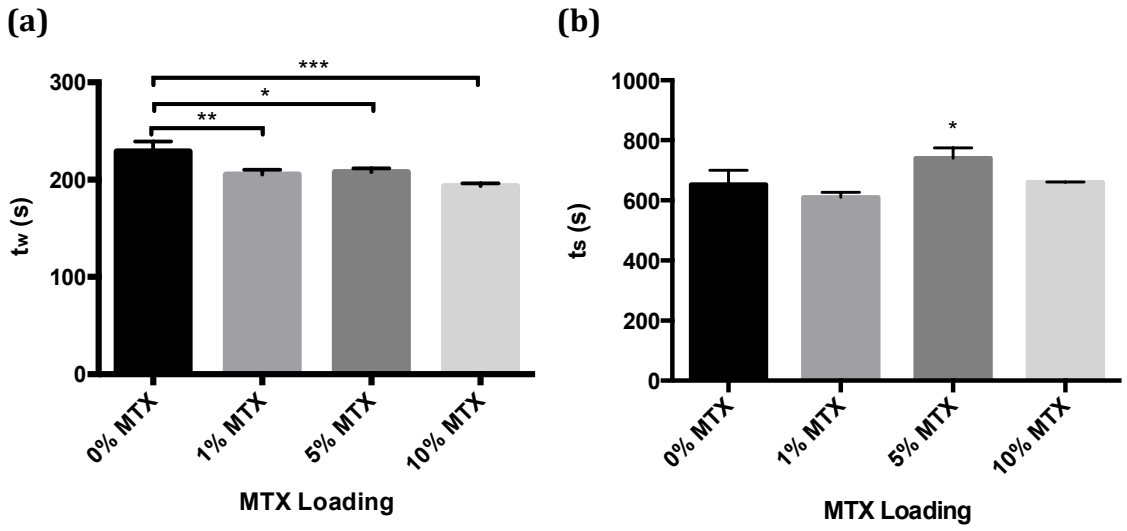

Figure 4.3: General trends in (a) t_w and (b) t_s with MTX addition.

The effect of MTX addition on t_w is similar to that observed for increased AC, as discussed in Section 4.2.1: MTX addition significantly reduced the t_w of the material. As MTX is a dicarboxylic acid, the drug could hypothetically increase the proton attack on the glass particles, increasing the overall reactivity of the setting process. Consistent with this idea would be an observed increase in t_s with MTX addition, as discussed in Section 4.2.1; however, as evidenced from Figure 4.3, no general trend in t_s was found in this experiment. Interestingly, in the preliminary experimental drug loading investigation (Section 4.1.2), 20 wt% MTX extended t_s indefinitely. This is worth mentioning, as it may be indicative of effects of increased acidity. Together, the

results of t_w and t_s suggest MTX may exert similar effects on the DG209-GIC setting process as those reported for increased AC, though no significant trends were observed between the 1 and 10 wt% loadings.

In the literature, similar effects to handling properties have been reported when the cationic bactericidal agent, chlorhexidine (CHX) was added to conventional GICs [121, 147]. Takashi *et al.* reported increases in t_s by 15 to 30 sec when CHX was loaded into a dental GIC at 2 to 3 wt%, respectively [121]. Palmer *et al.* also showed increases in t_s (by 12 to 18 min) with CHX addition (up to approximately 11 wt%), as well as increases in t_w (by 1.8 to 3.6 min), although this group adjusted the P/L of the material [147]. To describe the drug-cement interactions, Palmer *et al.* proposed the cationic, proton-pulling, properties of CHX may have interfered with the proton attack on the glass and/or the ion release from the glass [147]. Modifications of this theory may describe MTX behaviour in the DG209-GIC. MTX is likely an anionic molecule in the GIC system and thus its addition may both increase the proton attack on the glass and sequester released glass cations.

Overall, the results of this experiment suggest MTX may be loaded into the DG209-GIC up to 10 wt% with minimal effects to GIC handling. The maximum time difference between the t_w for the 0 wt% cement and MTX-loaded GICs was approximately 30 sec. As the optimized DG209-GIC (unloaded) falls short of the clinical requirements for t_w (Table 2.2), the reductions in t_w observed in this study suggest that drug loading would significantly compromise the application of this material in injectable procedures. However, should the t_w of the unloaded DG209-GIC be improved (extended), MTX addition would likely not compromise the clinical utility of this material. The DG209-GIC may be loaded up to 10 wt% with only losing 30 sec (maximum) of t_w.

4.4 Experiment 3: MTX and Ion Release from the MTX-Loaded DG209-GICs

The release investigation of this thesis work was divided into two sections: Part 1 involved quantification and characterization of MTX release, while Part 2 examined the ion release behaviour of the system.

4.4.1 MTX Release

This experiment compared the release of MTX from the 1, 5, and 10 wt% MTX DG209-GICs over 31 days. Compression cylinders were synthesized for each DG209-GIC, and each cylinder was immersed in PBS. The PBS was changed after one hour, daily for 10 days, and then again on days 30 and 31 to ensure the activity of the released drug could be tested over time (results for cytotoxicity testing shown in Section 4.6). The volume of PBS was adjusted as follows: 10 ml for the first hour and first day, 5 ml for the second day, and 2.5 ml for the remaining time points, in order to meet sink conditions and ensure that drug concentrations exceeded the minimum detection limit. The release profiles were examined in Prism 6 to compare the release efficiencies, $t_{1/2}$, and $t_{plateau}$ of the different MTX release profiles, and to apply kinetic models in an attempt to predict the mechanisms of release.

4.4.1.1 Quantification of Drug Release

Figure 4.4 (a-c) shows the raw MTX release profiles from the 1, 5, and 10 wt% MTX DG209-GICs. It is apparent that, for each GIC, there was an initial burst release over the first 24 h, which was followed by a significantly slower release for the remainder of the incubation period. Although increased drug loading significantly increased the amount of MTX released at each time point, increased drug loading did not significantly impact the percentage of MTX released, as shown in Table 4.6.

Table 4.6: Release efficiency values for the 1, 5, and 10 wt% DG209-GICs after 31 days.

MTX-Loading in DG209-GIC	Release Efficiency
1 wt%	1.7%
5 wt%	1.4%
10 wt%	1.7%

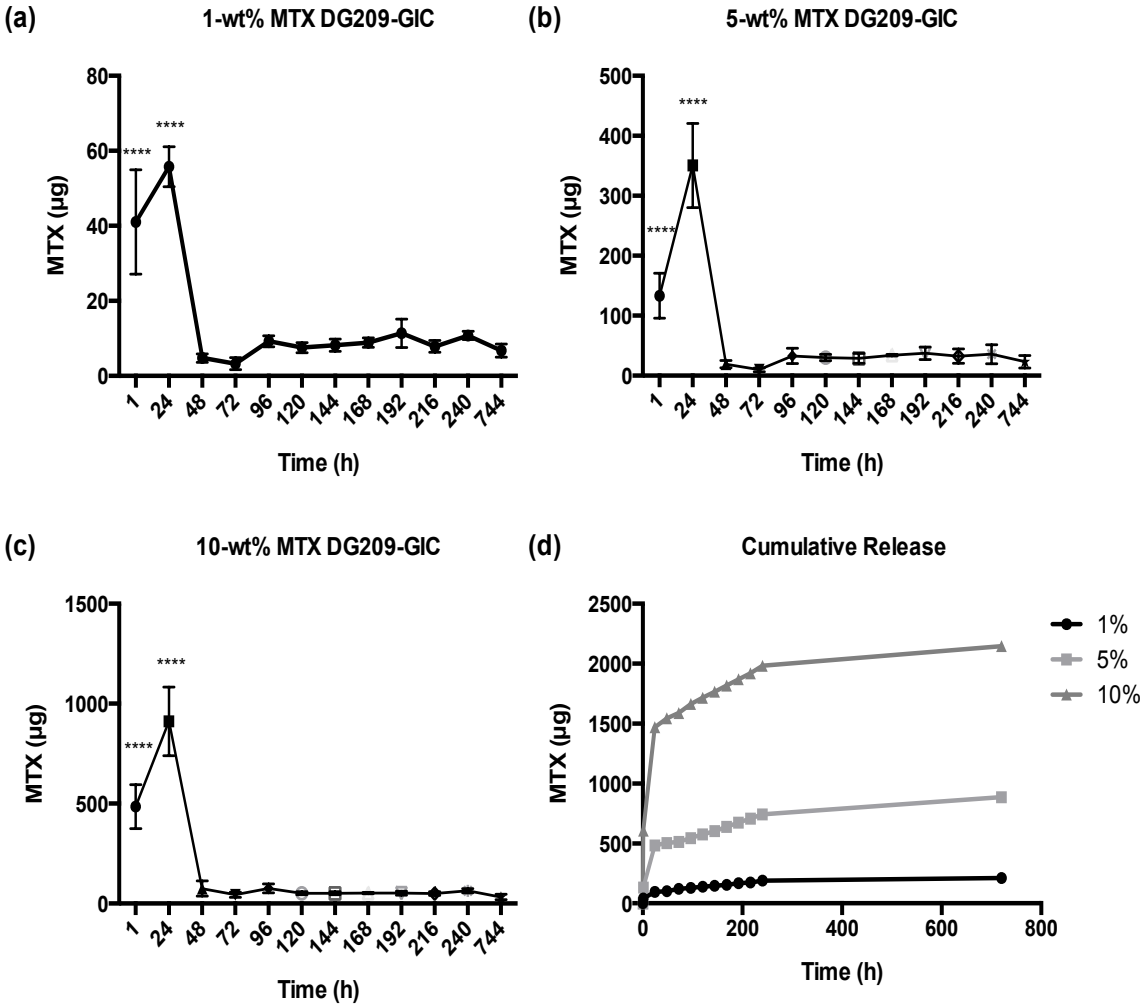

Figure 4.4: (a-c) Raw MTX release profiles (µg) for the 1, 5, and 10 wt% MTX DG209-GICs over 31 days (744 hours); (d) Cumulative MTX release profiles (µg) over 31 days (744 hours).

These results are comparable to MTX release reports from MTX-loaded PMMA [1, 57, 78]. Two phases of release were observed, though the time points at which the different release phases terminated/began differed: Hernigou *et al.* reported an initial rapid release over the first 2 hours, which decreased over the next 18 hours, and decreased further thereafter [78]; Maccauro *et al.* described an initial burst release within the first 5 min, with a rapid decay in the rate of MTX release thereafter, lasting for the 30-day test period [1]; and Gouran *et al.* found an initial burst release during the first day, which dramatically declined after the third [57]. These groups found that the highest MTX loading released the lowest percentage of incorporated drug, which suggests the higher MTX loadings were less efficient [1, 57]. Maccauro *et al.* proposed that initial release was driven by the surface characteristics of the cement and was related to the concentration of drug incorporated. Following this initial release phase, efficiency was affected by the bulk porosity of the cement. At later time points, release was impeded as the drug was entrapped in the PMMA; higher drug concentrations resulted in a larger amount of entrapped drug [1]. In the present experiment, no significant difference in release efficiency was found across the different MTX loadings (Table 4.6). However, the theory developed by Maccauro *et al.* may translate to the present work, as the heightened burst release (seen with the higher drug-loaded GICs) may offset the increase in amount of drug entrapped. Average release efficiency values reported by these groups varied between 6% and 10% [57, 78]. These are remarkably higher than that found for the DG209-GIC in the present work (Table 4.6), though it is difficult to accurately compare these results since (1) the surface-area-to-release-media ratios are not consistent (8.5 mm by 7.5 mm diameter samples and 4 mm by 3 mm diameter samples were used by Hernigou *et al.* and Gouran *et al.*, respectively, which 6 mm by 4 mm diameter samples were used in the present experiment), and (2) the release media differed (PBS and cell culture media were used by Hernigou *et al.* and Gouran *et al.*, respectively, while PBS was used in the current work) [57, 78].

As compared to antibiotic release from conventional GICs, the MTX-DG209-GICs demonstrated similar shaped release profiles [123, 147]. Palmer *et al*. observed

an initial burst release over the first 4 hours, which significantly decreased over the following 5-50 days, depending on the initial loading, and then plateaued thereafter. These authors proposed that the two phases of release resulted from two different mechanisms: an initial washout before the GIC fully set, followed by a slow diffusion-controlled process [147]. This theory may be applicable to the MTX-DG209-GIC system. The release efficiencies of conventional GIC delivery systems are significantly higher that those of the DG209-GIC [123, 147]. Palmer *et al.* found that between 3% and 10% of the initial drug (CHA) load was released over 240 days, and that these efficiencies were primarily dependent on the initial loading, as higher loadings resulted in higher release efficiencies [147]. Conversely, Takahashi *et al.* found that higher CHA loadings yielded lower release efficiencies from a GIC [121]. Although these authors reported similar release methods, it is difficult to compare these release reports as Palmer adjusted the P/L for different CHA loadings, while Takahashi did not [121, 147]. To explain these efficiency values, the authors proposed that CHA may be chemically or physically bound within the GIC matrix, thereby preventing full release, or that an equilibrium may have been established between CHA and GIC ions, also resulting in prevented release [147]. The relative increase in release with increased CHA loading, as seen in both the Takahashi and Palmer works, supports the former proposal, as a higher proportion of "free" CHA would be available for release in the higher drug loaded GICs [121, 147]. This idea may be extrapolated to this experiment as well, as higher MTX loadings resulted in higher release.

4.4.1.2 Comparison of Release Profiles

The cumulative release data, shown in Figure 4.4 (d), was compared using Prism 6 using exponential models to examine the effects of MTX loading on the general shape of the release profile. A comparison of a one-phase association model and a two-phase association model is shown in Table 4.8. Since the two models had a different number of parameters, the comparison could not be made simply based on which had the smaller sum-of-squares or larger R-squared value (goodness of fit); the two-phase association model had more parameters and thus more inflections points, which

automatically lead it closer to the actual data more frequently. To avoid this bias, the F-test was used to compare the improvements in the fit that were due to an increase in the number of parameters (using the difference in the sum-of-squares), and the improvements that were a result of pure chance (derived from the number of data points). A *p*-value of less than 0.05 was derived from this comparison, and therefore the one-phase model, which was set as the null hypothesis, was rejected. Table 4.8 outlines the generated model terms and applied diagnostics.

Table 4.7: Comparison of fits: one-phase association model versus two-phase association model. The two-phase association model best describes the MTX release profiles of the 1, 5, and 10 wt% MTX DG209-GICs.

Comparison of Fits	1% MTX	5% MTX	10% MTX
Null hypothesis	One-phase association	One-phase association	One-phase association
Alternative hypothesis	Two phase association	Two phase association	Two phase association
P value	< 0.0001	< 0.0001	< 0.0001
Conclusion (alpha = 0.05)	Reject null hypothesis	Reject null hypothesis	Reject null hypothesis
Preferred model	Two phase association	Two phase association	Two phase association
F (DFn, DFd)	13.65 (2,56)	56.60 (2,56)	19.11 (2,56)

Table 4.8: (a) Best-fit values and diagnostic results for the one-phase association model; (b) Best-fit values and diagnostic results for the two-phase association model.

(a)	One-phase association	1% MTX	5% MTX	10% MTX
	Best-fit values			
	Y0	= 0.0	= 0.0	= 0.0
	Plateau	181.3	668.6	1750
	Half-time	45.17	22.09	1.626
	95% Confidence Intervals			
	Plateau	160.8 to 201.8	625.0 to 712.2	1671 to 1828
	Half-time	33.28 to 70.28	16.57 to 33.10	1.076 to 3.328
	Hougaard's Measure of Skewness			
	Plateau	0.3060	0.1202	3.800e-005
	Goodness of Fit			
	R square	0.6966	0.7779	0.8053
	Normality of Residuals			
	P value	0.1457	0.0299	0.6869
	Passed normality test (alpha=0.05)?	Yes	No	Yes
	Replicates test for lack of fit			
	Discrepancy (F)	2.415	10.36	3.300
	P value	0.0204	< 0.0001	0.0025
	Evidence of inadequate model?	Yes	Yes	Yes

Table 4.8: (a) Best-fit values and diagnostic results for the one-phase association model; (b) Best-fit values and diagnostic results for the two-phase association model.

(b)	Two phase association	1% MTX	5% MTX	10% MTX
	Best-fit values			
	Plateau	215.5	941.2	2176
	Y0	= 0.0	= 0.0	= 0.0
	Fast HalfLife	0.9196	1.864	1.189
	Slow HalfLife	133.2	216.2	141.8
	95% Confidence Intervals			
	Plateau	183.8 to 247.3	825.0 to 1057	1930 to 2422
	PercentFast	22.96 to 47.69	38.98 to 51.11	52.99 to 72.62
	Fast HalfLife	0.4374 to +infinity	1.183 to 4.392	0.8045 to 2.280
	Slow HalfLife	83.97 to 322.0	142.2 to 451.0	80.01 to 624.1
	Hougaard's Measure of Skewness			
	Plateau	0.4330	0.8968	0.6417
	Goodness of Fit			
	R square	0.7961	0.9265	0.8843
	Normality of Residuals			
	P value	0.2897	0.6427	0.4198
	Passed normality test (alpha=0.05)?	Yes	Yes	Yes
	Replicates test for lack of fit			
	Discrepancy (F)	0.06262	0.2723	0.01814
	P value	0.9998	0.9719	1.0000
	Evidence of inadequate model?	No	No	No

To assess the validity of the model's predictions, Hougaard's test was applied to quantify the skew of the generated parameters. The two-phase model demonstrated noticeable skew, with Hougaard's values ranging between 0.25-1.00, while the one-phase model demonstrated a wider range of Hougaard's values, some ideal, and some concerning* [148]. The skew of the chosen model may explain the broad confidence intervals. The D'Agostino-Pearson Test for normality and the Replicates Test were also applied to the models to assess the distribution of the data around the model and the lack of fit, respectively. The two-phase model passed both of these tests, while the one-phase did not [148].

In conclusion, the two-phase association model fit the release profiles better than the one-phase association model. The chosen models are likely adequate in

*Typically, values <0.10 are ideal (almost linear), values between 0.10-0.25 are adequate, values between 0.25-1.00 are concerning, and values >1.00 indicate the model is not appropriate.

detailing the general trends for MTX release, but they are not sufficient for deriving exact time points. Consequently, these models were not used to compare the effects of MTX loading on the shape of the release profiles.

4.4.1.3 Drug Release Kinetics

To describe the release kinetics and attempt to understand the underlying mechanisms, the release profiles were modeled using various analytical definitions specific to diffusion, erosion, and dissolution. Since the release profiles were biphasic, it was evident that the release data would not fit a zero-order or first-order rate, as these relationships describe processes with constant release rates. Consequently, the Higuchi, Korsmeyer Peppas (KP), and the Hopfenberg models were applied [75]. Table 4.9 summarizes the R-squared values for each of these kinetic models.

Table 4.9: Summary of the R-squared values computed for each kinetic model.

Kinetic Model	1% MTX	5% MTX	10% MTX
Higuchi	0.6855	0.7731	0.6094
Korsmeyer Peppas	0.9392	0.9264	0.9290
Hopfenberg	0.5559	0.4248	0.2264

4.4.1.3.1 Higuchi release kinetics

The Higuchi model was applicable to the results of this experiment since (i) the initial drug concentration in the system was significantly higher than the drug solubility, (ii) the size of the drug particles was much smaller than the release device, (iii) the carrier material did not swell or dissolve, and (iv) the diffusion coefficient of the drug was assumed constant [75]. Higuchi describes drug release in terms of a diffusion process that is based on Fick's law; it is square-root-time-dependent, as shown:

$$M_t = A\left[\frac{D\varepsilon}{\tau} C_s(2C_0 - \varepsilon C_s)t\right]^{\frac{1}{2}}$$

where M_t is the amount of drug released in time (t), A is surface area, D is the diffusion coefficient, ε is the cement porosity, τ is the tortuosity of the cement, C_s is the solubility of the drug, and C_0 is the initial drug loading [75].

The R-squared values, shown in Table 4.9, indicated that the Higuchi model did not adequately describe the results of this experiment; the plot of percent-drug-release vs. square-root-time showed poor linearity, as depicted in Figure 4.5 (a).

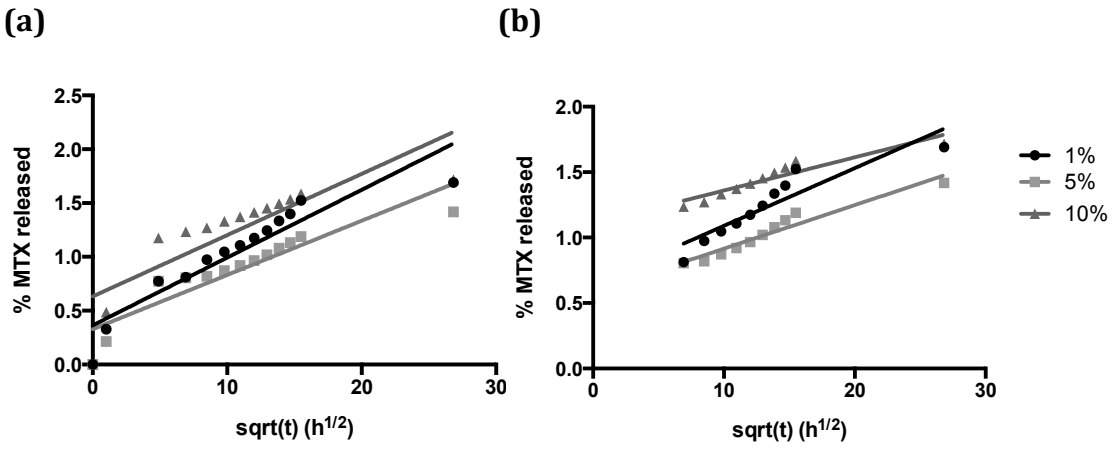

Figure 4.5: Application of the Higuchi model to the 1, 5, and 10 wt% DG209-GIC release profiles: percentage of MTX released in reference to the total amount of MTX released versus square-root-time (SD not shown). (a) Entire release period; (b) Release excluding the first three time points.

To determine whether the rate-limiting step or the sustained release involved diffusion, this model was applied to the 0- to 24-hour and the 48- to 720-hour time points, independently. Neither approach improved the R-squared values. However, when the averages for each data point were modeled using the Higuchi model, significant improvements to the R-squared values were observed. When the entire data set was modeled, the resulting R-squared values were 0.8639, 0.8379, and 0.6908 for the 1, 5, and 10 wt% MTX releases, respectively. Even greater improvements in R-squared values were found for the 5 and 10 wt% MTX releases when the first three time points (0- to 24-hours) were excluded from the model: 0.8444, 0.9354, and 0.8851 for the 1, 5, and 10 wt% MTX releases, respectively. This improvement is depicted in Figure 4.5 (b). This correction suggests that diffusion may be a primary mechanism of release for the 1, 5, and 10 wt% MTX DG209-GICs, and

that the poor fit seen in the initial application of the model was a result of the variability in the data. This idea is further supported by the tightening of the confidence intervals seen when the first three data points were excluded from the analysis, as shown in Table 4.10.

Table 4.10: A comparison of the 95% confidence intervals for slope when the Higuchi model was applied to the entire data set versus the data set excluding the 0-24 h time points.

	Entire Data Set	**Data Set Excluding Burst Release**
1% MTX	0.1562 to 0.5716	0.4298 to 0.8679
5% MTX	0.1434 to 0.5120	0.4819 to 0.6842
10% MTX	0.3155 to 0.9490	1.000 to 1.212

4.4.1.3.2 Korsmeyer-Peppas release kinetics

The KP model is a semi-empirical model that is often used to predict primary release mechanisms for polymeric systems. This model is only relevant to the first 60% of the drug release; consequently, the R-squared values in Table 4.9 only correspond to the first 60% of the total drug release [75]. The following equation was used to define the release exponent, *n:*

$$M_t/M_\infty = Kt^n$$

where M_t/M_∞ is the fraction of drug released at time, t, and K is the release rate constant. The n values were calculated as 0.2102, 0.2224, and 0.2155 for the 1, 5, and 10 wt% MTX DG209-GICs, respectively. Based on the KP definitions, these n values indicate that the primary mechanism of drug release was Fickian diffusion, and that release was not affected by erosion. Like what was seen for the Higuchi model, the R-squared values improved when the average of each data point was considered: 0.9914, 0.9485, and 0.9703 were derived for the 1, 5, and 10 wt% MTX releases when the averages of each data point were modeled. Again, this suggests that the variability in the data compromised the fit of the model.

Taken together with the results from the application of the Higuchi model, these results suggest that diffusion plays a key role in the release of MTX from the

DG209-GIC system. To confirm this, the Hopfenberg model was applied to rule out any potential influences of erosion.

4.4.1.3.3 Hopfenberg release kinetics

The Hopfenberg model was applied to investigate whether MTX addition interrupted the structural integrity of the GIC matrix. This model describes drug release from surface eroding polymers [75]. Palmer *et al.* hypothesized that CHA addition to a conventional GIC interfered with the acid-base setting reaction, and ultimately caused a breakdown of the structure at higher drug loadings. This idea was based on the observed decrease in CS [147]. Therefore, in order to predict whether MTX addition would cause erosion of the DG209-GIC, the following equation was applied each release profile:

$$M_t/M_\infty = 1 - \left[1 - \frac{k_0 t}{C_L a}\right]^n$$

where k_0 is the zero order rate constant that describes surface erosion, C_L is the initial drug loading, a is radius of the cylinder, and n=2 for cylindrical samples. The low R^2 values, shown in Table 4.9, suggest this model did not fit the data adequately, which implies erosion was not an influential factor in this release system.

★★★

In conclusion, MTX release from the DG209-GIC system was biphasic, demonstrating relatively low release efficiencies ranging 1.4% to 1.7%. Drug release was best characterized by the two-phase association model, although model adequacies were too low for deriving precise values to describe the release profiles ($t_{1/2}$ and $t_{plateau}$). In terms of kinetic release models, the KP model fit the data best, with n values <0.45, suggesting that MTX release occurred primarily through Fickian diffusion. These results are supported by the relatively good linearization of the Higuchi model, especially when the averages of each data point were modeled, and agree with the poor fit for the Hopfenberg model.

Overall, understanding the mechanisms of release for bone cement delivery systems is crucial for tailoring release and predicting cement behaviour *in vivo.* Given the results of this study, it is evident release efficiency merits improvement. In understanding release was primarily diffusion-mediated, methods, such as increasing porosity and wettability, may be implemented to ameliorate the efficiency issue [46]. This topic is further discussed below in Future Research Directions, Section 5.2.

4.4.2 Part 2: Ion Release

This supplementary experiment aimed to quantify ion release over time to investigate if MTX addition influenced the ionic activity of the DG209-GIC and to examine whether ion release correlated with any of the findings from the other experiments. It was proposed that relating MTX loading with ion release might provide support for theories involving the chemical interactions of MTX in the GIC matrix (developed from Experiments 2-5). Figure 4.6 summarizes the findings for the Zn^{2+}, Sr^{2+}, Si^{4+}, Ge^{4+}, and Ca^{2+} releases at 1, 7, and 31 days. No significance was found in the Na^{+} release from the system, as the sodium content of the PBS incubating solution saturated the system. Additionally, no Zr^{4+} release was measured from any of the GICs at any of the time points.

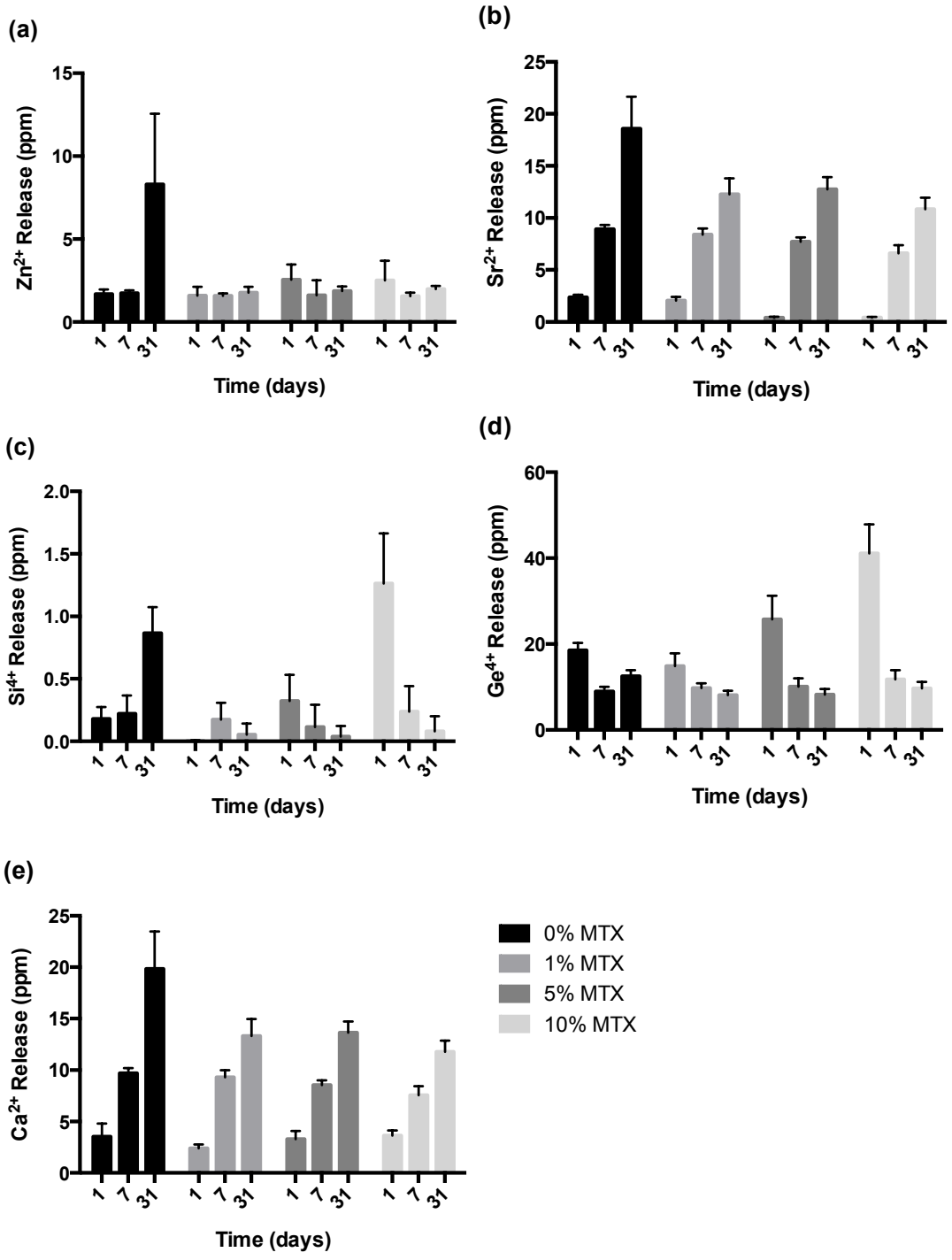

Figure 4.6: Ion release profiles (ppm) at 1, 7, and 31 days for 0, 1, 5, and 10 wt% MTX loadings. Ion concentrations represent ion release over the 24 hours preceding the time point.

At 1-day, the 10 wt% MTX DG209-GIC extracts showed significantly higher Ge^{4+} and Si^{2+} release in comparison to the 0, 1, and 5 wt% extracts. No other significant trends were observed at this time point. For the 7-day extracts, no significant differences were found in Ge^{4+} or Si^{2+} content across the different MTX-GICs; however, it appears that MTX addition significantly decreased Sr^{2+} and Ca^{2+} release at higher concentrations. At 7 days, the Sr^{2+} content of the 10 wt% MTX DG209-GIC was significantly lower than that of all other GICs, and the 5 wt% loading showed significantly lower Sr^{2+} release in comparison to the control (0 wt%). Additionally, Ca^{2+} content in the 10 wt% MTX DG209-GIC 7-day extracts was significantly lower in comparison to the 0 and 1 wt% MTX DG209-GIC extracts. At 31 days, all ion releases significantly decreased for each MTX loading, as compared to the control (0 wt%), though no significant decrease was observed between MTX loadings.

In terms of ion release over time, Ge^{4+} content of the 31-day extracts was significantly lower than that of the 1-day extracts for the 1, 5, and 10 wt% MTX DG209-GICs. Silica content of the 31-day 0 wt% MTX DG209-GIC extracts was significantly higher than that of the 1- and 7-day extracts, while the 1-day 10 wt% MTX DG209-GIC extracts showed significantly higher Si^{2+} release, as compared to the 7- and 31-day extracts. No significant difference was found in Si^{2+} release for the 1 and 5 wt% MTX DG209-GICs over time. For Sr^{2+} release, the 31-day extracts yielded significantly higher ppm, as compared to the other two time points, for all GICs. Finally, all GICs showed significant increases in Ca^{2+} over time.

Overall, the main objective in completing this analysis was to investigate whether MTX addition affected the ion release behaviour of the DG209-GICs. Cross-referencing the ion release data with the finding of the other experiments may support theories regarding the chemical nature of the drug in the cement matrix. Since MTX is a dicarboxylic acid, it may contribute to the proton attack during neutralization setting reaction of the GIC. This theory is supported by the increase in Ge^{4+} and Si^{2+} release seen in the 1-day extracts for the 10 wt% MTX DG209-GIC. The 1-day time point is of significant interest, as the GIC is in the early phase of the continued neutralized reaction, described by Nicholson *et al.* [108]. Increases in ion

release during this time period may be indicative of increases in the proton attack on the glass. This may correlate with the decreases in t_w observed in Experiment 2, which likely resulted from an increase in setting reactivity. Moreover, the observed decrease in the release of all ions at 31 days with increased MTX loading further suggests MTX chemically interfered with the GIC matrix. It is possible that MTX, which is likely an anion in the cement matrix, sequestered released glass cations, binding itself to the PAA of the GIC matrix. This theory may be supported by the relatively low release of the drug.

4.5 Experiment 4: Compressive Strength of the MTX-Loaded DG209-GICs

The primary objective of this experiment was to examine whether MTX loading compromised the mechanical integrity of the DG209-GIC. CS was used as a preliminary measure of mechanical strength, though it should be appreciated that there are several mechanical tests that must be performed prior to confirming MTX loading does not compromise strength. Cement cylinders were prepared and incubated exactly as those used for release experimentation (Experiment 3, Part 1) in order to accurately correlate strength findings with those of release.

The 1-, 7-, and 31-day CSs of the DG209-GICs are summarized in Figure 4.7. All DG209-GICs provided CSs that exceed that of the ideal bone cement: 30 MPa (Table 1.6). It was hypothesized that the addition of MTX would decrease the CS of the DG209-GIC. The results show no significant difference in CS between different MTX loadings after 1 or 7 days of incubation; however, it appears the 1 wt% MTX DG209-GIC had a significantly higher 31-day CS as compared to the other GICs (statistics shown in red in Figure 4.7). This was the only significance found between different MTX loadings.

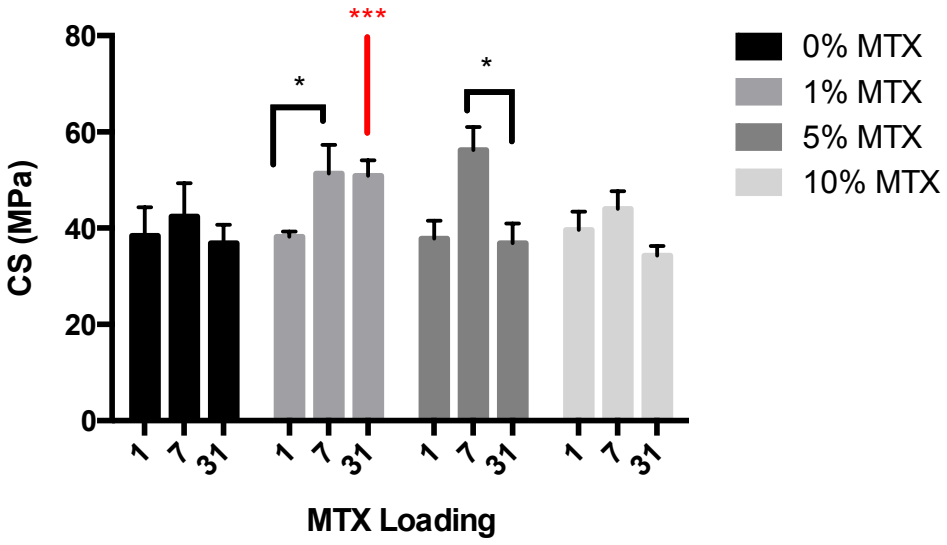

Figure 4.7: 1-, 7-, and 31- day CSs for the 0, 1, 5, and 10 wt% MTX DG209-GICs. Statistics shown in black refer to significance across different time points for a particular DG209-GIC composition, while statistics shown in red refer to significance across different DG209-GICs for a particular time point.

It was also hypothesized that the MTX-loaded DG209-GICs would demonstrate an increase in CS over time. The results of this experiment show no significant trend in CS over time (Figure 4.7). The 1 wt% MTX DG209-GIC showed an increase in strength between 1 and 7 days, and the 5 wt% MTX DG209-GIC showed a decrease in strength between 7 and 31 days; however, it is difficult to draw conclusions regarding these findings, as there is no observable trend in strength over time.

Interestingly, an increase in CS was observed over time when Brett Dickey conducted the CS analysis of the DG209-GIC (without MTX) [117]. As evidenced by Figure 4.7, the DG209-GICs analyzed in the present study did not generally increase in CS over the 1- to 31-day incubation period. Deviations between these observations may result from the test setup. The test setup employed by Brett Dickey is described in [4]: deionized water was used for the incubating medium and it was not changed at any time between the incubation start point and the mechanical test time. This deviates from the present study in which PBS was used as the incubating medium and it was changed at 1 hour, daily for 10 days, and on days 30 and 31. It is well understood that the incubating medium largely influences the release and degradation of bioactive glasses [149]. Deionized water may act as an ion-sink,

encouraging ion release from the GIC, whereas the ionic content of PBS may contribute to the maturation of the cement matrix, which results from the continued acid-base reaction of the material. Furthermore, the media exchange method used in the present work may have resulted in the removal of leached ions, which would have integrated with the cement matrix over time. Therefore, it is difficult to compare the findings of Brett Dickey with those of the present study.

In the literature, decreases in CS are generally observed for CHX-loaded dental GICs [121, 150]. Türkün *et al.* reported the 1-day CS of a conventional GIC decreased from 225 MPa to 180 MPa when CHX was added at 1.25 wt%, while Takahashi *et al.* reported significant decreases in both 1- and 7-day CS when the material was loaded at 1, 2, and 3 wt% [121, 150]. Although other groups attribute decreases in CS to drug elution, as the cements weaken over time [147], Takahashi *et al.* found no correlation between release and strength, concluding the decrease in mechanical properties must have resulted from CHX interactions with the cement setting process [121]. Takahashi *et al.* also observed extended t_s with CHX addition, proposing drug addition hampered the reaction of neutralization reaction, possibly through interfering with the proton attack or the ion release [121]. Similar theories pertaining to the acid-base reaction may apply to the present results. As discussed in Section 4.4.2, variations in ion release behaviour across the different drug loadings supports the idea that MTX interferes with the neutralization setting reaction. It is difficult to say, however, if CS correlates with drug release in the present study or not. From Figure 4.7, there is an obvious, though not significant, trend in strength over time: all GICs demonstrate an initial increase over the first 7 days, which decreases between days 7 and 31. This may represent a trade-off between maturation and drug elution, whereby the cements begin to increase in strength, but this process is counteracted by the drug release.

Overall, the results of the preliminary strength test suggest the DG209-GIC may be drug-loaded up to 10 wt% with no significant effects to CS. Further testing to elucidate the failure mechanisms of this material would provide clinical context for these data. At present, it can only be concluded that MTX addition does not affect the

quality of the DG209-GIC [138, 139]. As evidenced from Figure 4.7, no composition-property relationships were drawn from this experiment; no general trend in CS was observed between the different drug loadings. Additionally, the general effects of CS with maturation do no appear to be affected by the drug loading.

4.6 Experiment 5: Cytotoxicity of the MTX-Loaded DG209-GICs and Validation of Drug Activity

In vitro elution testing was conducted to quantify the cytotoxicity of the MTX-loaded GICs (relative to the 0 wt% MTX control cement) and to investigate whether the activity of the released MTX was compromised. An MTT assay using NIH-3T3 mouse fibroblast cells was conducted to establish composition-property relationships, correlating MTX wt%-loading with cell viability, and to evaluate differences in cytotoxic effect between cement extracts and fresh MTX solutions.

The results of the MTT assay are shown in Figure 4.8. It was hypothesized that the MTX-loaded cement extracts would yield significantly lower NIH-3T3 mouse fibroblast cell viability than the 0 wt% MTX cement extract at each time point due to the inhibitory effects of MTX on the metabolism of folic acid. The findings of this experiment validate this hypothesis; cement extracts containing MTX showed significantly lower cell viability at each time point in comparison to controls. It was also hypothesized that extracts containing higher MTX concentrations would yield lower NIH-3T3 in a dose-dependent manner. The results presented in Figure 4.8 falsify this second hypothesis; no statistical difference in cell viability was observed between extracts of the different MTX cements. Furthermore, no significant difference in cell viability was found for any of the cement extracts over time. Consequently, no composition-property relationships were drawn based on the cell viabilities of the different MTX-loaded cements.

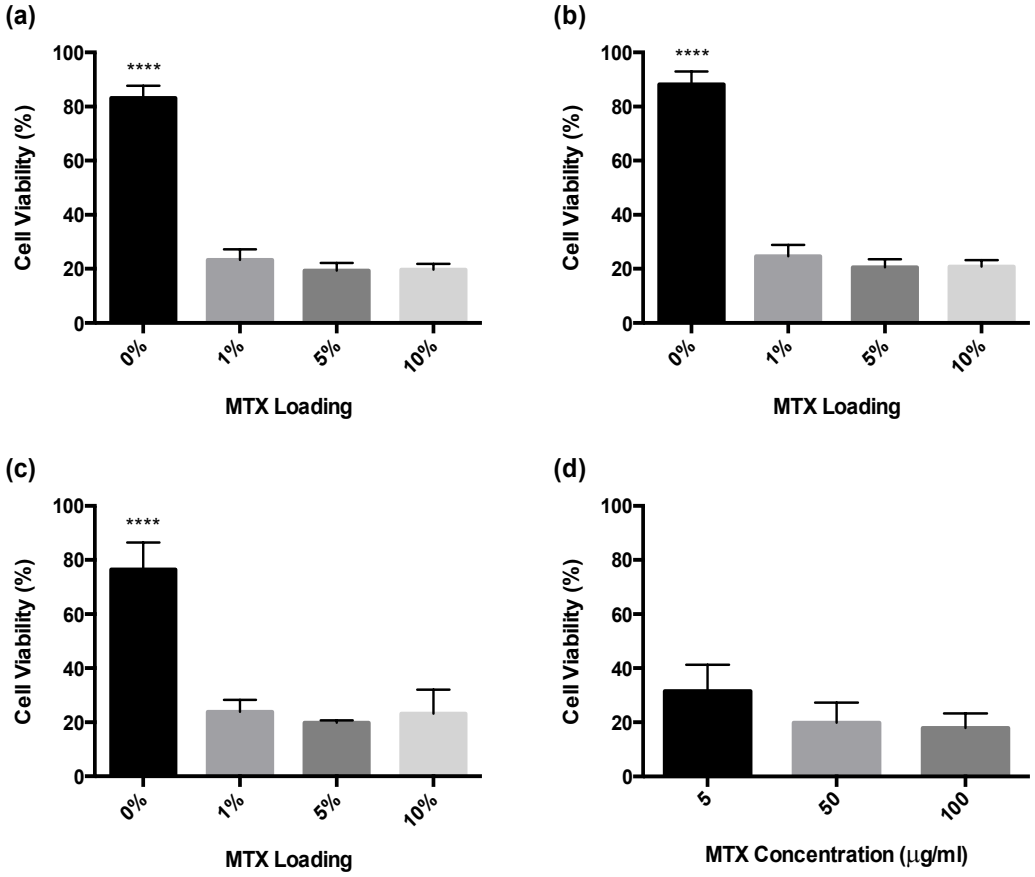

Figure 4.8: Cell viabilities (%) of NIH-3T3 mouse fibroblast cells exposed to 0, 1, 5, and 10 wt% MTX DG209-GIC extracts collect from 1-day (a), 7-day (b), and 31-day (c) release experiments (Experiment 3, Part 1); (d) Cell viability for fresh MTX solutions: 5, 50, and 100 μg/ml.

From Section 4.4.2, it is evident the DG209-GICs released a variety of ionic species into solution. In the literature, germanium has been discussed as a potential anticancer agent [151]. As discussed in her MASc. thesis, Victoria Dickinson investigated Ge^{4+}-release from the DG-series and its potential inhibitory action, as this material feature may be beneficial in the treatment of metastatic-related fractures [118]. This *in vitro* analysis found that up to 200 ppm of Ge^{4+} was released from these glasses into tissue culture water, but that no extracts yielded cytotoxic effects [118]. In the present work, Ge^{4+} release was enhanced with increase MTX loading; however, it not possible to drawn conclusions regarding the cytotoxic consequences of this event, as increased MTX was released from higher loaded cements. It does not appear ion release correlates with cell viability findings;

however, it should be noted that ion-mediated effects on cell viability cannot be completely ruled out based on the data collected.

Since MTX is a dicarboxylic acid (Figure 2.2), it may chemically participate in the neutralization setting reaction of the GIC and/or interact with the ionic species released from the DG209-GIC. Therefore, it was necessary to determine whether the GIC setting process interfered with the chemical activity of the drug. To do so, an MTT assay was performed using fresh solutions of MTX prepared at concentrations in the range of those observed from Experiment 3, Part 1, as summarized in Table 4.11. As compared to the MTT results for the cement extracts, the fresh MTX solutions produced similar cell viabilities (Figure 4.8 (d)). However, without drug concentrations that exactly match those of the cement extracts, it is difficult to make definitive statements regarding the cytotoxicity of the drug. Nonetheless, these results suggest that the cement did not likely compromise the activity of the released MTX since the fresh solutions resulted in cell viabilities in a similar range to those observed for the cement extracts.

Table 4.11: Mean and standard deviations (SD) of MTX concentrations (μg/ml) measured in 1-, 7-, and 31-day extracts for the 1, 5, and 10 wt% MTX DG209-GICs.

	1% MTX	**5% MTX**	**10% MTX**
1-day	5.583 ± 0.533	35.076 ± 7.03	91.26 ± 17.21
7-day	3.553 ± 0.486	13.534 ± 0.521	20.639 ± 1.545
31-day	6.758 ± 1.763	23.196 ± 10.37	32.091 ± 13.08

The good correlation between the cell viabilities measured for the fresh MTX solutions and the cement extracts insinuate MTX remained stable throughout the test period. MTX stability was a primary concern at the commencement of this thesis; the drug is only stable in solution for 1-7 days when stored between 4-8°C and 30 days when stored at -20°C [133, 141]. To avoid this stability issue, PBS was changed 24 hours prior to collecting the extracts and careful attention was made to ensure the extracts were stored in the absence of light as specified. These measures reduced the potential of MTX degradation, which could affect the activity of the drug.

The enduring cytotoxic effect observed in the present study compares to the results reported for antineoplastic-loaded PMMA systems. Rosa *et al.* observed a constant cytotoxic effect throughout a 15-day test period, while Gouran *et al.* reported a continued, though decreasing effect over a 30-day period [57, 72]. Gouran *et al.* found that the cytotoxic effect of MTX on stromal giant-cell tumour cells fell to 69% (31% cell viability) after 30 days; however, it is unclear whether this resulted from increased cell proliferation or decreased drug concentrations [57]. In the present work, no significant effects to cytotoxicity were observed over time (ANOVA; stats not shown in Figure 4.8).

With regards to CHX-releasing GIC systems, dose-effect responses vary extensively across the literature, with some groups finding antimicrobial activity was dependent on the concentration of the disinfectant [123, 152], and others finding no such correlation [121, 153]. The present experiment compares with the latter, as increased MTX loading did not correlate with increased cytotoxicity; rather all MTX-inclusive extracts, for each time point, exerted a significant cytotoxic effect *in vitro.*

4.6.1 Limitations with the MTT Assay

The MTT assay is a colorimetric assay based on the reduction of MTT to formazan crystals by living cells, which is indicative of mitochondrial activity. For the majority of cells, mitochondrial activity is related to the number of viable cells, and thus this method has been widely accepted by the peer-reviewed literature as a predictive tool for measuring the *in vitro* cytotoxic effects of drugs on cell lines [154]. MTT results become meaningful when comparing cell viabilities against a reference. In the present study, PBS was used as a control, from which %-cell viability was calculated for each cement extract.

It is important to consider the limitations with this technique when relying on its results to drawn conclusions. One such consideration is the potential for MTT reduction outside of the mitochondria. To rule out this concern, media with and without cells were added as controls in this study. Another hypothetical issue with

this particular test setup was the potential for colorimetric interference as MTX is a bright yellow compound. Accordingly, the MTT assay was selected over the simpler MTS (3-(4,5-dimethylthiazol-2-yl)-5-(3-carboxymethoxyphenyl)-2-(4-sulfophenyl)-2H-tetrazolium inner salt) assay as the intermittent steps of the MTT method removes traces of coloured compounds.

4.7 Summary of Composition-Property Relationships for the MTX-Loaded DG209-GIC

The primary objective of this thesis was to investigate the drug loading and delivery potential of the DG209-GIC using MTX. To do so, MTX was loaded into the DG209-GIC at 0, 1, 5, and 10 wt% and the handling properties, MTX release, ion release, CS, and cytotoxicity of the GICs were examined. The following points summarize the key composition-property relationships observed from the present work:

- MTX addition significantly decreased the t_w of the DG209-GIC as compared to the 0 wt% control. However, MTX loading between 1-10 wt% did not correlate with decreased t_w; no significant differences in t_w were observed across the variable MTX loadings. No significant trend in t_s was observed across the 0, 1, 5, and 10 wt% MTX DG209-GICs.
- Increased MTX loading resulted in increased MTX release; however, the release efficiencies were constant across all drug loadings. No difference in release mechanism was observed across the different drug loadings. For each DG209-GIC, the KP equation fit the data best, suggesting release was primarily diffusion-mediated and erosion likely did not affect release.
- Increased concentrations of Si^{4+} and Ge^{4+} in the 1-day cement extracts were observed with increased MTX loading, while decreases in all ion species were observed at 31 days between the 0 wt% control and the MTX-loaded GICs.
- No significant trend in CS was observed relative to MTX addition at any of the tested time points. No general trend in CS was observed over the 31-day incubation period for any of the DG209-GICs.
- MTX addition significantly increased the cytotoxic effect of the DG209-GIC on NIH-3T3 mouse fibroblast cells. However, increased MTX loading did not correlate with decreased cell viability. The released MTX demonstrated maintained activity, as compared to fresh MTX solutions prepared in the range of that observed in cement extracts.

CHAPTER 5

Limitations, Conclusions, and Future Research Directions

5.1 Limitations

- The ISO 9917 test for t_w is a simple measurement used to compare the ease of handling of different bone cements and approximate their injectability [4]. Although this measure is used widely across the literature, it is burdened by several inherent problems, such as user inconsistency and environmental variability [138]. In the present study, t_w analysis was conducted by a single operator under constant conditions to minimize external factors that could affect the variability of the data set. However, the author cautions comparing these results with those of the literature. Furthermore, although the composition-property relationships derived herein correlate MTX loading with handling properties, the author recommends that a full injection study be completed to accurately determine whether MTX addition influences the clinical utility of this material.
- The ISO 9917 test for CS has been subject to significant controversy in recent years, as it does not account for the failure mechanism and offers no predictive measure of strength [138]. The author stresses the present study only intended to preliminarily investigate whether MTX addition affected the mechanical properties of the cement, rather than predict GIC performance. Three-point bending and/or biaxial testing could provide context for the mechanical effects of MTX in the GIC matrix.

- *In vitro* testing is appropriate for establishing composition-property relationships and predicting the efficiency and efficacy of release systems; however it is necessary to interpret *in vitro* results with caution, as these conditions do not represent those of the body in full. Many factors, including blood supply, tumour location, and mechanical loading can significantly influence release kinetics [57, 88]. When comparing the drug release results of this study to other works, it is necessary to consider the effects of the release medium, surface-to-volume ratio, and incubation environment.
- Cytotoxicity analysis using the MTT assay is an internationally accepted method for the preliminary testing of drug activity. Although the methods used in the present study suggest the released MTX maintained its activity, investigating the mechanism of cell death would be beneficial to confirm the activity of the drug was not altered. Furthermore, using a more relevant cell line for the intended application, such as a breast adenocarcinoma cell line, may be valuable. The rapid multiplication of cancer cell lines may produce differences in cell viability between the different MTX cements.

5.2 Future Research Directions

Given the findings of this work, the author believes there are two primary aspects of this research that merit future investigation: (1) the optimization of the DG209-GIC properties for PVP/PKP, and (2) the drug release efficiency of the MTX-DG209-GIC. Beyond these projects, it may prove useful to implement a DOE approach to optimize the MTX-DG209-GIC delivery system through using the data acquired in this thesis.

5.2.1 Optimization of the DG209-GIC

The optimized DG209-GIC, developed in Experiment 1, is suboptimal for PVP/PKP. The derived formulation (P/L=1.5/1.0 and AC=50%) yielded only 4:10 min:s of t_w, when 5-10 min is required for PVP/PKP [80]. It was hypothesized that the t_w of the material could be extended without compromising t_s or CS through using a DOE approach adjusting both P/L and AC. The results of this experiment showed that decreasing P/L and AC increased the t_w of the material, but significantly compromised CS. Increasing AC significantly improved CS, but extended t_s beyond what is clinically acceptable (10-20 min) [80]. Unfortunately, adjustments to P/L and AC did not produce a clinically practical balance t_w, t_s, and CS for the DG209-GIC.

The author proposes altering other cement components to attempt to tailor the material to better meet the needs of PVP/PKP. Previously, several groups have shown the effects of PAA M_w, additives, surface treatments, and particle size on GIC properties [97, 132, 155]. M_w influences the handling and mechanical properties of GICs, as it influences the degree of chain entanglement. Dowling and Fleming showed that increasing M_w (15,250-80,650) increased the viscosity and CS of a commercial GIC and reported mixing different molecular weights to optimize the rheological and mechanical properties of the material [132]. With regards to cement additives, Boyd *et al.* reported the addition of trisodium citrate extended t_w and t_s without compromising CS. Trisodium citrate has been shown to form complexes with the GIC matrix that inhibit the formation of stable metal polyacrylate anion complexes and thus slow the setting reaction [97]. Crowley *et al.* also showed reductions in setting

reactivity, but through pre-treating the glass component with acetic acid. Acid washing depletes the ionic content of the glass surface, which reduces the initial rate of ion-release and therefore delays the onset of crosslinking [156]. Alternatively, cement reactivity can be controlled through modifying particle size distribution. Leon *et al.* found that increasing the proportion of smaller particles (3.34 μm) in an experimental GIC increased the CS, while an increase in larger particles (9.60 μm) decreased the viscosity of the material. Particle size is a complex subject whereby GICs composed of large particles form non-cohesive pastes and GICs comprising small particles set too fast [155]. In conclusion, introducing additional factors to the DOE in Experiment 1, such as these listed here, may produce a DG209-GIC composition with improved properties for injectable skeletal applications.

5.2.2 Improving Drug Delivery

From a drug delivery standpoint, the primary shortcoming observed in this study was the relatively low release efficiencies of the MTX-GIC systems. In comparison to the popular PMMA, the DG209-GIC showed MTX release efficiencies that were 3-5 times lower [74]. Ideally, release efficiency should be maximized in order to augment the therapeutic potential of the material, but also to reduce the concentration of drug that remains localized within the patient. Improving this component of the system would be an appropriate future research direction for this material.

It is appreciated that both cement microstructure and drug chemistry dictate drug release from bone cement delivery systems [46]. Therefore, these two domains merit investigation to advance this material towards clinical utility. The results of Experiment 3, Part 1 suggest release was primarily diffusion-mediated; consequently, increasing the porosity and hydrophilicity of the cement would likely result in improved efficiency [46]. In this regard, establishing composition-property relationships involving PAA M_w and cement additives may be beneficial for understanding the effects of free volume and porosity (respectively) on release from the material [46].

As mentioned, MTX is a dicarboxylic acid, and therefore it may interact with the GIC neutralization reaction. The altered ion release profiles may support this hypothesis; it is possible the drug interacted with released glass cations, chemically binding itself to the GIC matrix, impeding drug release. Investigating the addition of different chemotherapeutics may be beneficial in this regard, as different drugs have shown unique release behaviour in conventional bone cement systems [46].

5.2.3 Optimization of the MTX-DG209-GIC Delivery System

DOE is an efficient tool for material design whereby the effects of multiple variables may be analyzed concomitantly on several different material properties. The findings of this thesis provide preliminary composition-property relationships relating MTX loading to handling properties, drug and ion release, CS, and cytotoxicity. Using this data, and the data collected from the future research recommendations discussed above (Sections 5.2.1 and 5.2.2), a DOE approach could be implemented to derive an optimal MTX-DG209-GIC composition. As mentioned, further improvement is required to ameliorate issues with clinical utility and low release efficiencies; however, should these problems be addressed, the author recommends implementing a DOE approach to derive an optimal material in terms of what is considered idea for the treatment of metastatic-induced VCFs.

5.3 Conclusions

The addition of chemotherapeutics to bone cements may provide an attractive means of local drug delivery in the treatment of cancer-related fractures requiring cement injection for stabilization. Significant effort has been made to evaluate the drug loading and delivery potential of conventional bone cements; however, current materials fail to provide adequate biocompatibility and/or mechanical strength. Recently, Dickey *et al.* published a series of Al-free GIC compositions (DG series) that may address the concerns with conventional materials. Of these materials, the DG209-GIC offers the most appropriate balance in t_w, t_s, and CS for injectable skeletal applications, and has shown promising preliminary biocompatibility results. Prior to this study, the drug loading and delivery potential of this material were not known.

The present study examined composition-property relationships to correlate MTX loading with handling properties, mechanical strength, drug release, ion release, and cytotoxic effect. Prior to conducting the MTX loading experimentation, the DG209-GIC formulation was optimized in terms of clinically desired t_w, t_s, and CS for PVP/PKP using a DOE approach in which *both* P/L and AC were adjusted. This experiment presents the first set of predictive regression models that involve the *combined* effects of these two factors. The resulting response models showed high model adequacies, but proved to be poor predictors of optimal cement formulation. The centroid design point of the design space (P/L=1.5/1.0, AC= 50%) yielded better results (t_w=4:10 min:s, t_s=10:40 min:s, CS=39 MPa) in comparison to the model predictions. This formulation was deemed optimal and used in the subsequent MTX loading investigations.

Overall, MTX addition (1, 5, and 10 wt%) imparted minimal effects on GIC handling properties with no effects to strength. Release profiles were biphasic, with the initial burst release phase lasting approximately 24 hours, and the slow steady release phase persistent throughout the 31-day test period. With increased drug loading, higher drug release was observed; however, no significant difference was found in the release efficiencies of the different MTX-GICs. The release profiles were

best described by the Korsmeyer-Peppas model, which suggests release was primarily diffusion-mediated. To develop theories pertaining to ion-drug interactions, ICP analysis was conducted on release extracts. Significant differences in ion release were observed between drug loadings: MTX addition significantly decreased all ion releases at 31 days. These results may imply MTX chemically integrated with the GIC matrix. Finally, all MTX-loaded GICs showed significant cytotoxicity in comparison to the 0 wt% MTX DG209-GIC at 1, 7, and 31 days.

This thesis comprises the first study that investigates the effects of chemotherapeutic loading on GIC matrices. Overall, these results of this preliminary study support the clinical suitability of the MTX-loaded DG209-GIC for use in the management of cancer-related VCFs and justify the need for additional research to improve the clinical utility of the DG209-GIC and its release efficiency.

Bibliography

[1] G. Maccauro, A. Cittadini, M. Casarci, F. Muratori, D. De Angelis, C. Piconi, M. A. Rosa, A. Spadoni, M. Braden and A. Sgambato. Methotrexate-added acrylic cement: Biological and physical properties. *Journal of Materials Science. Materials in Medicine. 18(5),* pp. 839-844. 2007.

[2] G. Lewis. Injectable bone cements for use in vertebroplasty and kyphoplasty: State-of-the-art review. *Journal of Biomedical Materials Research. Part B, Applied Biomaterials. 76(2),* pp. 456-468. 2006.

[3] E. Engelbrecht, G. von Foerster and G. Delling, "Ionogran in revision arthroplasty." *Journal of Bone and Joint Surgery. British Volume.,* vol. 82, pp. 192-199, 2000.

[4] B. Dickey, S. Kehoe and D. Boyd, "Novel adaptations to zinc-silicate glass polyalkenoate cements: The unexpected influences of germanium based glasses on handling characteristics and mechanical properties." *Journal of the Mechanical Behavior of Biomedical Materials.,* vol. 23, pp. 8-21, 2013.

[5] *Canadian Cancer Society: Bone Metastases.* 2014. http://www.cancer.ca/en/cancer-information/cancer-type/metastatic-cancer/bone-metastases/?region=on Accessed: Sept. 2014.

[6] G. Selvaggi and G. Scagliotti. Management of bone metastases in cancer: A review. *Crit. Rev. Oncol. 56(3),* pp. 365-378. 2005.

[7] R. E. Coleman. Metastatic bone disease: Clinical features, pathophysiology and treatment strategies. *Cancer Treat. Rev. 27(3),* pp. 165-176. 2001.

[8] R. E. Coleman, P. Smith and R. D. Rubens. Clinical course and prognostic factors following bone recurrence from breast cancer. *Br. J. Cancer 77(2),* pp. 336-340. 1998.

[9] *American Cancer Society: Bone Metastasis*. 2014. http://www.cancer.org/treatment/understandingyourdiagnosis/bonemetastasis/bone-metastasis-detailed-guide-toc Accessed: Sept. 2014.

[10] F. Cardoso, N. Harbeck, L. Fallowfield, S. Kyriakides and E. Senkus. Locally recurrent or metastatic breast cancer: ESMO clinical practice guidelines for diagnosis, treatment and follow-up. *Annals of Oncology. 23(S7),* pp. 7-9. 2012.

[11] J. Strasser, N. Amin, G. Dickerson, N. Cersonsky, M. Stinauer, B. Peterson and T. Birney, "Advancing the Care of Cancer Patients with Vertebral Compression Fractures: A Radiation Oncology Expert Panel Discussion.**
**," *Oncology and Hematology Review.,* vol. 8, pp. 12-17, 2012.

[12] J. Brown, R. Cook, A. Lipton, L. Costa and R. Coleman. Prognostic factors for skeletal complications from metastatic bone disease in breast cancer. *Breast Cancer Res. Treat. 123(3),* pp. 76-79. 2010.

[13] S. Kushchayev, Y. Kushchayeva, N. Theodore, M. Preul and O. Clark. Percutaneous vertebroplasty for thyroid cancer metastases to the spine. *Thyroid 20(5),* pp. 555-560. 2010.

[14] B. Georgy. Metastatic spinal lesions: State-of-the-art treatment options and future trends. *American Journal of Neuroradiology. 29(9),* pp. 1605-1611. 2008.

[15] J. E. Brown, C. S. Thomson, S. P. Ellis, S. A. Gutcher, O. P. Purohit and R. E. Coleman. Bone resorption predicts for skeletal complications in metastatic bone disease. *Br. J. Cancer 89(11),* pp. 2031-2037. 2003.

[16] N. Rasulova, V. Lyubshin, F. Djalalov, K. Kim, L. Nazirova, N. Ormanov and D. Arybzhanov. Strategy for bone metastases treatment in patients with impending cord compression or vertebral fractures: A pilot study. *World Journal of Nuclear Medicine. 10(1),* pp. 14-19. 2011.

[17] F. Saad, A. Lipton, R. Cook, Y. Chen, M. Smith and R. Coleman. Pathologic fractures correlate with reduced survival in patients with malignant bone disease. *Cancer 110(8),* pp. 1860-1867. 2007.

[18] R. Coleman, "Clinical Features of Metastatic Bone Disease and Risk of Skeletal Morbidity." *American Association of Cancer Research.,* vol. 12, pp. 6243-6249, 2006.

[19] A. Cotten, F. Dewatre, B. Cortet, R. Assaker, D. Leblond, B. Duquesnoy, P. Chastanet and J. Clarisse. Percutaneous vertebroplasty for osteolytic metastases and myeloma: Effects of the percentage of lesion filling and the leakage of methyl methacrylate at clinical follow-up. *Radiology 200(2),* pp. 525-530. 1996.

[20] A. Weill, J. Chiras, J. Simon, M. Rose, T. Sola Martinez and E. Enkaoua. Spinal metastases: Indications for and results of percutaneous injection of acrylic surgical cement. *Radiology 199(1),* pp. 241-247. 1996.

[21] H. Deramond, C. Depriester, P. Galibert and D. Le Gars. Percutaneous vertebroplasty with polymethylmethacrylate. technique, indications, and results. *Radiol. Clin. North Am. 36(3),* pp. 533-546. 1998.

[22] R. Pflugmacher, F. Kandziora, R. Schroeder, I. Melcher, N. Haas and C. Klostermann. Percutaneous balloon kyphoplasty in the treatment of pathological vertebral body fracture and deformity in multiple myeloma: A one-year follow-up. *Acta Radiol. 47(4),* pp. 369-376. 2006.

[23] R. Izzo, G. Guarnieri, G. Guglielmi and M. Muto, "Biomechanics of the spine. Part I: Spinal stability." *European Journal of Radiology.,* 2012.

[24] S. Ferreira, I. Dormehl and M. Botelho. Radiopharmaceuticals for bone metastasis therapy and beyond: A voyage from the past to the present and a look to the future. *Cancer Biotherapy and Radiopharmaceuticals. 27(9),* pp. 535-551. 2012.

[25] M. Goodman and K. Weiss, "Surgical Approach to Metastatic Bone Disease." *Operative Techniques in Orthopedics.,* vol. 24, pp. 85-90, 2014.

[26] M. Robson and N. Dawson. How is androgen-dependent metastatic prostate cancer best treated? *Hematol. Oncol. Clin. North Am. 10(3),* pp. 727-747. 1996.

[27] B. Roedel, F. Clarençon, S. Touraine, E. Cormier, L. Molet Benhamou, L. Le Jean, H. Brisse, S. Neuenschwander and J. Chiras. Has the percutaneous vertebroplasty a role to prevent progression or local recurrence in spinal metastases of breast cancer? *Journal of Neuroradiology. Article in Press*pp. 1-7. 2014.

[28] E. Dunning, J. Butler and S. Morris. Complications in the management of metastatic spinal disease. *World Journal of Orthopedics. 3(8),* pp. 114-121. 2012.

[29] N. Eastley, M. Newey and R. Ashford. Skeletal metastases - the role of the orthopaedic and spinal surgeon. *Surg. Oncol. 21(3),* pp. 216-222. 2012.

[30] A. Bhatt, J. Schuler, M. Boakye and S. Woo. Current and emerging concepts in non-invasive and minimally invasive management of spine metastasis. *Cancer Treat. Rev. 39(2),* pp. 142-152. 2013.

[31] J. Dunn. Percutaneous vertebroplasty in the management of a patient with malignant pain and associated osteolytic compression fractures. *Curr. Pain Headache Rep. 6(6),* pp. 436-443. 2002.

[32] A. N. Serafini. Therapy of metastatic bone pain. *The Journal of Nuclear Medicine 42(6),* pp. 895-906. 2001.

[33] N. Kohno, K. Aogi, H. Minami, S. Nakamura, T. Asaga, Y. Iino, T. Watanabe, C. Goessl, Y. Ohashi and S. Takashima. Zoledronic acid significantly reduces skeletal complications compared with placebo in japanese women with bone metastases from breast cancer: A randomized, placebo-controlled trial. *Journal of Clinical Oncology. 23(15),* pp. 3314-3321. 2005.

[34] F. Saad, D. Gleason, R. Murray, S. Tchekmedyian, P. Venner, L. Lacombe, J. Chin, J. Vinholes, J. Goas and B. Chen. A randomized, placebo-controlled trial of zoledronic acid in patients with hormone-refractory metastatic prostate carcinoma. *J. Natl. Cancer Inst. 94(19),* pp. 1458-1468. 2002.

[35] A. Gangi and X. Buy. Percutaneous bone tumor management. *Seminars in Interventional Radiology. 27(2),* pp. 124-136. 2010.

[36] V. Salapura and M. Jeromel. Minimally invasive (percutaneous) treatment of metastatic spinal and extraspinal disease--a review. *Acta Clinica Croatica. 53(1),* pp. 44-54. 2014.

[37] *Harvard: Treating osteoporotic fractures of the spine.* 2014. http://www.health.harvard.edu/newsletters/Harvard_Womens_Health_Watch/2008/December/Treating_osteoporotic_fractures_of_the_spine Accessed: Sept. 2014.

[38] D. J. Magee, J. E. Zachazewksi and W. S. Quillen, *Pathology and Intervention in Musculoskeletal Rehabilitation.* Swift Current, SK: Saunders, Elsevier, 2009.

[39] K. Harrington. The use of methylmethacrylate for vertebral-body replacement and anterior stabilization of pathological fracture-dislocations of the spine due to metastatic malignant disease. *The Journal of Bone & Joint Surgery 63(1),* pp. 36-46. 1981.

[40] S. Dudeney, I. Lieberman, M. Reinhardt and M. Hussein. Kyphoplasty in the treatment of osteolytic vertebral compression fractures as a result of multiple myeloma. *Journal of Clinical Oncology. 20(9),* pp. 2382-2387. 2002.

[41] C. Chew, L. Craig, R. Edwards, J. Moss and P. J. O'Dwyer. Safety and efficacy of percutaneous vertebroplasty in malignancy: A systematic review. *Clin. Radiol. 66(1),* pp. 63-72. 2011.

[42] Y. Yimin, R. Zhiwei, M. Wei and R. Jha. Current status of percutaneous vertebroplasty and percutaneous kyphoplasty--a review. *Medical Science Monitor. 19*pp. 826-836. 2013.

[43] D. Reidy, H. Ahn, P. Mousavi, J. Finkelstein and C. Whyne. A biomechanical analysis of intravertebral pressures during vertebroplasty of cadaveric spines with and without simulated metastases. *Spine. 28(14),* pp. 1534-1539. 2003.

[44] B. Cortet, A. Cotten, N. Boutry, F. Dewatre, R. M. Flipo, B. Duquesnoy, P. Chastanet and B. Delcambre. Percutaneous vertebroplasty in patients with osteolytic metastases or multiple myeloma. *Revue Du Rhumatisme. 64(3),* pp. 177-183. 1997.

[45] D. Grönemeyer, S. Schirp and A. Gevargez. Image-guided radiofrequency ablation of spinal tumors: Preliminary experience with an expandable array electrode. *The Cancer Journal. 8(1),* pp. 33-39. 2002.

[46] K. Anagnostakos and J. Kelm. Enhancement of antibiotic elution from acrylic bone cement. *Journal of Biomedical Materials Research. Part B, Applied Biomaterials. 90(1),* pp. 467-475. 2009.

[47] M. Ginebra, T. Traykova and J. Planell, "Calcium phosphate cements as bone delivery systems: A review." *Journal of Controlled Release.,* vol. 113, pp. 102-110, 2006.

[48] J. Healey, F. Shannon, P. Boland and G. DiResta. PMMA to stabilize bone and deliver antineoplastic and antiresorptive agents. *Clin. Orthop. (415),* pp. S263-S275. 2003.

[49] J. Webb and R. Spencer. The role of polymethylmethacrylate bone cement in modern orthopaedic surgery. *The Journal of Bone and Joint Surgery. British Volume. 89(7),* pp. 851-857. 2007.

[50] E. Erbe, T. Clineff and G. Gualtieri. Comparison of a new bisphenol-a-glycidyl dimethacrylate-based cortical bone void filler with polymethyl methacrylate. *European Spine Journal. 10(2),* pp. S147-S152. 2001.

[51] S. Larsson and T. Bauer. Use of injectable calcium phosphate cement for fracture fixation: A review. *Clin. Orthop. (395),* pp. 23-32. 2002.

[52] I. Lieberman, D. Togawa and M. Kayanja. Vertebroplasty and kyphoplasty: Filler materials. *The Spine Journal. 5(6),* pp. 305-316S. 2005.

[53] H. van de Belt, D. Neut, D. Uges, W. Schenk, J. van Horn, H. van der Mei and H. Busscher. Surface roughness, porosity and wettability of gentamicin-loaded bone cements and their antibiotic release. *Biomaterials 21(19),* pp. 1981-1987. 2000.

[54] H. Buchholz and H. Engelbrecht. Depot effects of various antibiotics mixed with palacos resins. *Chirurg 41(11),* pp. 511-515. 1970.

[55] G. Josefsson and L. Kolmert. Prophylaxis with systematic antibiotics versus gentamicin bone cement in total hip arthroplasty. A ten-year survey of 1,688 hips. *Clin. Orthop. (292),* pp. 210-214. 1993.

[56] D. Weisman, M. Olmstead and J. Kowalski. In vitro evaluation of antibiotic elution from polymethylmethacrylate (PMMA) and mechanical assessment of antibiotic-PMMA composites. *Veterinary Surgery. 29(3),* pp. 245-251. 2000.

[57] D. Gouran Savadhoohi, P. Sadeghipour, H. Attarian, S. Sardari, A. Eslamifar and M. A. Shokrgozar, "Cytotoxic effect of drugs eluted from polymethylmethacrylate on stromal giant-cell tumour cells." *The Journal of Bone and Joint Surgery. British Volume.,* vol. 90, pp. 973-979, 2008.

[58] B. Thomes, P. Murray and D. Bouchier Hayes. Development of resistant strains of staphylococcus epidermidis on gentamicin-loaded bone cement in vivo. *The Journal of Bone and Joint Surgery. British Volume. 84(5),* pp. 758-760. 2002.

[59] B. Picknell, L. Mizen and R. Sutherland. Antibacterial activity of antibiotics in acrylic bone cement. *The Journal of Bone and Joint Surgery. British Volume. 59(3),* pp. 302-307. 1977.

[60] S. Hughes, C. Field, M. Kennedy and C. Dash. Cephalosporins in bone cement: Studies in vitro and in vivo. *The Journal of Bone and Joint Surgery. British Volume. 61(1),* pp. 96-100. 1979.

[61] J. Medcraft and A. Gardner. The use of an antibiotic bone cement combination as a different approach to the elimination of infection in total hip replacement. *Med. Lab. Technol. 31(4),* pp. 347-353. 1974.

[62] K. Marks, C. Nelson and E. Lautenschlager. Antibiotic-impregnated acrylic bone cement. *Journal of Bone and Joint Surgery American Volume. 58(3),* pp. 358-364. 1976.

[63] D. Kuechle, G. Landon, D. Musher and P. Noble. Elution of vancomycin, daptomycin, and amikacin from acrylic bone cement. *Clin. Orthop. (264),* pp. 302-308. 1991.

[64] D. Neut, H. van de Belt, J. van Horn, H. van der Mei and H. Busscher. The effect of mixing on gentamicin release from polymethylmethacrylate bone cements. *Acta Orthop. Scand. 74(6),* pp. 670-676. 2003.

[65] A. Baker and L. Greenham. Release of gentamicin from acrylic bone cement. elution and diffusion studies. *The Journal of Bone & Joint Surgery. 70(10),* pp. 1551-1557. 1988.

[66] K. Anagnostakos, J. Kelm, T. Regitz, E. Schmitt and W. Jung. In vitro evaluation of antibiotic release from and bacteria growth inhibition by antibiotic-loaded acrylic bone cement spacers. *Journal of Biomedical Materials Research. Part B, Applied Biomaterials. 72(2),* pp. 373-378. 2005.

[67] M. Penner, B. Masri and C. Duncan. Elution characteristics of vancomycin and tobramycin combined in acrylic bone-cement. *J. Arthroplasty 11(8),* pp. 939-944. 1996.

[68] M. Tunney, A. Brady, F. Buchanan, C. Newe and N. Dunne. Incorporation of chitosan in acrylic bone cement: Effect on antibiotic release, bacterial biofilm formation and mechanical properties. *Journal of Materials Science. Materials in Medicine. 19(4),* pp. 1609-1615. 2008.

[69] A. McLaren, S. McLaren, R. McLemore and B. Vernon. Particle size of fillers affects permeability of polymethylmethacrylate. *Clin. Orthop. 461*pp. 64-67. 2007.

[70] A. McLaren, C. Nelson, S. McLaren and G. DeCLerk. The effect of glycine filler on the elution rate of gentamicin from acrylic bone cement: A pilot study. *Clin. Orthop. (427),* pp. 25-27. 2004.

[71] J. Klekamp, J. Dawson, D. Haas, D. DeBoer and M. Christie. The use of vancomycin and tobramycin in acrylic bone cement: Biomechanical effects and elution kinetics for use in joint arthroplasty. *J. Arthroplasty 14(3),* pp. 339-346. 1999.

[72] M. Rosa, G. Maccauro, A. Sgambato, R. Ardito, G. Falcone, V. De Santis and F. Muratori. Acrylic cement added with antiblastics in the treatment of bone metastases. ultrastructural and in vitro analysis. *Bone and Joint Journal. 85(5),* pp. 712-716. 2003.

[73] R. Bayston and R. Milner. The sustained release of antimicrobial drugs from bone cement. an appraisal of laboratory investigations and their significance. *The Journal of Bone and Joint Surgery. British Volume. 64(4),* pp. 460-464. 1982.

[74] S. Wasserlauf, A. Warshawsky, R. Arad Yelin, Y. Mazur, R. Salama and S. Dekel. The release of cytotoxic drugs from acrylic bone cement. *Bulletin - Hospital for Joint Diseases. 53(1),* pp. 68-74. 1993.

[75] S. Dash, P. Murthy, L. Nath and P. Chowdhury. Kinetic modeling on drug release from controlled drug delivery systems. *Acta Pol. Pharm. 67(3),* pp. 217-223. 2010.

[76] P. Costa and J. Sousa Lobo. Modeling and comparison of dissolution profiles. *European Journal of Pharmaceutical Sciences. 13(2),* pp. 123-133. 2001.

[77] E. Díez Peña, G. Frutos, P. Frutos and J. Barrales Rienda. Gentamicin sulphate release from a modified commercial acrylic surgical radiopaque bone cement. I. influence of the gentamicin concentration on the release process mechanism. *Chem. Pharm. Bull. 50(9),* pp. 1201-1208. 2002.

[78] P. Hernigou, J. Thiafry, J. Benoit, M. Voisin, P. Leroux, G. Hagege, G. Delepine and D. Goutallier. Methotrexate diffusion from acrylic cement. local chemotherapy for bone tumours. *Journal of Bone and Joint Surgery. British Volume. 71(5),* pp. 804-811. 1989.

[79] E. Lautenschlager, J. Jacobs, G. Marshall and P. Meyer. Mechanical properties of bone cements containing large doses of antibiotic powders. *J. Biomed. Mater. Res. 10(6),* pp. 929-938. 1976.

[80] P. Heini and U. Berlemann. Bone substitutes in vertebroplasty. *European Spine Journal. 10(2),* pp. S205-S213. 2001.

[81] M. DiCicco, T. Duong, A. Chu and S. Jansen. Tobramycin and gentamycin elution analysis between two in situ polymerizable orthopedic composites. *Journal of Biomedical Materials Research. Part B, Applied Biomaterials. 65(1),* pp. 137-149. 2003.

[82] M. Otsuka, M. Sawada, Y. Matsuda, T. Nakamura and T. Kokubo. Antibiotic delivery system using bioactive bone cement consisting of bis-GMA/TEGDMA resin and bioactive glass ceramics. *Biomaterials 18(23),* pp. 1559-1564. 1997.

[83] M. Otsuka, M. Sawada, Y. Matsuda, T. Nakamura and T. Kokubo. Effects of water-soluble component content on cephalexin release from bioactive bone cement consisting of bis-GMA/TEGDMA resin and bioactive glass ceramics. *Journal of Materials Science. Materials in Medicine. 10(1),* pp. 59-64. 1999.

[84] M. Otsuka, H. Fujita, T. Nakamura and T. Kokubo. Effects of ceramic component on cephalexin release from bioactive bone cement consisting of bis-GMA/TEGDMA resin and bioactive glass ceramics. *Biomed. Mater. Eng. 11(1),* pp. 11-22. 2001.

[85] J. Verlaan, W. van Helden, F. Oner, A. Verbout and W. Dhert. Balloon vertebroplasty with calcium phosphate cement augmentation for direct restoration of traumatic thoracolumbar vertebral fractures. *Spine. 27(5),* pp. 543-548. 2002.

[86] M. Otsuka, Y. Matsuda, D. Yu, J. Wong, J. Fox and W. Higuchi. A novel skeletal drug delivery system for anti-bacterial drugs using self-setting hydroxyapatite cement. *Chem. Pharm. Bull. 38(12),* pp. 3500-2. 1990.

[87] M. Otsuka, Y. Matsuda, Y. Suwa, J. Fox and W. Higuchi. A novel skeletal drug delivery system using a self-setting calcium phosphate cement. 5. drug release behavior from a heterogeneous drug-loaded cement containing an anticancer drug. *J. Pharm. Sci. 83(11),* pp. 1565-1568. 1994.

[88] Z. Yang, D. Li, B. Gao, K. Duan, Z. Li, X. Li and J. Li. Release kinetics of methotrexate loaded calcium phosphate cement and histological evaluation of the osteogenesis in rabbits. *32(5),* pp. 543-548. 2010.

[89] Z. Yang, J. Han, J. Li, X. Li, Z. Li and S. Li. Incorporation of methotrexate in calcium phosphate cement: Behavior and release in vitro and in vivo. *Orthopedics 32(1),* pp. 27. 2009.

[90] C. Hamanishi, K. Kitamoto, S. Tanaka, M. Otsuka, Y. Doi and T. Kitahashi. A self-setting TTCP-DCPD apatite cement for release of vancomycin. *J. Biomed. Mater. Res. 33(3),* pp. 139-143. 1996.

[91] M. Bohner, J. Lematre, H. Merkle and B. Gander. Control of gentamicin release from a calcium phosphate cement by admixed poly(acrylic acid). *J. Pharm. Sci. 89(10),* pp. 1262-1270. 2000.

[92] M. Takechi, Y. Miyamoto, Y. Momota, T. Yuasa, S. Tatehara, M. Nagayama, K. Ishikawa and K. Suzuki. The in vitro antibiotic release from anti-washout apatite cement using chitosan. *Journal of Materials Science. Materials in Medicine. 13(10),* pp. 973-978. 2002.

[93] A. Ratier, M. Freche, J. L. Lacout and F. Rodriguez. Behaviour of an injectable calcium phosphate cement with added tetracycline. *Int. J. Pharm. 274(1-2),* pp. 261-268. 2004.

[94] T. Tani, K. Okada, S. Takahashi, N. Suzuki, Y. Shimada and E. Itoi. Doxorubicin-loaded calcium phosphate cement in the management of bone and soft tissue tumors. *In Vivo 20(1),* pp. 55-60. 2006.

[95] B. Magnan, M. Bondi, T. Maluta, E. Samaila, L. Schirru and C. Dall'oca. Acrylic bone cement: Current concept review. *Musculoskeletal Surgery.* 2013.

[96] N. Dunne, J. Orr, M. Mushipe and N. Dunne. The relationship between porosity and fatigue characteristics of bone cements. *Biomaterials 24(2),* pp. 239-245. 2003.

[97] D. Boyd, O. Clarkin, A. Wren and M. Towler. Zinc-based glass polyalkenoate cements with improved setting times and mechanical properties. *Acta Biomaterialia. 4(2),* pp. 425-431. 2008.

[98] D. San Millan Ruiz, K. Burkhardt, B. Jean, M. Muster, J. Martin, J. Bouvier, J. Fasel, D. Rufenacht and A. Kurt. Pathology findings with acrylic implants. *Bone 25(2),* pp. 85S-90S. 1999.

[99] J. Sturup, L. Nimb, M. Kramhafft and J. Jensen. Effects of polymerization heat and monomers from acrylic cement on canine bone. *Acta Orthop. Scand. 65(1),* pp. 20-23. 1994.

[100] F. Vale, M. Castro, J. Monteiro, F. Couto, R. Pinto and J. Gião Toscano Rico. Acrylic bone cement induces the production of free radicals by cultured human fibroblasts. *Biomaterials 18(16),* pp. 1133-1135. 1997.

[101] D. Togawa, T. Bauer, I. Lieberman and S. Takikawa. Histologic evaluation of human vertebral bodies after vertebral augmentation with polymethyl methacrylate. *Spine. 28(14),* pp. 1521-1527. 2003.

[102] J. Orr, N. Dunne and J. Quinn. Shrinkage stresses in bone cement. *Biomaterials 24(17),* pp. 2933-2940. 2003.

[103] D. Boyd, M. Towler, A. Wren and O. Clarkin. Comparison of an experimental bone cement with surgical simplex P, spineplex and cortoss. *Journal of Materials Science. Materials in Medicine. 19(4),* pp. 1745-1752. 2008.

[104] G. J. Pomrink, M. P. DiCicco, T. D. Clineff and E. M. Erbe. Evaluation of the reaction kinetics of CORTOSS, a thermoset cortical bone void filler. *Biomaterials 24(6),* pp. 1023-1031. 2003.

[105] W. Geurtsen. Biocompatibility of resin-modified filling materials. *Critical Reviews in Oral Biology and Medicine. 11(3),* pp. 333-355. 2000.

[106] R. O'Hara, N. Dunne, J. Orr, F. Buchanan, R. Wilcox and D. Barton. Optimisation of the mechanical and handling properties of an injectable calcium phosphate cement. *Journal of Materials Science. Materials in Medicine. 21(8),* pp. 2299-2305. 2010.

[107] P. Hatton, K. Hurrell Gillingham and I. Brook. Biocompatibility of glass-ionomer bone cements. *J. Dent. 34(8),* pp. 598-601. 2006.

[108] J. Nicholson. Chemistry of glass-ionomer cements: A review. *Biomaterials 19(6),* pp. 485-494. 1998.

[109] J. Renard, D. Felten and D. Béquet. Post-otoneurosurgery aluminium encephalopathy. *Lancet. 344(8914),* pp. 63-64. 1994.

[110] P. Hantson, P. Mahieu, M. Gersdorff, C. Sindic and R. Lauwerys. Encephalopathy with seizures after use of aluminium-containing bone cement. *Lancet. 344(8937),* pp. 1647-1647. 1994.

[111] D. Boyd and M. Towler. The processing, mechanical properties and bioactivity of zinc based glass ionomer cements. *Journal of Materials Science. Materials in Medicine. 16(9),* pp. 843-850. 2005.

[112] O. Clarkin, D. Boyd and M. Towler. Strontium-based glass polyalkenoate cements for luting applications in the skeleton. *J. Biomater. Appl. 24(6),* pp. 483-502. 2010.

[113] A. Wren, A. Coughlan, L. Placek and M. Towler. Gallium containing glass polyalkenoate anti-cancerous bone cements: Glass characterization and physical properties. *Journal of Materials Science. Materials in Medicine. 23(8),* pp. 1823-1833. 2012.

[114] F. Gomes, R. Pires and R. Reis. Aluminum-free glass-ionomer bone cements with enhanced bioactivity and biodegradability. *Materials Science & Engineering. Biomimetic Materials, Sensors and Systems. 33(3),* pp. 1361-1370. 2013.

[115] M. Darling and R. Hill. Novel polyalkenoate (glass-ionomer) dental cements based on zinc silicate glasses. *Biomaterials 15(4),* pp. 299-306. 1994.

[116] A. Wren, A. Kidari, N. Cummins and M. Towler. A spectroscopic investigation into the setting and mechanical properties of titanium containing glass polyalkenoate cements. *Journal of Materials Science. Materials in Medicine. 21(8),* pp. 2355-2364. 2010.

[117] B. Dickey, "PhD Candidate, Dalhousie University, bretttdickey@gmail.com," 2014.

[118] V. Dickinson, "Composition-Property Relationships in Multicomponent Germanium-Based Polyalkenoate Cements," *Dalhousie University,* 2014.

[119] J. Hu, X. Du, C. Huang, D. Fu, X. Ouyang and Y. Wang. Antibacterial and physical properties of EGCG-containing glass ionomer cements. *J. Dent.* 2013.

[120] M. Farret, E. de Lima, E. Mota, H. Oshima, V. Barth and S. de Oliveira. Can we add chlorhexidine into glass ionomer cements for band cementation? *Angle Orthod. 81(3),* pp. 496-502. 2011.

[121] Y. Takahashi, S. Imazato, A. Kaneshiro, S. Ebisu, J. Frencken and F. Tay. Antibacterial effects and physical properties of glass-ionomer cements containing chlorhexidine for the ART approach. *Dental Materials. 22(7),* pp. 647-652. 2006.

[122] G. Palmer. Chlorhexidine release from an experimental glass ionomer cement. *Biomaterials 25(23),* pp. 5423-5431. 2004.

[123] J. Ribeiro and D. Ericson. In vitro antibacterial effect of chlorhexidine added to glass-ionomer cements. *Scand. J. Dent. Res. 99(6),* pp. 533-540. 1991.

[124] J. Jedrychowski, A. Caputo and S. Kerper. Antibacterial and mechanical properties of restorative materials combined with chlorhexidines. *J. Oral Rehabil. 10(5),* pp. 373-381. 1983.

[125] A. Lebugle, A. Rodrigues, P. Bonnevialle, J. Voigt, P. Canal and F. Rodriguez, "Study of implantable calcium phosphate system for the slow release of methotrexate." *Biomaterials.,* vol. 23, pp. 3517-3522, 2002.

[126] *Dictionary of Pharmacology*. Methotrexate 2014. http://www.thekanjifoundrypress.com/m.html Accessed: Sept. 2014.

[127] S. Ayyappan, N. Sundaraganesan, V. Aroulmoji, E. Murano and S. Sebastian. Molecular structure, vibrational spectra and DFT molecular orbital calculations (TD-DFT and NMR) of the antiproliferative drug methotrexate. *Spectrochimica Acta. Part A, Molecular and Biomolecular Spectroscopy. 77(1),* pp. 264-275. 2010.

[128] Pubchem, Methotrexate. 2013. http://pubchem.ncbi.nlm.nih.gov/summary/summary.cgi?cid=126941&loc=ec_rcs Accessed: Sept. 2014

[129] A. Dowling and G. Fleming. The influence of poly(acrylic) acid number average molecular weight and concentration in solution on the compressive fracture strength and modulus of a glass-ionomer restorative. *Dental Materials. 27(6),* pp. 535-543. 2011.

[130] G. Fleming, A. Farooq and J. Barralet. Influence of powder/liquid mixing ratio on the performance of a restorative glass-ionomer dental cement. *Biomaterials 24(23),* pp. 4173-4179. 2003.

[131] V. Zahra, S. Kohen and R. Macchi. Powder-liquid ratio and properties of two restorative glass ionomer cements. *Acta Odontológica Latinoamericana. 24(2),* pp. 200-204. 2011.

[132] A. Dowling and G. Fleming. Can poly(acrylic) acid molecular weight mixtures improve the compressive fracture strength and elastic modulus of a glass-ionomer restorative? *Dental Materials. 27(11),* pp. 1170-1179. 2011.

[133] Sigma-Aldrich, Inc. "Product Information: Methotrexate hydrate" 2008.

[134] K. Gowthamarajan and S. Singh, "Dissolution Testing for Poorly Soluble Drugs: A Continuing Perspective." *Dissolution Technologies.,* pp. 24-32, 2010.

[135] S. Decker, W. Winkelmann, B. Nies and F. van Valen, "Cytotoxic effect of methotrexate and its solvent on osteosarcoma cells in vitro." *The Journal of Bone and Joint Surgery. British Volume.,* vol. 81, pp. 545-551, 1999.

[136] A. Hoppe, N. Guldal and A. Boccaccini, "A review of the biological response to ionic dissolution products from bioactive glasses and glass-ceramics." *Biomaterials.,* vol. 32, pp. 2757-2774, 2011.

[137] ISO, "Dentistry - Water-based cements - Part 1: Powder/liquid acid-base cements," *British Standard: ISO 9917,* 2007.

[138] G. Fleming, A. Dowling and O. Addison. The crushing truth about glass ionomer restoratives: Exposing the standard of the standard. *J. Dent. 40(3),* pp. 181-188. 2012.

[139] A. Dowling, G. Fleming, E. McGinley and O. Addison. Improving the standard of the standard for glass ionomers: An alternative to the compressive fracture strength test for consideration? *J. Dent. 40(3),* pp. 189-201. 2012.

[140] M. Bohner and J. Lemaitre. Can bioactivity be tested in vitro with SBF solution? *Biomaterials 30(12),* pp. 2175-2179. 2009.

[141] Cayman Chemical. Product Information: Methotrexate. 2012.

[142] S. Kehoe, M. Langman, U. Werner Zwanziger, R. Abraham and D. Boyd. Mixture designs to assess composition-structure-property relationships in SiO2-CaO-ZnO-La,,2O3,f-TiO,,2-MgO-SrO-Na2O glasses: Potential materials for embolization. *J. Biomater. Appl. 28(3),* pp. 416-433. 2013.

[143] H. Wang, C. Galasko, S. Crank, G. Oliver and C. Ward. Methotrexate loaded acrylic cement in the management of skeletal metastases. biomechanical, biological, and systemic effect. *Clin. Orthop. (312),* pp. 173-186. 1995.

[144] R. Billington, J. Williams and G. Pearson. Variation in powder/liquid ratio of a restorative glass-ionomer cement used in dental practice. *Br. Dent. J. 169(6),* pp. 164-167. 1990.

[145] Stat-Ease Inc., "Design Expert" 2011.

[146] M. Anderson and P. Whitcomb, *DOE Simplified - Practical Tools for Effective Experimentation.* New York: Productivity Press, 2007.

[147] G. Palmer, R. Billington and G. Pearson. Chlorhexidine release from an experimental glass ionomer cement. *Biomaterials 25(23),* pp. 5423-5431. 2004.

[148] Graph Pad, "Prism" 2014.

[149] F. Shah, D. Brauer, R. Wilson, R. Hill and K. Hing. Influence of cell culture medium composition on in vitro dissolution behavior of a fluoride-containing bioactive glass. *Journal of Biomedical Materials Research. Part A. 102(3),* pp. 647-654. 2014.

[150] L. Turkun, M. Turkun, F. Ertuarul, M. Atea and S. Brugger. Long-term antibacterial effects and physical properties of a chlorhexidine-containing glass ionomer cement. *Journal of Esthetic and Restorative Dentistry. 20(1),* pp. 29-45. 2008.

[151] G. Gerber and A. Léonard. Mutagenicity, carcinogenicity and teratogenicity of germanium compounds. *Mutation Research - Fundamental and Molecular Mechanisms of Mutagenesis. 387(3),* pp. 141-6. 1997.

[152] M. Botelho. Inhibitory effects on selected oral bacteria of antibacterial agents incorporated in a glass ionomer cement. *Caries Res. 37(2),* pp. 108-114. 2003.

[153] J. Jedrychowski, A. Caputo and S. Kerper. Antibacterial and mechanical properties of restorative materials combined with chlorhexidines. *J. Oral Rehabil. 10(5),* pp. 373-381. 1983.

[154] J. van Meerloo, G. Kaspers and J. Cloos. Cell sensitivity assays: The MTT assay. *Methods Mol. Biol. 731*pp. 237-245. 2011.

[155] L. Prentice, M. Tyas and M. Burrow. The effect of particle size distribution on an experimental glass-ionomer cement. *Dental Materials. 21(6),* pp. 505-510. 2005.

[156] C. Crowley, J. Doyle, M. Towler, N. Rushe and S. Hampshire. Influence of acid washing on the surface morphology of ionomer glasses and handling properties of glass ionomer cements. *Journal of Materials Science. Materials in Medicine. 18(8),* pp. 1497-1506. 2007.

[157] G. Babighian. Use of a glass ionomer cement in otological surgery. A preliminery report. *J. Laryngol. Ontol. 106(11)* pp. 854-959. 1992.

[158] R.T. Ramsden, R.C. Herdman, and R.H. Lye. Ionomeric bone cement in neuro-otological surgery. *J. Laryngol. Otol. 106(11)* pp. 949-953. 1992.

[159] G. Geyer and J. Helms. Ionomer-based bone substitute in otologic surgery. *European archives of oto-rhino-laryngology. 250(5)* pp. 253-256. 1993.

[160] H.G. Kempf, P.R. Issing, and T. Lenarz. Ionomer cement in cochlear implant surgery-applications and lont-term outcome. *Laryngo-Rhino-Otologie. 75(7)* pp. 388-391. 1996.

[161] A.I. Khuri and S. Mukhopadhyay. Response surface methodology. *WIRE Computational Statistics. vol 2* pp 128-149. 2010.

[162] J. Wang, Z. He, J. Oh, and S. Park. Multi-Response Robust Optimization Using Desirability Function. *Applied Stochastic Models in Business and Industry. 26(2)* pp. 157-171. 2010.

APPENDIX

Preliminary Experimentation: XRD & T_g Data

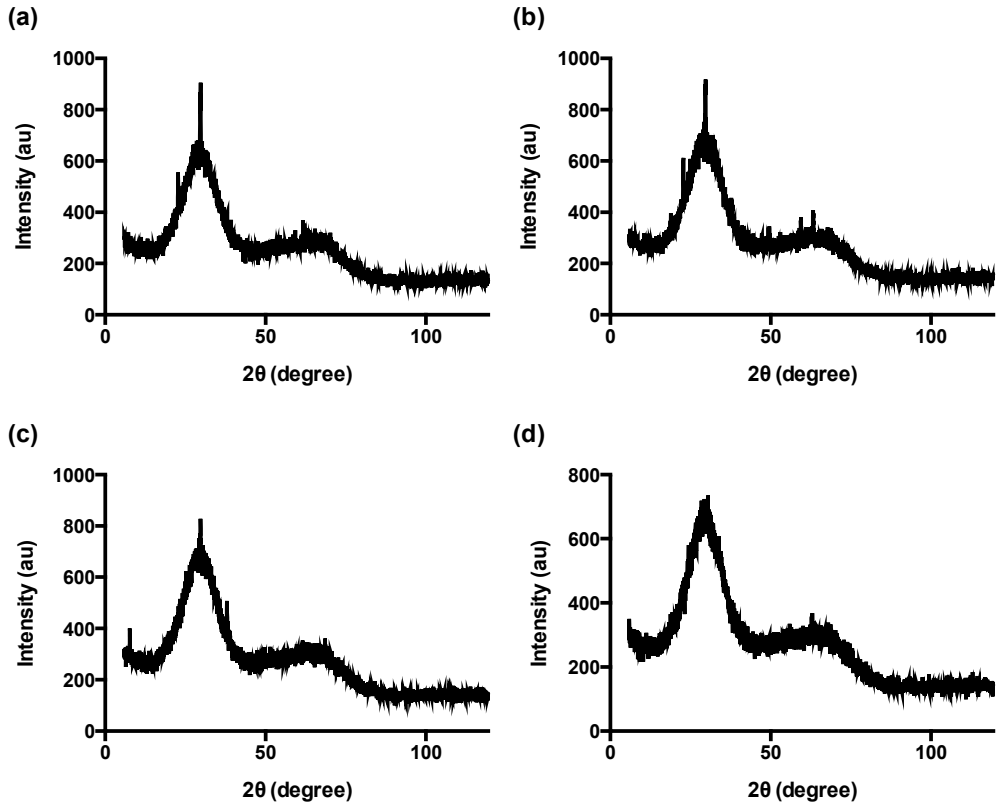

Figure 7.1: XRD plots for the four batches of DG209 glass synthesized, as detailed in Section 3.1; (a) Batch 1, (b) Batch 2, (c) Batch 3, (d) Batch 4; au: arbitrary units.

Table 7.1: Mean T_g and standard deviation for each batch of DG209 glass synthesized, as detailed in Section 3.1. T_g reported by Dickey *et al.* [4].

Batch No.	T_g (°C)
1	618 ± 0.0
2	605 ± 16.2
3	617 ± 1.2
4	616 ± 6.8
Dickey *et al.*	624

n=3 for each batch